Heating and Treating Water with Sunlight:
Solar Photocatalytic-Thermal Systems for a Sustainable Built Environment

By

Vivek Rao

A dissertation submitted in partial satisfaction of the

requirements for the degree of

Doctor of Philosophy

in

Engineering - Mechanical Engineering

in the

Graduate Division

of the

University of California, Berkeley

Committee in charge:

Professor Slawomir Hermanowicz, Co-Chair
Professor Alice Agogino, Co-Chair
Professor Maria-Paz Gutierrez
Professor Lisa Pruitt

Spring 2018

Abstract

Heating and Treating Water with Sunlight: Solar Photocatalytic Thermal Systems for a Sustainable Built Environment

by

Vivek Rao

Doctor of Philosophy in Mechanical Engineering

University of California, Berkeley

Professor Slawomir Hermanowicz, Co-Chair
Professor Alice Agogino, Co-Chair

Global water scarcity will be a defining challenge of the coming decades, with 2.5 billion of the world's population expected to live under water stress by 2050. Scarcity, and the accelerating factors of the food-energy-water nexus, population growth, and climate change will converge on the built environment, where buildings account for an estimated 25% of water use and 40% of energy use globally. Urban water re-use presents a promising opportunity to manage this crisis. However, current efforts to realize water reuse are generally capital-intensive, owing to centralization of recycling plants, or problematic for the food-energy-water nexus, as decentralized or building-scale plants employ recycling technologies that are energy-intensive. This dissertation presents my research to use sunlight to heat and treat domestic greywater in building facades. I propose a synergistic solar photocatalytic greywater recycling and solar thermal heating system in an envelope easily integrable into facades, enabling water re-use and energy savings at the building scale. To support this proposal, my dissertation explores greywater quality and properties, basic solar photocatalytic reactor design, and simultaneous solar photocatalytic reaction and solar thermal collection. Together, these research pursuits develop a foundation of knowledge to support the realization of new energy-offsetting and water-recycling systems at the building scale.

In Chapter 2, I describe research to understand the input, greywater, and its poorly-understand optical parameters that are essential to understand for any photodependent treatment process. I show that greywater absorbs heavily in the UVA/B range, a characteristic modeled by few currently-published synthetic greywater formulations, and that the absorbance is correlated to relatively high chemical oxygen demand (COD) and soluble COD. These results indicate that as UV-based methods for water recycling gain traction, careful consideration of the inherent absorbance of the greywater matrix must be accounted for in system design.

In Chapter 3, I explore the underlying treatment process proposed, solar photocatalysis via titanium dioxide, and characterize it for a simple inclined plate reactor system. I report that inclined plate photocatalytic reactors under simulated solar light show performance that is primarily governed by light intensity and light capture, rather than hydrodynamics and mass transfer, even when the two are coupled through system design parameters (e.g., inclination angle). This result is in agreement with previous literature on UV-driven inclined plate reactors, and offers new insight as to the operation of solar photocatalysis under low-UV and laminar or transitionary Reynolds number regimes.

In Chapter 4, I explore how the basics of the inclined plate reactor can be scaled up to a design relevant for building façades, and propose, fabricate, and characterize the Vertically Integrated Multistep (VIMS) reactor. Under real solar conditions in Berkeley, CA, I show that the VIMS system effectively decolorizes methylene blue in a westward-facing afternoon sun condition. Based on volumetric performance modeling, I suggest that the VIMS system can, at a $9m^2$-scale, treat up to 60L of greywater per day, although these results are substantially reduced under limited solar intensity, e.g., cloudy conditions.

In Chapter 5, I show how integration of solar photocatalytic systems, including VIMS and a simple flate-plate façade collector, can couple with simultaneous solar thermal gain to yield a multifunctional system. This research represents, to my knowledge, the first reported simultaneous solar photocatalytic water treatment and solar thermal gain system. Under simulated solar conditions, I experimentally demonstrate that ASHRAE measures of solar thermal collector efficiency and photocatalytic reaction performance are opposed to each other in multifunctional systems. However, given the relatively warm temperatures of greywater entering the system in real-world application, I suggest that significant promise exists for high solar photocatalyic treatment performance.

These results indicate that buildings and their facades present a promising platform to offset water scarcity through re-use, and point to further research in multifunctional façade-integrated systems to realize sustainability in urban energy and water.

Table of Contents

List of figures

List of tables

Acknowledgments

I am continually inspired by and grateful for the wonderful community who has supported me throughout my work on this research.

First, this work would not have been possible without the generous support of the National Science Foundation (NSF) through the Emerging Frontiers in Research Innovation Program. The NSF's willingness to fund and support this project enabled truly unique research to occur at UC-Berkeley, and I am a stronger, more confident researcher for it. I would also like to acknowledge the Tsinghua-Berkeley Shenzhen Institute's generous funding of my research.

Second, I would like to thank my fellow students in the UC Berkeley community for helping me realize this dissertation. Henry Kagey, David Campbell, Yuan Li, Pablo Hernandez, Dylan Kato, Elly Lin, Matthew Kozuch, Burcu Ozdemir, John Stevens, Shuk Chan, and many, many more colleagues helped me with every aspect of completing this work, from programming microcontrollers to recommending papers to review to providing much-needed feedback on research results.

Next, I would like to thank my academic committee. I am truly fortunate to have had four faculty members – all of whom I consider role models – engage with me throughout my graduate school experience. Professor Lisa Pruitt has been an inspiration for her commitment to research, pedagogy, and her students, and I appreciate her unyielding support of me throughout my graduate study. Professor Maria-Paz Gutierrez has been instrumental in my development as a researcher, urging me to explore engineering research with a design-centric lens, and vice versa. Her leadership and vision earned the NSF EFRI award that supported this work, and would not have been possible without her. Professor Alice Agogino has been an incredible inspiration for me both personally and professionally since my undergraduate studies here at UC-Berkeley, and has been a wonderful source of support and guidance throughout my graduate work. Without her belief in and continued support of my exploration of research outside of traditional Mechanical Engineering fields, I would not have completed this research work. Finally, I am forever grateful for Professor Slav Hermanowicz's close guidance and advising throughout my graduate career. He welcomed me into his research group and laboratory, and provided me a unique combination of inspiration, independence, and deeply empathetic counsel to explore engineering research in ways I wouldn't have imagined.

Finally I would like to acknowledge my family and partner. My brother Vikram, and parents Mohan and Kala all resolutely encouraged and supported me throughout my research work in graduate school, and cultivated my curiosity about engineering research from an early age. I am indebted to my partner Jenny Flaherty, who embodies the tenacity and grace of meaningful scholarship and strong partnership, and who never ceases to inspire me.

1. Introduction

1.1 Motivation & Research Opportunity

Provision of sustainable, adequate water supplies will be a defining challenge of the 21st century [1]. Two-thirds of the world's population currently experiences water scarcity at least one month out of the year [2], and by 2030, global water demand is expected to exceed readily available supply (as quantified in 2009) by more than 40% [3]. If current efforts to reconcile this gap continue unabated – through groundwater pumping, increasing withdrawals from existing reservoirs, and other approaches – ecosystems will suffer severe damage [4]. While the vast majority of global water withdrawals – more than 70% - are related to agriculture, proportions used in industrial (~19%) and domestic and sanitation applications (~10%) are expected to expand significantly [5], and the smaller quantity of water used for domestic applications and sanitation is crucial for public health and human comfort [6].

These projections are driven by a range of forces as complex as water systems themselves. However, water scarcity will be particularly exacerbated by three factors that uniquely converge on water resources and human society: climate change and the energy-water nexus; rapid urbanization and further expansion of cities; and legacy approaches to infrastructure.

Climate change will affect both the supply and energy demand of water. Climate change is likely to put increased strains on water resources [7], which will impact urban areas in terms of water supply [8]. Besides the immediate concern of diminished accessible water supply, climate change will require reconsideration of the energy embodied in water, as 80% of global energy is produced via combustion of greenhouse gas-producing fossil fuels [9]. For example, by the time of its end-use in urban domestic environments in the United States, water has embodied energy of 15400 MJ/person/year across the pre-consumption, use, and post-consumption stages [10]. While significant energy use is associated with transport (primarily pumping) and wastewater treatment (primarily aerobic biological treatment) [11], more than 70% of embodied energy in urban water is attributable to water heating in the US [10]. In many regions of the world, the interdependence of water and energy is particularly extreme, with substantial embodied due to treatment or transport costs: in the United Arab Emirates, seawater desalination can account for more than 20% of the nation's electricity demand [12], while in California, approximately 19% of the state's electricity is involved in water systems, with up to 3% of the state's power dedicated to move water from Northern California to the Los Angeles area via the State Water Project alone [13]. The large embodied energy of urban water, owing to heating and the often highly intensive treatment and transport of water supply, are one aspect of the energy-water nexus [14] that will exacerbate existing issues of water scarcity.

Second, rapid, continued urban population growth will yield greater stresses on water resources [15]. A study of large cities in Africa and Asia projected an increase in the number of urban residents anticipated to experience by water scarcity by 2050 by a factor of 5 and 10, respectively [16]. This is driven by the combined effect of increased water withdrawals, owing to population growth, and climate change on existing water resources.

Third, the dominant paradigm on water infrastructure is ill-suited to meet the current range of water challenges facing the urban population. For example, large-scale infrastructure, such as dams and centralized treatment systems, what Peter Gleick calls 'the hard path' [17], may not account for complex social and environmental issues to come, compromising intended results [18] [19]. While many studies on the topic examine dams, much of today's water infrastructure and approach to water development reflects insufficient consideration for conditions of scarcity, population and climate change [20].

However, each of these exacerbating forces can be re-framed as opportunities for impactful innovation (Fig 1.1). This framing is cause for optimism about the future of water resources.

To re-frame climate change and the energy-water nexus as opportunities, a paradigm of minimizing the energy demand of water and maximizing the value of energy spent on water can be adopted. Decentralized water treatment and supply in urban environments can help offset significant amounts of energy involved in transport and conveyance of water [21]. Similarly, the use of solar and other renewable energy sources to power water supply and treatment [22], and solar energy to heat water before use [23] are established approaches that promise to minimize the greenhouse gas impact of water supply. To maximize the value of energy embodied in water, wastewater can be broadly viewed as a resource. First, wastewater recycling promises to provide water for a fraction of the energy used for desalination [24]. If only greywater is recycled (see Section 2.1), 10-25% of urban water demand could be satisfied by nonpotable reuse [25]. Second, heat in wastewater can be collected to offset energy demand at local or building scales [26], an approach commercially implemented in sewers [27] and showers [28]. Thus, by embracing the energy demand of water as an opportunity, decentralized water treatment, renewable energy, and harvesting wastewater for its thermal and resource properties can be more readily realized.

Urban population growth and corresponding development can also be re-framed as an opportunity to develop cities responsibly and institute responsible water management practices. Careful consideration of urban design, governance, and user behavior can help cities manage water demand and resources proactively [29], [30]. For example, progressive approaches to urban water governance enabled both Singapore and Windhoek, Namibia to offset roughly one-quarter of their water needs with recycled wastewater [31]. In the United States, San Francisco implemented a building-scale recycled water ordinance to advance the city towards a vision of district-scale water reuse [32]. These examples and methods illustrate that achieving simultaneous urban growth

and sustainable water use is possible with proactive governance, design, and collaboration.

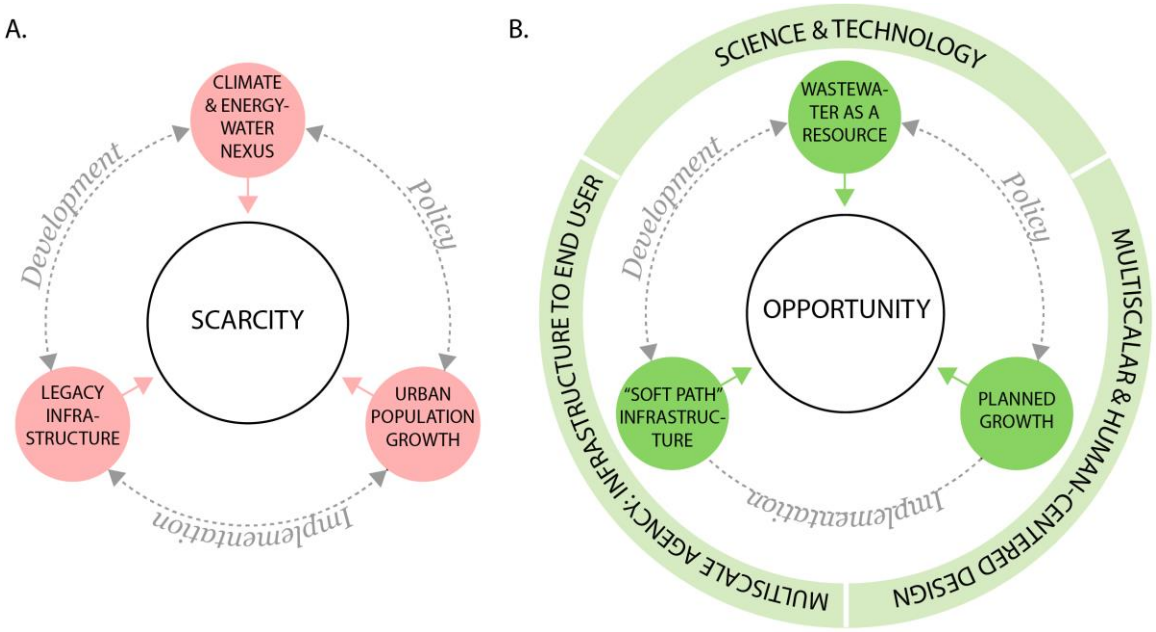

Figure 1.1. A drivers and opportunities framework maps how the condition of water and energy scarcity **(a)**, articulated around current approaches to resources, implementation, and development, is exacerbated by legacy infrastructure, climate change and the energy-water nexus, and urban population growth. This condition can be re-envisioned into a framework around scarcity as opportunity **(b)**, in which science and technology, design, and new paradigms of agency to both infrastructure and end users enable realization of "soft path" infrastructure, wastewater as a resource, and planned growth. Together, this re-frame views water and energy scarcity as an opportunity for innovation. This dissertation explores one possible pathway to explore the emergent opportunity around water and energy in the context of scarcity.

Finally, while legacy thinking about centralized, 'hard path' infrastructure dominates, it clearly points to an opportunity for more sustainable water infrastructure, what Gleick calls 'the soft path' [17]. The soft path is characterized by community-scale systems operating in complement to existing centralized water infrastructure. Such systems are supported by equitable water markets and decision making, and a suite of water efficiency interventions. David Sedlak extends on this concept with his Water 4.0 framework [33], which champions a portfolio of infrastructural and efficiency interventions ranging from greywater reuse to smart irrigation systems to stormwater management and reclamation. While both Gleick and Sedlak readily admit that the paradigm will be challenging

to realize, together, their arguments present a paradigm to approach the future as one of opportunity rather than abject crisis.

Inspired by the soft path and Water 4.0 approaches, this work fully embraces the reframe of urban water scarcity into an opportunity for research and innovation. Here, I describe the conception, design, and characterization of a building-integrated system to heat and treat greywater using sunlight. The system is powered by sunlight to minimize energy inputs, and uses wastewater as a water and thermal resource at the building scale, to maximize the value of energy invested in urban water. This work seeks to establish hybrid water- and energy-harvesting systems as a viable technology to help resolve urban water scarcity.

1.2 Structure of this Document

In the subsequent chapters, the key underlying challenges in realizing the proposed system will be addressed. This dissertation is presented as four chapters representing several research thrusts that establish knowledge essential to the realization of onsite greywater recycling systems in the built environment. Although each chapter draws on substantially different research methods, experimental setups, and disciplinary backgrounds, they are interdependent in that the findings from each chapter inform the others. Thus, while each chapter is closely connected to the previously and subsequently presented work, it is framed as an independent contribution to allow for discrete engagement with its specific methods and background.

First, in Chapter 2, the nature of greywater to be considered in treatment is discussed, with a focus on the challenges inherent in its composition, specifically, unknown optical properties.

Next, in Chapter 3, the fundamental issues surrounding photocatalytic reactor design are considered, namely, the relationship between important design parameters and overall reaction performance under solar conditions. This relationship is explored using the inclined plate reactor as a model system.

In Chapter 4, the baseline system of the solar photocatalytic inclined plate reactor system is multiplexed to realize a building-façade integrated water recycling system. The proposed design, the Vertically Integrated Multistep (VIMS) system, is designed, fabricated, and characterized under real sunlight conditions.

In Chapter 5, a hybrid solar photocatalytic treatment and solar thermal gain system is designed to interface with a building façade. As of this writing, this is the first system to characterize the relationship between photocatalytic oxidation performance and solar thermal collector efficiency. Laboratory- and sub-pilot scale systems are fabricated and characterized under real and simulated solar conditions.

2. Survey and Optochemical Characterization of Real and Synthetic Greywaters

2.1. Introduction

2.1.1. Definition, Quantity, and Characteristics of Greywater

Greywater is water that originates from sinks, showers, and laundry in the domestic environment – in short, anything that does not come into contact with sewage or toilet waste. It represents between 46% [34] to greater than 90%, if vacuum-based toilets are employed [35], of all domestic wastewater effluent (Figure 2.1). Greywater is also further classified into 'light' or 'low strength' – originating from showers, sinks, and baths only – and 'heavy' or 'high strength' – which includes greywater from laundry, kitchens, and other sources. This classification helps distinguish greywater heavy with biological matter from greywater with relatively little biological content.

The actual quantity of greywater available depends on local water infrastructure (e.g., piped water versus a community well) and water use behaviors, and can vary between 20-30 liters per person per day (LPD) in low-income regions (e.g., rural Mali) and 100-220 LPD in high-income regions (e.g. urban Switzerland) [36]. A recent report indicated that in the United States, greywater quantities were between 127-151 LPD [37]. This thesis focuses primarily upon high-income urban environments, because much of the published work in the field converges on the resource needs of these regions, and the thrust of this scholarship is at the intersection of new technologies and the urban built environment.

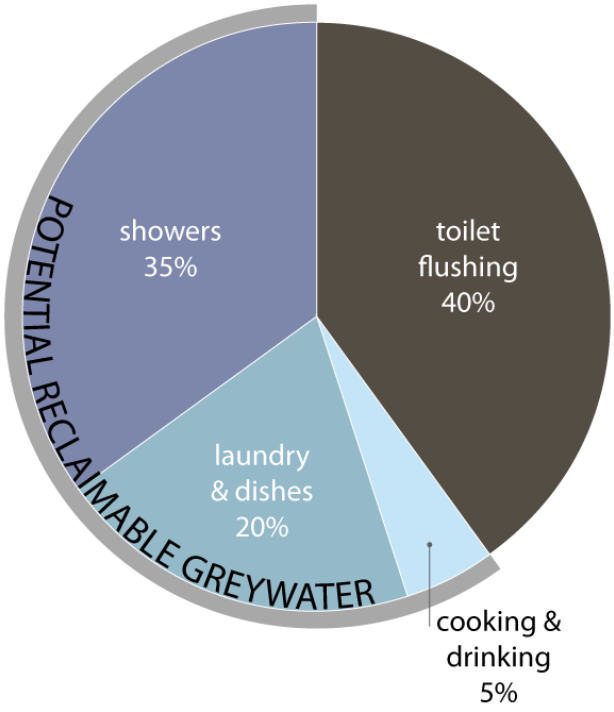

Figure 2.1. Potential Reclaimable Greywater, by Source [38]–[40]

Regardless of region, the quantity of greywater represents significant water resource with great potential for assuaging local water demand; using recycled greywater for toilet flushing applications alone could reduce water consumption by 40-60 LPD [39]. This, combined with its relatively low organic loading levels (greywater typically has roughly 50% of the chemical oxygen demand (COD) of sewage [35]), makes greywater an attractive target for water recycling technologies.

Greywater's high variability in chemical and biological composition has been widely reported. Beyond significant heterogeneity in water quality by location, greywater characteristics have been shown to vary significantly across a single day [41], owing to differences in sources of residential greywater production. Greywater composition can be considered first in terms of traditional water quality indicators (Table 2.1), and by these parameters, greywater exhibits a significant range; for example, BOD can vary by an order of magnitude [42] [43] [40]. Should recycled greywater be used solely for environmental applications, such as irrigation, a careful understanding of these parameters, along with mineral content, could suffice to meet re-use standards (see 2.2.2).

	Mixed Greywater
pH	6.3-8.1
Total Suspended Solids (TSS) (mg/L)	25-183
Turbidity (NTU)	29-375
Chemical Oxygen Demand (COD) (mg/L)	100-700
Biochemical Oxygen Demand (BOD) (mg/L)	47-466
Total Kjeldahl Nitrogen (TKN) (mg/L)	1.7-34.3
Total Phosphorous (TP) (mg/L)	0.11-22.8
Total Coliforms (CFU/100mL)	56-8.03E7
Fecal Coliforms (CFU/100mL)	.1-1.5E8

Table 2.1: Characteristics of Greywater (Adapted from [42]).

However, because domestic nonpotable applications for recycled greywater, such as toilet flushing and laundry applications, are very promising, careful consideration of human health risks from micropollutants and emerging contaminants is crucial, especially if on-site recycling is to be realized. Based on the content of personal care products, detergents, and other household chemicals, nearly 900 xeniobiotic organic compounds (XOC's) have been identified as possibly resident in greywater [43]; further screening studies reported detecting more than 190 compounds via gas chromatography mass spectrometry (GC-MS), including many, such as illicit drugs and pesticides, that did not originate from commercial products [44]. A subsequent analysis of the human health risks originating from 280 compounds contained in greywater indicated that while lifetime exposure risk to these chemicals was insignificant, 14 chemicals were of concern for potential potable water use [45]. The authors suggested triple-barrier treatment process involving a membrane bioreactor (MBR), ozone-based advanced oxidation process (AOP), and

activated carbon adsorption (AC), which has been reported to effectively manage the breakdown of detected micropollutants [46].

Greywater thus represents a significant water resource with great potential to reduce the water needs of the urban environment. However, it is characterized by highly heterogeneous chemical and biological composition, and particular concern exists around micropollutants that could pose health risks. Thus, careful design of treatment processes is essential if decentralized greywater recycling is to be realized.

2.1.2. Standards and Current Treatment Processes Applicable to Greywater

Much of recycled greywater finds re-use in toilet-flushing and irrigation/gardening [47], and despite these being nonpotable applications, stringent standards governing such nonpotable reuse (NPR) exist. United States EPA Guidelines suggest below limit-of-detection quantity of fecal coliforms (0 CFU / 100mL) and < 10mg/L biological oxygen demand (BOD_5) for unrestricted usage; however, actual implemented policies vary widely between states [48]. Among implemented standards, some of the most stringent exist in California, where Title 22 requires a total coliform count of < 2.2 CFU / 100 mL and a demonstrated 5-log reduction in poliovirus or chlorine CT times of (450 mg/L)-min (USEPA, 2004) [49] exhibited by the treatment process. It is important to note that current US NPR standards do not account for micropollutant content. Treatment technologies intending to recycle greywater must satisfy these criteria.

A range of technologies exist to treat greywater, following the heterogeneity of both greywater quality and reuse standards. Many technologies been proposed and characterized in the academic literature, and several commercialized systems are operational and online. Solutions have ranged from constructed wetlands [50] to nanofiltration [51], and the range of greywater treatment technologies has been covered in excellent detail elsewhere [42] [40]. In addition to various treatment *technologies*, solutions also include incorporating other water sources, such as rainwater [52], and involving novel process control methods such as model-predictive control [53] to govern system operation. For building-integrated technologies, where footprint and simplicity of operation are crucial, MBR and multi-stage treatment processes have established themselves as the most promising candidates for on-site greywater treatment, and the majority commercially-installed systems involve either process [54].

MBR's have achieved popularity for their combination of physical and biological processes into a relatively small footprint [41], while multi-stage systems ensure compliance with NPR disinfection guidelines. MBR's have been shown to effectively treat greywater to compliance with a variety of countries' standards at a variety of scales: at the 600-L scale to treat household greywater to compliance with Turkish standards [55], to the 3 m^3-scale to treat selected shower greywater from a 441-room room hotel to meet Spanish water re-use requirements [56]. Multistage systems involve essentially miniaturizing water treatment trains to involve primary, secondary, and tertiary treatment in a single module, and may include an MBR as an intermediate process. Installations in

San Francisco, California, and Pittsburgh, PA, use the Aquacell G20 system, which begins with screening for solids removal, followed by an MBR, and subsequently ultrafiltration, UV-disinfection, and chlorination [57] [58]. Other non-commercialized systems proposed in the literature follow a similar design, albeit with different biological treatment and disinfection technologies [39] [46] [59].

A key limitation of existing water recycling technology lies in the significant energy demand of MBR operation. Owing to aeration and membrane scouring, which can be as high as 6-7 kWh / m^3 for systems operating in the 1000 gallons-per-day (gpd) [~ 4 m^3/day] range; energy demand falls with increasing system size, and the specific energy demand for treatment is nearly an order of magnitude lower for 100000 gpd [~400 m3/day] MBRs [21]. However, most building-scale applications for greywater recycling are typically much smaller, and thus do not enjoy such economy of scale: for example, an installed greywater treatment system at 181 Fremont in San Francisco, California, has a design capacity of 5000 gpd [~20 m^3/day], for a 42600 ft^2 [4000 m^2] building [60], while of systems surveyed across the US, none exceeded 50000 gpd [200 m^3/day] [54]. Thus, the promise and effectiveness of leading greywater recycling systems is constrained by their energy demand.

Recent work has suggested that a significantly streamlined treatment process could achieve NPR standards [61]. In this work, researchers studied 'light greywater' originating from showers and sinks, and then filtered greywater through a 10*u*m filter. Subsequently, greywater was subject to UV disinfection, which the authors determined to be the most cost-effective disinfection process. The researchers demonstrated that effluent from the system was in compliance with California Title 22 regulations. Thus, by targeting a specific category of greywater, which forms the majority of greywater effluent (Figure 2.1), the researchers were able to meet NPR standards solely with tertiary treatment following a basic filtration step. Considering the high energy cost of operating a multi-stage system, filtration followed by disinfection schemes are highly appealing.

2.1.3. Optical Properties of Greywater and Synthetic Greywater

Given that many possible tertiary and advanced treatment processes are light-driven, such as UV, UV/H_2O_2, and UV-TiO_2, a careful understanding of the optical properties of greywater is necessary. Even at low turbidity levels, filtered water can attenuate light via scattering and absorption [62] to compromise the delivery of sufficient fluence for effective treatment. A clear relationship between turbidity and reduction in effective UV dose has been demonstrated for raw drinking water: waters with a turbidity range of 1 – 10 NTU decreased effective UV dose by 5-33% respectively, although the exact effects and mechanism of particle size remains unclear [63]. Among the light driven processes, UV-TiO_2 advanced oxidation is particularly promising because of its potential to be powered by sunlight, and thus, to resolve much of the energy demand issues of onsite treatment.

Limited understanding of greywater's optical properties exists in literature. Work has been done to examine the effect of particulate shielding of microorganisms in greywater on UV photolysis, but no systematic examination of attenuation was reported [64]. Specific to advanced oxidation processes, a study treating hotel greywater with UV/TiO_2 via a UV-C lamp and suspended TiO_2 nanoparticles reported a 65% decrease in dissolved organic carbon (DOC) [65], while another study reported UV-C/H_2O_2 treatment of real greywaters yielded 87% COD reduction [66]. Both studies indicate that advanced oxidation can effectively treat greywater, but neither considers the effect of optical properties on overall treatment performance. In addition, both studies use greywaters of significantly different characteristics, making it difficult to compare performance.

In this effort, existing synthetic greywater formulations – that is, formulations for greywater consisting of laboratory reagents, and thus, repeatable – are studied to understand their optical properties. Three studies, by Fenner [64], Hourlier [51], and Surendran [67], provided a clear rationale for their synthetic greywater formulation and detailed discussion of the formulations' constituent parts. By identifying the optical profile of these synthetic greywaters, and comparing these profiles to real greywater, the synthetic greywaters that optically model real greywater closely are identified, and thus, the formulations that should be used to characterize light-dependent treatment processes can be revealed.

2.3. Materials and Methods

Synthetic Greywater Sample Preparation

Constituents of each synthetic greywater formulation (Table 2.1) were laboratory grade reagents (Sigma-Aldrich) unless otherwise specified. For each synthetic greywater, constituents were added to 2L of deionized water, and were magnetically stirred for two hours. Between experiments, samples were stored in a refrigerator (4^oC), and were magnetically stirred prior to re-use to re-suspend any settled solids. A preparation of Surendran's synthetic greywater formulation was altered to omit cooking oil and shampoo, as light greywater precludes kitchen effluent, and the authors were not specific about what type of shampoo was used in their formulation; the original formulation was also prepared using vegetable oil (Crisco), and shampoo (Dove).

Each synthetic recipe called for some proxy for microbiological load, either as settled sewage (Surendran), *E. coli* culture (Fenner), or septic effluent (Hourlier). As this study did not focus on biological analyses, and the influence of the small quantities of these proxies (10mL/L) on chemical properties was deemed insignificant, these constituents were not included in the greywater formulations below.

Real Greywater Sample Collection

To recreate domestic light greywater, 48 volunteers at the University of California, Berkeley, were instructed to wash their hands in a modified sink with effluent capture using Dial Soap, the second most-widely used liquid handsoap in the U.S. [68]. The

resulting greywater was completely mixed with a paddle mixer, and 2L was sampled and kept refrigerated between experiments. Samples were magnetically stirred prior to re-use to re-suspend any settled solids.

Analytical Methods

UV-Vis-NIR Spectrophotometry

Full spectrum scans were conducted using a spectrophotometer (HACH DR 5000, HACH Company, Loveland, CO) with a wavelength range of 200 – 1100 nm. 10mL samples were taken and loaded into a quartz-glass cell with path length 2.54cm. Three filtered samples were run and results averaged.

Water Quality Analysis

Colorimetric analysis was used to study key water quality parameters using a spectrophotometer (HACH DR 2400). COD was quantified using HACH Methods (Method #8000), and triplicate samples were taken and averaged. Nitrate, nitrite, and ammonia were quantified using HACH Methods (#8039), (#8153), and (#10031), respectively, with single samples.

Filtration

Filtration of samples was conducted using a 50mL syringe with a 0.450 micrometer syringe filter. Soluble COD (SCOD) was taken as the COD value for the filtrate, while COD refers to the raw greywater's value.

	Fenner	Surendran	Hourlier
Dextrin (mg/L)	85	85	
Ammonium Chloride (mg/L)	75	75	
Yeast Extract (mg/L)	70	70	
Soluble Starch (mg/L)	55	55	
Sodium Carbonate (mg/L)	55	55	70
Washing Powder (mg/L)		30	
Sodium Dihydrogen Phosphate (mg/L)	11.5	11.5	
Potassium Sulfate (mg/L)		4.5	
Potassium Phosphate (mg/L)	4.5		
Shampoo (mL/L)		.1*	
Cooking oil (mL/L)		.1*	
Sodium dodecyl Sulfate (mg/L)	10		50
Lactic Acid (mg/L)			100
Cellulose (mg/L)			100
Glycerol (mg/L)			200
Sodium Sulfate (mg/L)			50

Table 2.2. Synthetic Greywater Compositions. *A preparation of Surendran's greywater omitting these components was prepared, as well.

2.3. Results

Water Quality Parameters

Water quality parameter studies align closely with published literature (Table 2.2) – synthetic formulations fall within the ranges specified in their original studies, while real greywater falls into the broad range of values described for greywater. It is clear that the Surendran formulations – the first without cooking oil and shampoo, as these were poorly specified, and the second, 'Surendran+' including these ingredients – are highly divergent in properties. Hourlier's formulation shows the highest COD of all. Except for Hourlier's formulation, all greywaters, including the real sample, exhibit >60% significant amounts of COD as insoluble.

	Fenner	**Surendran**	**Surendran+**	**Hourlier**	**Real Greywater (RGW)**
COD (mg/L)	254	228	475	675	459
SCOD (mg/L)	101	82	135	553	259
Nitrate (mg/L)	1.2	0.6	0.5	1.5	1.4
Nitrite (mg/L)	2	3	27	10	4
Ammonia (mg/L)	0.86	ND	20.4	ND	ND

Table 2.3. Water quality parameters for real greywater. ND indicates 'not detected' - the analysis produced results below the range of detection of the technique.

Optical Characterization

Attenuation of the five greywater varieties across the UV-Vis-NIR range (Fig. 2.2) indicates roughly similar attenuation of UV light by Fenner, Surendran, and RGW. Surendran+ exhibits substantially higher attenuation, and a substantially different absorbance drop-off with increasing wavelength – the formulation absorbs much higher than RGW and other formulations well into the visible wavelength range. Hourlier shows significantly less attenuation.

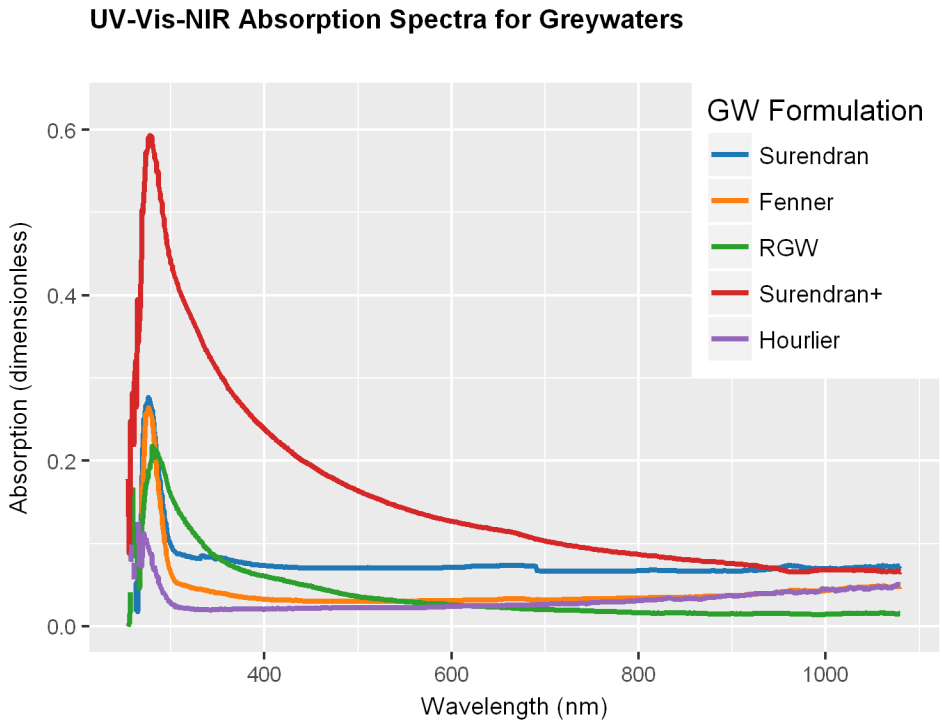

Figure 2.2. UV-Vis-NIR Absorption for synthetic and real greywaters.

Next, to quantify the intensity of COD relationship to attenuation in each sample, attenuation results were normalized by both COD (Fig. 2.3) and SCOD (Fig. 2.4). In these plots, it is apparent that Surendran, Fenner, and Surendran+ all exhibit similar COD attenutation intensities. Real greywater and Hourlier have substantially lower attenuation intensities. For SCOD attenuation intensity, these trends largely stay the same, but with more dispersion between Surendran, Fenner, and Surendran+.

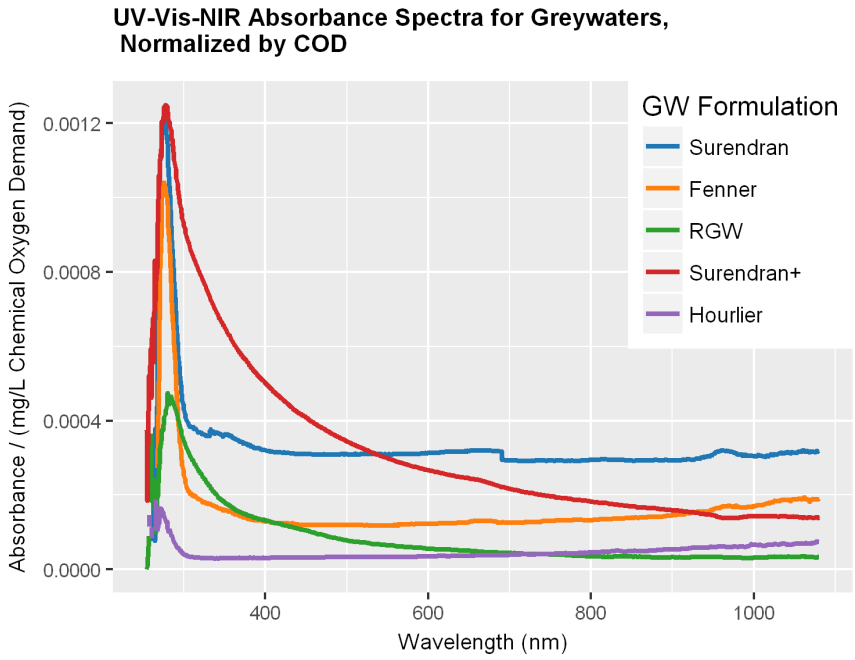

Figure 2.3. UV-Vis-NIR Absorption, normalized by chemical oxygen demand.

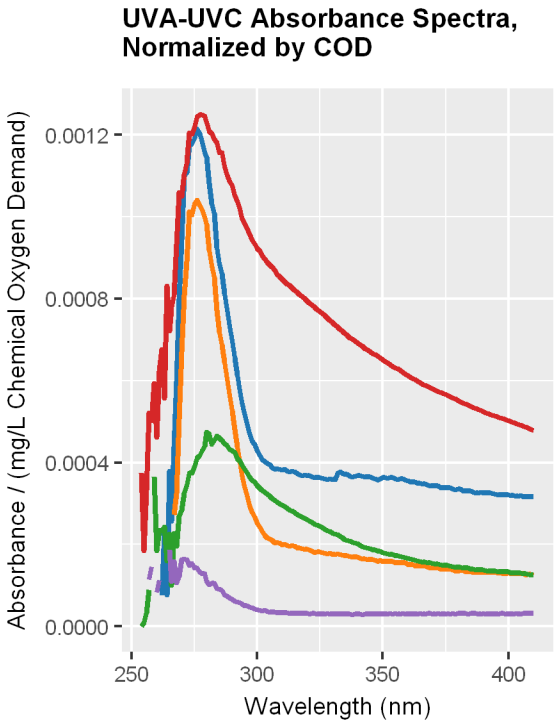

Figure 2.4. Enlargement of UVA-UVC region from Figure 2.3.

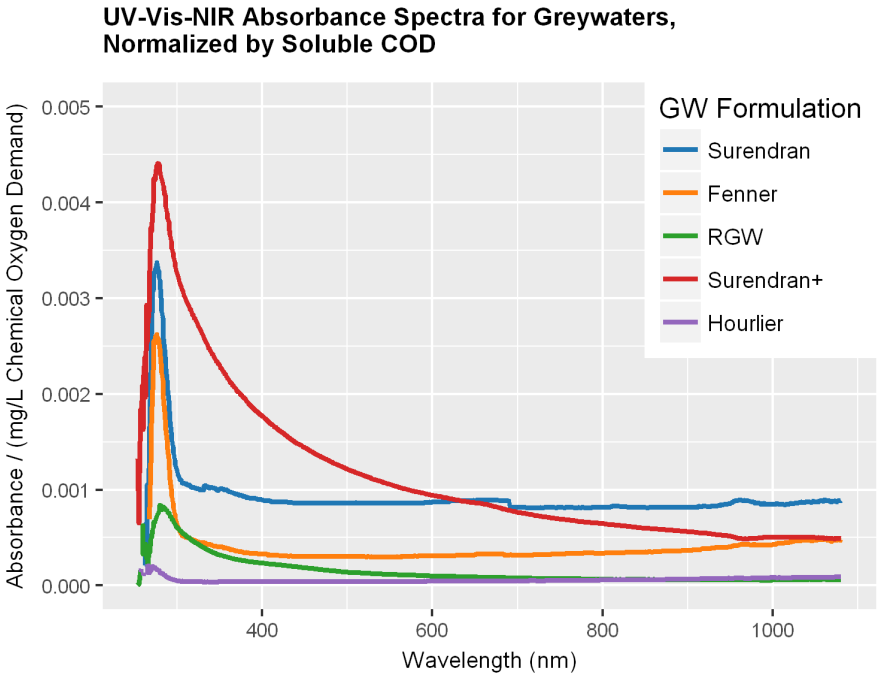

Figure 2.5. UV-Vis-NIR Absorption, normalized by soluble COD.

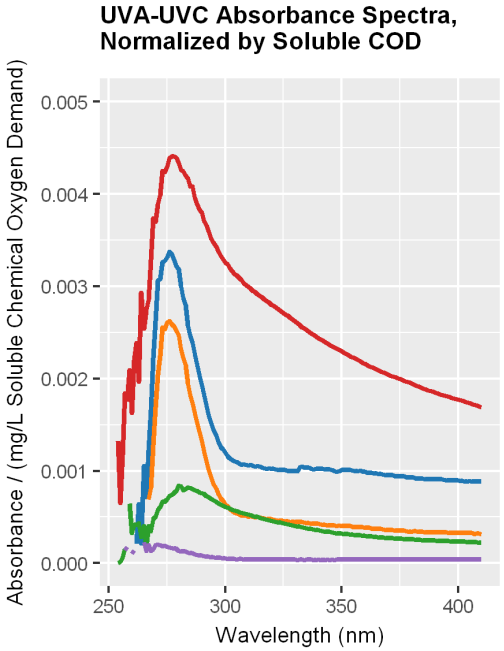

Figure 2.6. Enlargement of UVA-UVC region from Figure 2.3.

While the Fenner, Surendran, and RGW may diverge in terms of COD attenuation intensity, their overall attenuation remains quite similar. Examining these waters' attenuation in the UV range, where they exhibit peak attenuation and where the action spectra of UV-based treatment processes lie, reveals significant overlap between the three formulations. While Surendran and Fenner attenuate UV more heavily in the UVC region, < 280 nm, RGW attenuates more heavily in the UVA-UVB regions. Integrating the attenuation vs. wavelength curves indicate that while Surendran and RGW have similar UV-range integrated attenuations, Fenner attenuates substantially less over the UV range.

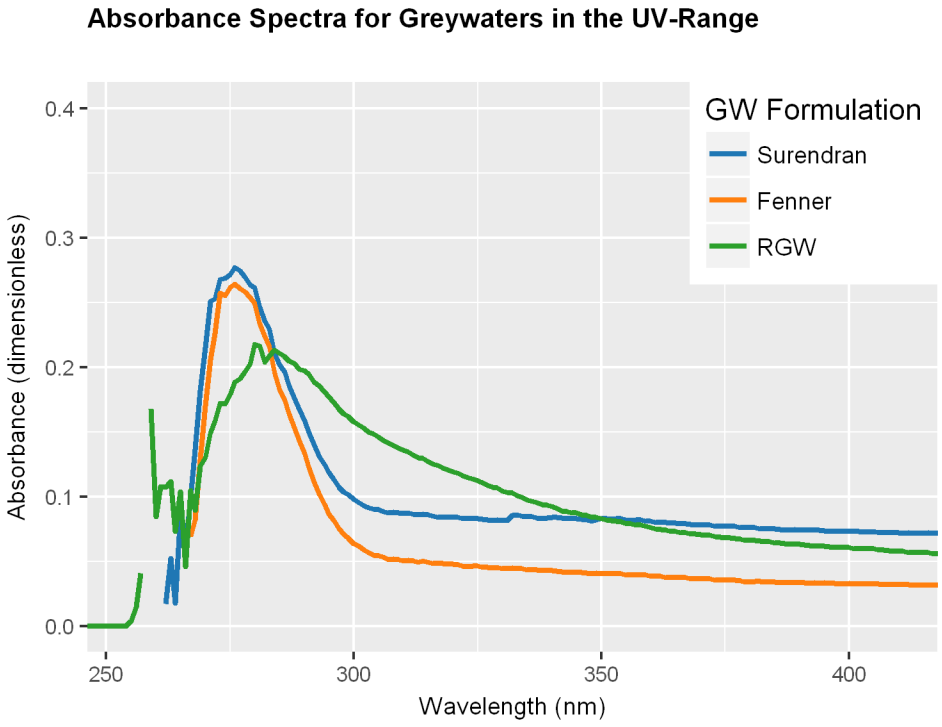

Figure 2.7. Absorbance of Surendran, Fenner, and Real Greywaters in the UV region (254nm – 410nm). A measurement discontinuity was repeatedly observed at the 254nm wavelength for the RGW sample.

2.4 Discussion

Just as various greywaters exhibit a wide range of water quality parameters, so do synthetic recipes exhibit a large range of attenuation profiles. Significantly, as samples are filtered before spectra are analyzed, the difference between Surendran and Surendran+ suggest that a small quantity of chemicals can apparently have a dramatic impact on the attenuation of various waters. If a further round of verifications confirms this, representative attenuation profiles cannot forgo inclusion of microbiological contributors (e.g., septic effluent).

The SCOD attenuation intensity plot indicates how challenging a realistic synthetic water matrix formulation will be. While in terms of attenuation only, Fenner and Surendran represent RGW attenuation in the UV range somewhat well, they do so with far less SCOD; in fact, their SCOD attenuation intensities are more than 2.5 and 3 times higher than RGW's, respectively. This indicates that the SCOD present in RGW is less highly scattering and absorbing than those found in existing synthetic greywater recipes, or, that inorganic substances play a key role in the optical attenuation of greywaters.

Regardless of the underlying drivers, a closer examination of the Fenner and Surendran formulations for candidacy as an optically realistic greywater is warranted. Based on the integration of attenuation over the wavelength range studied, Surendran's formulation presents a much closer analogue to RGW in the UV range, which is the crucial range of interest for treatment processes. Thus, Surendran's formulation is a strong point of departure for further development of synthetic greywater formulations. Future iterations should seek to increase COD content while minimizing changes to its UV attenuation profile.

It is important to note, however, that RGW varies widely in composition and over time. Significant follow-on work must be done to understand how optical attenuation can vary between samples of RGW, across different RGW sources, across seasons, and throughout the day.

2.5 Conclusions

Leading formulations of synthetic greywater were collected from literature and recreated, along with real domestic "light" greywater generated by 48 volunteers in a modified sink setup. COD, soluble COD, Nitrate/nitrite/ammonia, and optical attenuation of all waters were studied to determine which synthetic matrices could best model RGW both chemically and optically.

While no synthetic formulation accurately represented RGW in terms of optical attenuation, Surendran's formulation followed it closely. One caveat is the significant divergence in overall COD and SCOD attenuation intensity between Surendran and RGW.

These results indicate that further study into nature of optical attenuation in greywater is warranted. This has two implications. First, optical attenuation introduces a new parameter to be modeled by future synthetic greywater recipes. An investigation into the variation of optical attenuation across RGW sources and times could inform a model of RGW composition and optical properties, which in turn could help optimize water treatment technologies. Second, the specific mechanism of attenuation in greywaters – whether absorbance or scattering – must be elucidated for integration into optical simulation approaches, whether with analytic optics or raytracing. Thus, incorporating knowledge of greywater's optical properties from process technology and simulation perspectives promises to a path to the most effective and energy-efficient light-dependent greywater treatment processes.

3. Solar Photocatalysis on an Inclined Plate

3.1 Introduction

Providing a safe, sustainable water supply is a crucial challenge of the 21st century, and it is a challenge exacerbated by pollution, climate change, and population growth [69]. A key opportunity to surmounting this challenge lies in technologies that facilitate the re-use of wastewater and treatment of emerging contaminants and micropoullutants in wastewater at low energy intensity [70]. While many technologies such as nanofiltration menbranes [71], membrane bioreactors and full advanced treatment trains [72] promise some of these benefits, the opportunity to reduce electrical energy demand across all water treatment operations remains substantial [73].

As a follow-on step to well-characterized primary (physical-sedimentation) and secondary (biological) treatment processes, heterogeneous semiconductor photocatalysis using titanium dioxide and solar ultraviolet (UV) light holds great promise as a low-energy tertiary 'polishing' treatment process to target recalcitrant pollutants in wastewater [74]. Semiconductor photocatalysis is the absorption of photons at sufficient energy by a semiconductor material, exciting an electron to the conduction band and leaving a positively-charged "hole" in the valence band [75]. The electron and hole may recombine or migrate to the semiconductor surface, where they are available to drive oxidative and reductive reactions with species adsorbed on the surface [76]. In aqueous systems, one outcome of these surface reactions is the production of reactive oxygen species (ROS) [77], including the hydroxyl radical OH^o, a powerful oxidizing agent that is the basis of many advanced oxidation processes (AOPs) in water treatment [78], [79]. Brief equations describing one reaction mechanism underlying OH^o generation via TiO_2 photocatalysis by a photon with energy *hv* in an aqueous system are shown below, adapted from Hermann [75].

$$hv + TiO_2 \rightarrow e^- + p^+ \tag{3.1}$$

$$\left(H_2O \leftrightarrow H^+ + OH^-\right) + p^+ \rightarrow H^+ + OH^o \tag{3.2}$$

Since the discovery of semiconductor photocatalysis via titanium dioxide (TiO_2) in 1972 [80], and the first demonstration of its use to oxidize cyanide ion in contaminated ponds [81], the process has attracted substantial interest from the environmental remediation and water treatment research communities (Fig. 3.1). As the 3.2 eV bandgap of anatase-form TiO_2 requires photoexcitation by light of wavelength 387 nm or less [82], significant research has been dedicated to both the design of photocatalytic treatment processes under UV lamps [83] and more recently UV LEDs [84]–[86], and the

development of materials and fabrication processes to reduce the bandgap energy of semiconductor photocatalysts [87], [88]. However, while promising high treatment effectiveness, these approaches are constrained by potentially high operating costs of operating artificial illumination [89] and the stability, durability, and reproducibility of novel photocatalysts [90]–[92], respectively. It is important to note, however, that all of these limitations are the focus of active research.

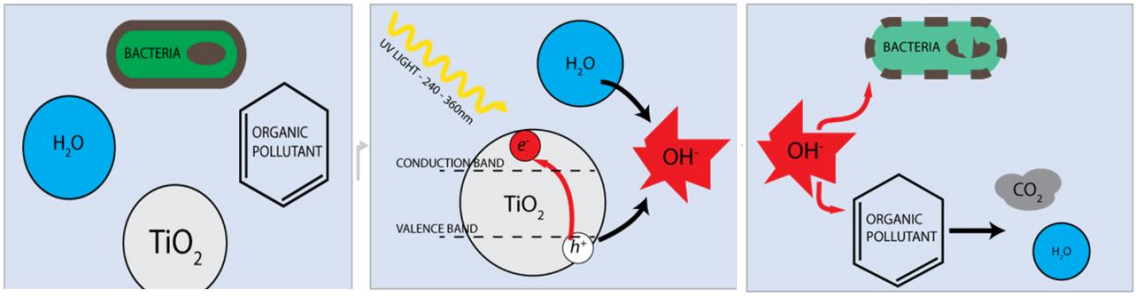

Figure 3.1. Schematic of TiO_2 photocatalytic degradation of water pollutants and pathogens.

UV light represents 4% of incident sunlight on earth, making solar photocatalysis with unmodified TiO_2 possible. Solar photocatalytic water treatment has accordingly attracted a range of reactor designs which have been characterized in a number of studies, from the laboratory to pilot scales [93]. Solar photocatalytic reactors must balance the need for high irradiance in the reactor to drive the reaction and the need for good mass transfer and adsorption onto the catalyst surface [93], [94]. Such constraints have led the majority of solar photocatalytic reactor research to converge on three reactor designs: the parabolic trough collector (PTC); the compound parabolic collector (CPC); and the inclined plate collector (IPC), also knowing as the non-concentrating collector (NCC) or thin-film fixed-bed reactor (TFFBR) [93]–[95].

PTC designs are a direct adoption from the field of solar thermal engineering, where they have found commercial application since the 1970s [96], and have more recently been explored as a photocatalytic reactor platform [97]. While PTC promise high solar concentration ratios, easily achieving 90-sun concentration, the design can only accept direct sunlight [98], thus requiring single- or dual-axis tracking systems; even with advanced tracking, the systems do not function at all in diffuse light (e.g., cloudy) conditions [99]. This is especially pertinent for two reasons. First, many geographies have significantly more diffuse light than direct [100], and second, crucially for photocatalytic applications, ~70% of UV light incident on Earth's surface is present as diffuse light, with an increasing proportion represented as diffuse light at higher-energy wavelengths [101].

In contrast, the CPC design accepts diffuse light and obviates the need for active tracking [102]. While its concentration is much lower than that offered by PTC's, the delivered

irradiance to the reaction zone is typically beyond the saturation limit of the photocatalytic reaction [103] . Owing to these properties, CPC's have been widely studied as platforms for photocatalytic applications [104], [105]. However, published designs of PTC and CPC systems typically use suspensions of TiO_2 nanoparticles for successful operation, requiring post-treatment separation [83]. While separation of TiO_2 nanoparticles has been demonstrated, the cost [106] and reliability [107], [108] of this separation at scale remain an open question, and is particularly pertinent owing to concerns about the effects of TiO_2 nanoparticles on human and ecological health [109].

The IPC configuration offers a simple method of capturing diffuse light with non-concentrating optics, and can accommodate immobilized photocatalyst rather than suspensions. To examine the general field of IPC designs, I consider reactors featuring both suspended and immobilized photocatalyst. Several reports have characterized IPC performance in destroying organic pollutants such as phenolic compounds [110], pesticides [111], textile and dye wastewaters [112], [113], and agricultural processing wastes [114], among other compounds. Across all studies, a clear, nearly linear, relationship between UV light intensity and reaction performance has been repeatedly demonstrated [115] [116] [117], as would be anticipated from photocatalytic reaction engineering theory given the UV photon flux range in sunlight [75]. Accordingly, several studies define the optimal incline plate angle to be parallel to the local latitude [110], [111] to maximize sunlight capture.

However, other studies conducted analysis at other incline angles [118], arguing that mass transfer considerations related to flow regime and flow film thickness must be considered in reactor performance. These reports can be contradictory, however; one report suggested that shallower angles, and thus, longer hydraulic residence times (HRT) yielded more effective treatment [119] , while another suggested that steeper angles were superior [112]. One of the few systematic studies, from Zou et al., on the influence of angle and flow rate on treatment performance studied a suspended nanoparticle IPC configuration, and reported that a peak reaction rate was discovered at a film thickness of 1.0 mm [120]. In Zou's work, however, purely UV light was used, and lamps remained normal to the IPC surface, regardless of incline orientation. This setup poorly represents solar operating conditions with systems lacking active tracking mechanisms, however, as deviation of IPC angle from the solar angle will lead to a tradeoff between irradiance and mass transfer. While Zou's work reports relatively thin flow films, it uses suspended nanoparticles, which will behave differently than a fixed photocatalyst configuration. Both Zou's study and the work of Wyness et al. [115] examined flows with Reynolds numbers in the range of 350 – 3000. Studies of mass transfer effects in an immobilized-photocatalyst spinning disk reactor illuminated by UV light found no consistent relationship between Reynolds number or film height and the overall photocatalytic reaction rate, as measured by decolorization of methylene blue and degradation of dihydroabietic acid [121], [122].

In this work, I offer a detailed analysis of the relationship between hydrodynamic parameters inherent to the IPC, solar illumination, and reaction rate for immobilized TiO_2 systems. Using a bench-scale fixed-catalyst IPC with multiple tracks under artificial solar illumination, I study the decolorization of methylene blue at Re from ~40 to ~750, and model pseudo first order decolorization rates. The implications for IPC operation in large-scale systems, and the potential operational instructions that these results suggest, are discussed.

3.2 Materials and Methods

IPC Design and Experimental Set-up

Two generations of IPC systems were fabricated, both following roughly the same system architecture. TiO_2-coated glass slides as per the procedure developed in the following section were mounted on a CNC-milled aluminum track. An acrylic stand with pre-defined angle guides was designed and fabricated with a lasercutter (Universal Laser Systems). A variable-drive peristaltic pump (ColePalmer MasterFlex) drove methylene blue solution from a continuously stirred reservoir into a flow distributor, from which it was delivered onto the TiO_2-coated surface (Fig. 3.2). Liquid flowed down the surface and was collected through custom-designed funnels, where it was pumped back into the reservoir. For the first-generation IPC design, which included two separate tracks, the photocatalyst surface on each track measured 75 mm x 150 mm per track. In order to maximize frequency and flexibility of experiments, and ensure even liquid film coverage of the photocatalyst surface, a second-generation design with four separate tracks was constructed, featuring a photocatalyst surface measuring 25mm x 225mm per track.

The light source used was a xenon-arc lamp with daylight filter (Atlas SunTest XLS+), designed to model the AM1.5 solar spectrum. Lamp power output was manually varied, and incident irradiation spectra on the IPC surface were measured using a spectradiometer (Stellarnet SpectraWiz EPP2000) with UV-Vis-NIR wavelength sensitivity (280 – 1180 nm). These measurements reported both total irradiance and wavelength-specific irradiance.

To calculate UV-irradiance-normalized reaction rates, total UV power was calculated by first measuring the irradiance at three positions along the long axis of each track in the IPC, for each combination of IPC angle and lamp irradiance. These results were integrated in the UV wavelength range to produce a total UV power incident on the photocatalyst area.

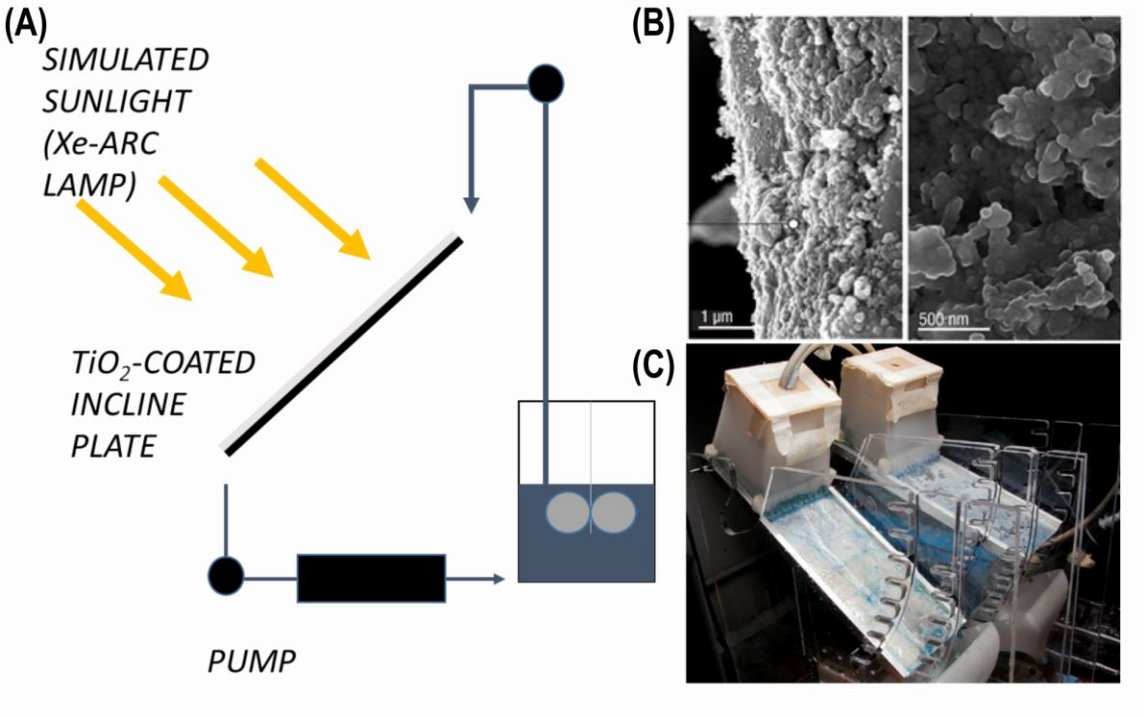

Figure 3.2. Experimental Setup for IPC Photocatalytic experiments. The system setup **(a)** includes a continuously stirred tank of Methylene Blue, driven by a peristaltic pump. SEM micrograph of photocatalyst surface **(b)** and first-generation IPC system photograph **(c).**

Photocatalyst Preparation and Immobilization

Preparation and immobilization of TiO_2 photocatalyst followed a nanopowder-modified alkoxide sol-gel process reported by Balasubramanian et al. [123], chosen for its generation of resilient and thick photocatalyst films. As indicated, a dip-coating procedure was used to immobilize film of consistent photocatalyst on substrates.

All reagents listed were purchased from SigmaAldrich. Briefly, a 0.5 M solution of titanitum tetraisopropoxide (TTIP) in isopropanol (iPrOH) was prepared, and diethanolamine was added to yield a molar ratio of DEA:TTIP of 1:4. After vigorous magnetic stirring, deionized water was added, dropwise, to reach a molar ratio of H_2O:TTIP of 2:1. After the solution was completely mixed, 30g/L titanium dioxide nanopowder (Evonik Degussa P-25) was slowly added to create a highly viscous sol-gel.

Quartz glass substrates at 50mm x 75mm (IPC first generation) or 25mm x 75mm (IPC second generation) (Fisher Scientific) were spray-cleaned with 30% isopropanol (iPrOH) in water and allowed to air-dry. Using a modified 3D Printer, glass substrates were fixtured to a gantry and submerged in the prepared sol-gel. The substrates were extracted

at a rate of 1 mm/s, and promptly dried at 130° C for 30 minutes. Substrates were removed from the oven and returned to room temperature, and were processed through one more dip-coating cycle. Following another drying cycle at 130° C, substrates were calcinated at 550° C for 1 hour, and allowed to cool naturally for 16 hours. Glass substrates were mounted in a fixture and ultrasonicated in a bath of deionized water at 20kHz for 30 minutes, to release any unbound catalyst. Substrates were air-dried and mounted in the IPC system using a water-tight sealant.

Experimental Protocol

Methylene Blue (Sigma Aldrich) was dissolved in sufficient deionized water to produce a 20 micromolar solution and was continuously stirred. 200mL of methylene blue (MB) solution was collected in stirred reservoirs, and continuously stirred throughout the reaction period. Upon the start of the reaction period, the pump was turned on, beginning the flow of MB from the reservoir into the holding tank. At each sample interval, triplicate 3.5mL samples were pipetted from each reservoir and analyzed using a spectrophotometer (HACH DR2000) at absorbance peak 665nm. Absorbance was recorded, and samples returned to the respective reservoir. The system was run for a 60-minute dark period, to dissociate the effect of dye adsorption from photocatalytic dye degradation during the experiment. Following the dark experiment, the lamp was turned on, and samples were taken at 15-minute intervals for a total reaction period of 2-hours.

Flow rate in first-generation experiments was varied between 45 mL/min and 130 mL/min. During second-generation experiments, flowrate was varied between 50 mL/min and 1000 mL/min. Angle of inclination was varied between 5 degrees and 40 degrees, measured from the horizontal, in both experiments.

Following an experiment, 1L of deionized water was pumped through the system, to remove any residual dye from the system or catalyst surface.

Using the second-generation experimental platform, a total of 14 trials across four reactors were conducted, plus three controls featuring dark conditions or no photocatalyst.

3.3 Results and Discussion

Reaction Kinetics and Order

Many studies indicate that photocatalytic reactor performance can be characterized by Langmuir-Hinshelwood kinetics, owing to the reliance of photocatalytic oxidation on surface adsorption [124], as defined by:

$$r = k\left(\frac{KC}{1+KC}\right) \tag{3.2}$$

Where k is the true rate constant, K is the equilibrium constant of adsorption, and C is the instantaneous reactant concentration, in this case, methylene blue. The Langmuirian

model can be extended to incorporate light intensity and other parameters as well. However, for dilute solutions, with C < 10^{-3} M, the Langmuirian expression reduces to apparent first order behavior as *KC* << 1:

$$r = kKC \tag{3.3}$$

$$r = k'C \tag{3.4}$$

With pseudo-first-order reaction constant *k'* [75]. For conditions where the reactant completely covers the adsorbing surface owing to high concentration, *KC* in the original Langmuir expression becomes >> 1, and apparent zero order behavior is observed:

$$r = k \tag{3.5}$$

With *k* representing the pseudo-zero-order reaction rate constant [125], [126]. Considering the widely-discussed linear dependence of photocatalytic reaction rate on incident UV light intensity in the irradiance intensity range of sunlight, a light-normalized reaction rate can be developed:

$$r_I = \frac{k}{I} \tag{3.6}$$

With *I* the UV irradiance in W/m^2.

In an IPC system, both first- and zero-order results have been reported. Given the specified experimental parameters, with reactant concentration on the order of 10^{-5}, pseudo-first-order reaction kinetics were hypothesized. A small number of reports [127], [128] reported second-order kinetics for photocatalytic dye degradation, but offered little mechanistic insight into why this was the case, although other sources suggest this could be driven by charge carrier recombination within TiO_2, which has been demonstrated to be a second-order process [126]. Higher reaction orders have been reported, but also lack any mechanistic basis. While attempts to model similar systems as plug-flow reactors across the area of the photocatalyst surface have been reported [129], since the presented system operates with recirculation to a continuously-stirred reservoir, I model it with a bulk reaction rate.

To verify the reaction kinetics model of the IPC experiments, a comparison between zero-, first-, and second-order kinetics was performed. Experimental data were fit using linearized least-squares regression for each kinetic model, indicating that the data, as expected, most strongly fit first-order kinetics (Fig. 3.2). Because modeling results indicate many reactions nearly fit zero-order behavior, it is possible that the TiO_2 surface becomes saturated over subsequent runs, despite the washing/desorption step post-

experiment, perhaps behaving as a pseudo-zero-order system. However, as observed in Fig. 3.2(a), there is an observable, systematic deviation from zero order behavior that tends towards first-order kinetics, suggesting that first order kinetics are more appropriate for this experiment.

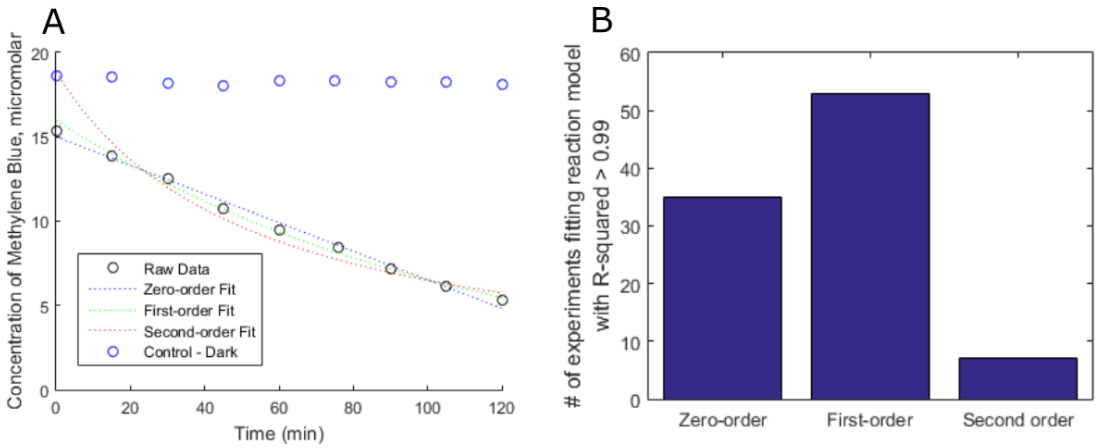

Figure 3.3. Example Kinetics from Second Generation IPC Performance (a), which indicate good fits to zero- and first-order reaction models. However, data analysis across all experimental results **(b)** indicated that 53 out of 56 experiments fit pseudo-first-order kinetics with an R^2-value of > 0.99, compared to 35 > 0.99 R^2 correlations for pseudo-zero-order kinetics.

Hydrodynamic Modeling

For flow over an infinite incline plate, the relationship between film thickness *h* and volumetric flow rate *Q* can be written as follows [130]s:

$$h = \left(\frac{3\upsilon Q}{gW sin(\alpha)}\right)^{\frac{1}{3}} \tag{3.7}$$

With acceleration of gravity *g*, kinematic viscosity υ, width of plate *W*, and inclination angle from the horizontal α. This expression, developed from the Nusselt formulation, does not account for the presence of rivulets and waves on the surface of a flow film, which are clearly present; it accounts for a completely laminar, still surface. Significant research combining theory and experiment to understand the relationship between flow regime and film thickness in inclined plate flow has been published; Yu's work [131] established an empirical correlation for inclined plate systems that accounts for the experimentally-observed over-prediction of film thickness by the Nusselt relationship:

$$h = (0.462 * Re^{0.422})\left(\frac{\upsilon^2}{g\ sin(\alpha)}\right)^{\frac{1}{3}} \tag{3.8}$$

for Reynolds numbers between 80 and 900, with *Re,* the Reynolds number, defined by

$$Re = \frac{uL}{v} \tag{3.9}$$

with *L* the characteristic length of the system. In the case of the inclined plate, *L* is the film thickness. As Yu's expression relies on the Reynolds number, it cannot be adopted here for use, as the film thickness was not directly measured; the Nusselt expression will be employed for calculating film height. It is important to note that reports on inclined plate photocatalytic reaction systems that measure film thickness do so by measuring the 'volume remaining in the reactor' and averaging the film height across the plate area [115], [120]. This method produced film thicknesses up to an order of magnitude larger than predicted by Yu's model, which is developed from real-time imaging and software analysis. This suggests that either the volume-remaining method is insufficient to describe film height, or that Yu's model does not describe the specific conditions of those experiments. Thus, the Nusselt film thickness used in subsequent analysis in this work is viewed as a likely over-prediction of actual film thickness, as described previously.

Hydraulic residence time, HRT, is defined as:

$$HRT = \frac{L_x}{u_x} \tag{3.10}$$

With u_x defined from the Nusselt velocity as:

$$u_x = \frac{g \sin\alpha \, h^2}{3v} \tag{3.11}$$

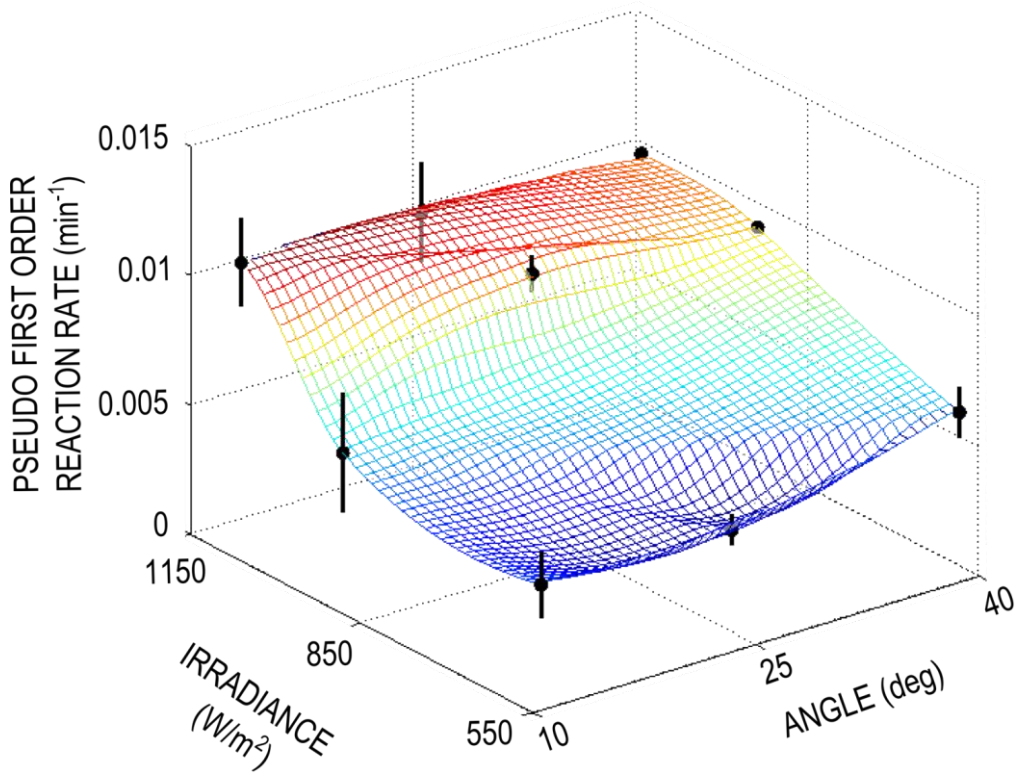

Figure 3.4. Dependence of the IPC first generation on light intensity and angle. Error bars indicate the standard deviation between reaction rate results for the combination of parameters at that data point.

Experimental Results – First Generation Experiments

First generation experiments, using low flow rates representing Re from 15 to 43, and examining irradiance from 550 W/m^2 to 1150 W/m^2 were performed. As expected, these results indicated strong dependence, although not clearly linear dependence, of pseudo-first-order reaction rate on irradiance (Fig. 3.4). There was apparently minimal dependence of reaction rate on hydrodynamic conditions. Changing flow rate and angle had an apparently inconclusive effect on reaction rate (Fig. 3.5); accordingly, film thickness as per Eq, 3.6 reveals no conclusive relationship to reaction rate across the range of variables studied (Fig. 3.6). The results reported in Fig. 3.4, 3.5, and 3.6 are thus effectively decoupled from mass transfer considerations, and therefore do not convincingly address the fundamental question of this chapter: understanding the relationship between mass transfer, hydrodynamics, light capture, and reaction rate, governed by reactor hydraulics and design parameters.

The limited range of Re studied, along with the relative inconclusiveness of the results of the hydrodynamic experiments, motivated the second-generation experiments.

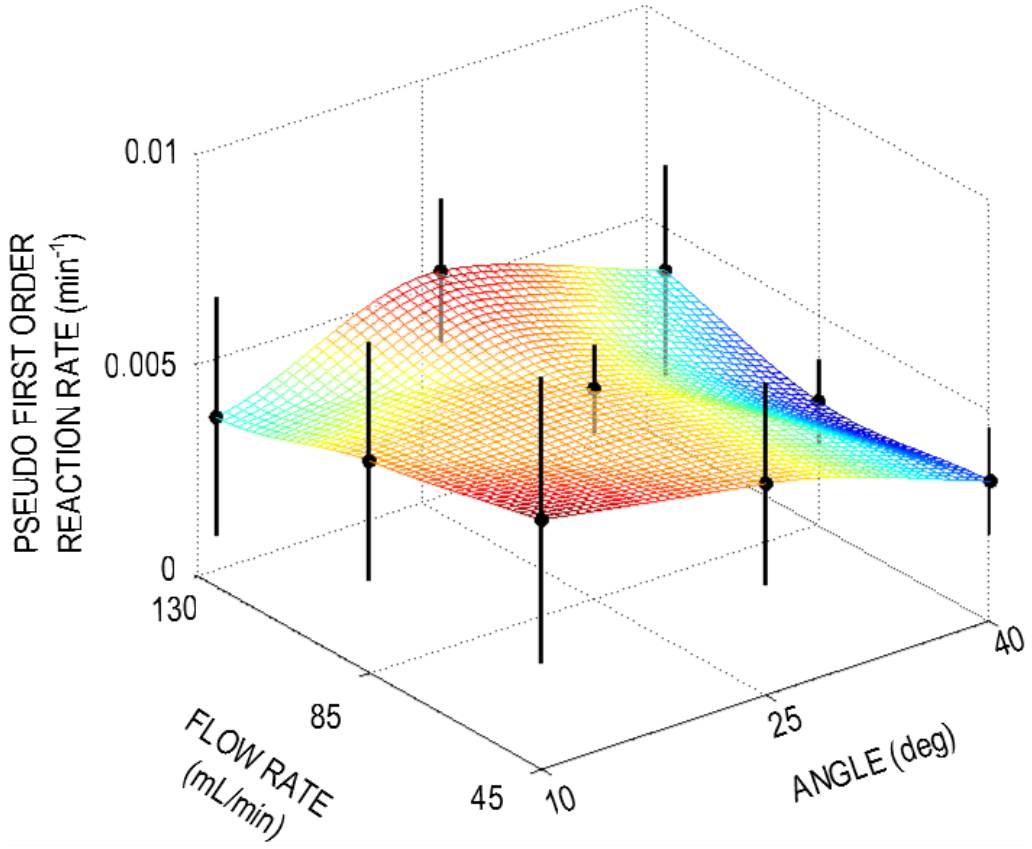

Figure 3.5. Relationship between mass-transfer parameters and reaction in IPC first generation. Error bars indicate the standard deviation between reaction rate results for the combination of parameters at that data point. Substantial error bars on all points support data from Fig. 3.4, indicating that trends across hydrodynamic parameters like angle and flow rate are overshadowed by irradiance.

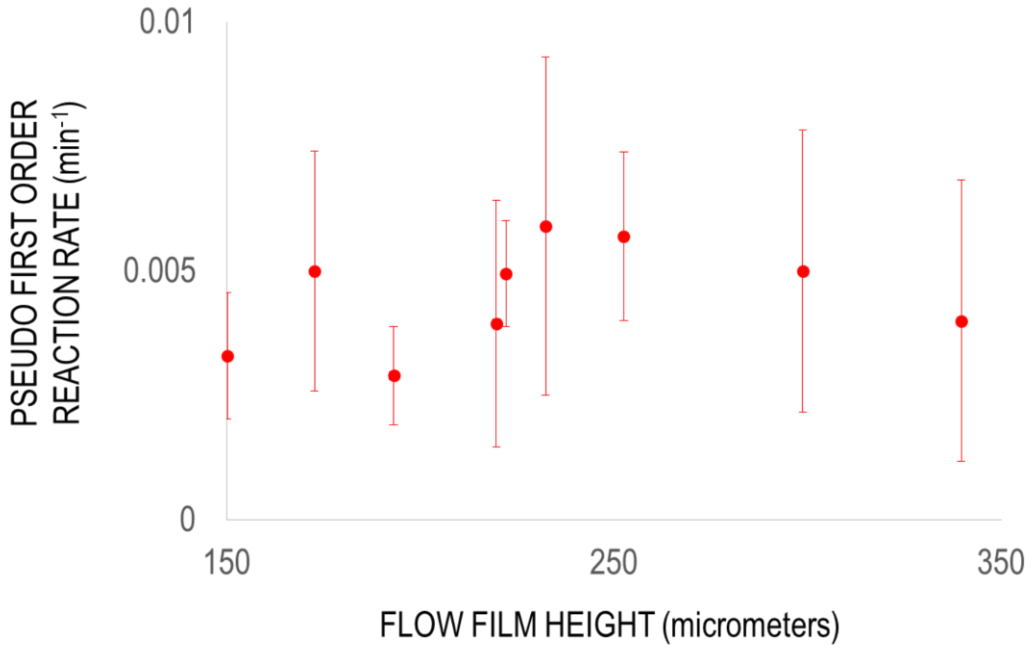

Figure 3.6. Relationship between Nusselt film thickness (analytically calculated) and pseudo-first-order reaction rate. Error bars indicate the standard deviation between reaction rate results for the combination of parameters at that data point.

Experimental Results – Second Generation Experiments

By utilizing a wider range of flowrates, the second generation experiments investigated a larger range of hydrodynamic conditions, with Re varying from ~30 to ~750. Film thickness was analytically calculated to range between 0.2 and 1.3 mm, and HRT on the photocatalyst surface ranged between 0.1 and 2.1 s. For ease of visualization and clearer understanding of trends, results (Fig. 3.7) were plotted with Re rounded to the nearest integer value, film thickness rounded to the nearest m x 10^{-4} (tenth of a mm), and HRT rounded to the nearest s x 10^{-1} (tenth of a second).

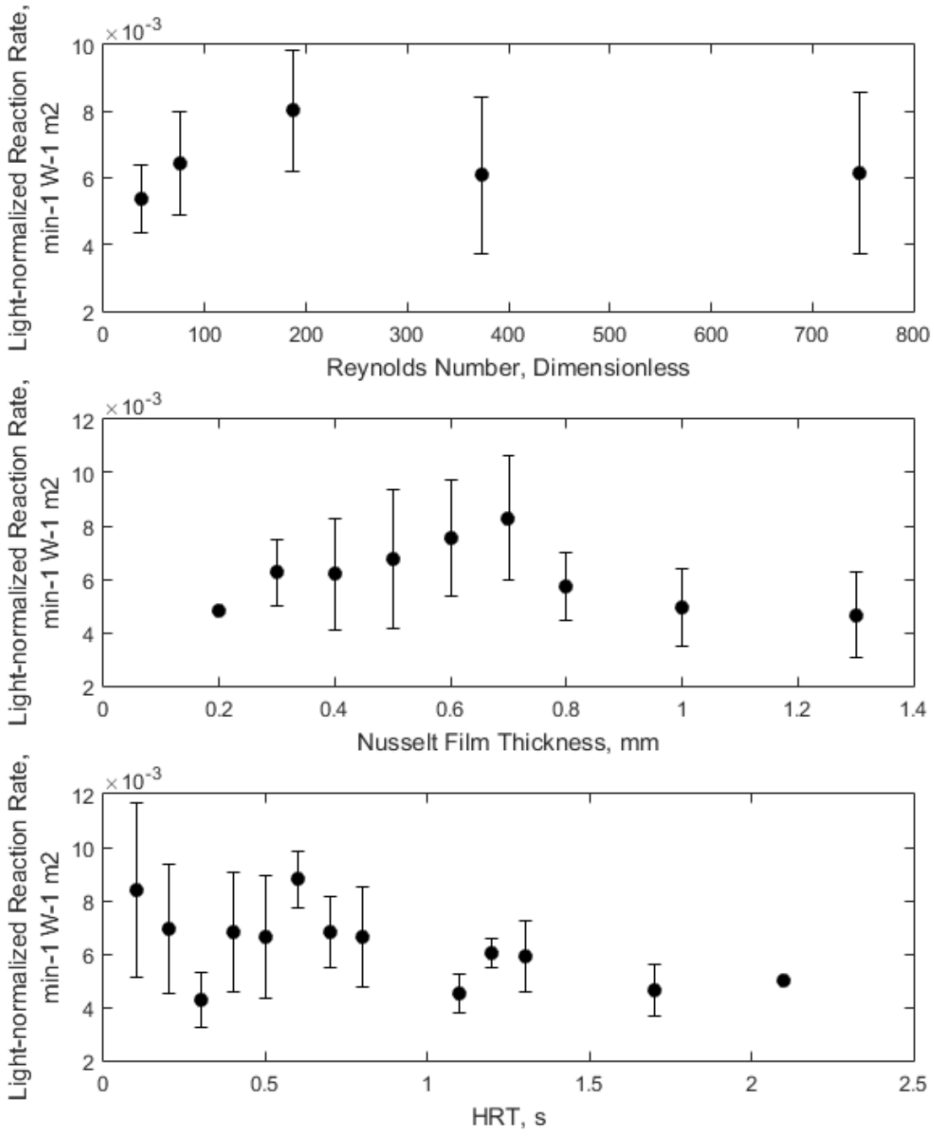

Figure 3.7. Light-normalized reaction rates as a function of hydrodynamic parameters: Reynolds number (top), analytically calculated (Nusselt) film thickness (middle), and Hydraulic Residence Time on plate surface (bottom).

Reaction rate is observed to peak at Re = 200, although experimental error limits confidence in this conclusion. Similarly, a peak in reaction rate at a calculated film thickness of roughly 0.7 mm is apparent as well, again with significant error. Both of these results are somewhat surprising, as previous reports from Boiarkina for an immobilized TiO_2 spinning disk reactor strongly suggest a decreasing reaction rate with increasing film thickness [129]. Zou et al. report a peak reaction rate at a film thickness

of 1.4 mm, although it is unclear what Re or hydrodynamic conditions this corresponds to. Zou's results also suggest that reaction rate increases with flow rate at an angle of 20 degrees, until a system flow rate of ~1000 L/h, equivalent to a Re of 1160, after which reaction rate no longer increases with flow rate [120]. Zou's work, however, relies on suspended catalyst, and thus embodies different mass transfer constraints. The peak at Re = 200 is near the transition from a wavy flow regime to a turbulent flow regime, which has been reported to be at Re = 250 [132].

To clarify underlying mechanisms of the reaction rate peak identified at 0.7 mm thickness, an open question lies in whether the IPC becomes photon-flux constrained owing to absorption through the thickness of flowing film layer. Absorption is governed by the Beer Lambert Law:

$$\log(\frac{I_o}{I}) = \varepsilon LC \tag{3.12}$$

with ε the extinction coefficient of the compound, in this case methylene blue dissolved in water; L the path length, in this case, the film thickness; C the concentration of methylene blue; I the intensity exiting the absorption zone, and I_o the incident intensity. Note that the Beer-Lambert Law accounts only for molecular absorption, and attenuation through other means, e.g. scatter off of the film surface, will not be accounted for. While methylene blue exhibits high molar extinction coefficients in the UVC and short-wavelength UVB range, these wavelengths represent a small fraction of the UV present in sunlight. UVA represents a greater fraction of incident solar UV, and methylene blue absorbs up to an order of magnitude less light intensity in these wavelengths. Accordingly, even using a high molar extinction coefficient of 10000 $M^{-1}cm^{-1}$, the difference light intensity passing through a film of 1mm thickness versus a film of 0.7mm is less than 2%, which cannot account for the observed decrease in reaction rate evident above.

Another possible inhibition attributable to film thickness is the availability of oxygen at the catalyst surface to act as an electron scavenger. In the case of thin-film flows, this proved difficult to measure. Dissolved oxygen is well-known to influence the photocatalytic reaction rate, and previous studies on the diffusion of oxygen through laminar flows on an incline plate indicate that reactive surfaces on inclined plates, such as biofilms, can be oxygen-starved if flows are not sufficiently aerated [133]. Instituting surface roughness or moving into a turbulent flow regime, could also potentially increase oxygen transfer to the surface [134], but with the added risk of creating further 3-D instabilities (see below). Thus, further work will involve modeling of gas transfer from the liquid flow surface to the photocatalytic reaction site, and the relationship between oxygen transfer and surface instability. The influence of this parameter on IPC performance would partially explain the differences between the experimental results reported here and Zou's work, which were collected using an IPC with TiO_2 slurry. It is expected, however, that given the recirculatory nature of the experimental design, and the

unobstructed exposure of the entire reaction zone to atmosphere, it is highly unlikely that oxygen starvation is a key determinant of reaction performance in the reported IPC results.

The peak reaction rate was detected at Re ~200. This does not coincide exactly with a transition to turbulence, reported at Re = 250, although as described previously, it approaches it [132]. As observed, Re = 200 is well within the range of surface instabilities, e.g. solitary and periodic waves [131]. Such instabilities have been reported as either enhancing or inhibiting mass transfer, depending on the dimensional nature of the surface waves generated from instabilities (2- or 3-D) [121]. Thus, it is possible that increasing Re beyond 200 moves the hydrodynamic behavior into instabilities that serve to inhibit mass transfer, rather than promote it. Follow-up studies to examine the specific characteristics of emergent instabilities, and their correspondence to flows characterized by different Reynolds numbers, will be necessary to elucidate the mechanisms behind the unexpected relationship between hydrodynamic behavior and reaction rate. Furthermore, additional study into the potential inhibition of reaction rate by the onset of turbulent flow conditions, whether due to mass transfer, surface instabilities, or other phenomena, is needed.

Reaction rate is shown to decline with HRT on the incline plate surface, although the correlation for a linear fit was very weak, at $R^2 = 0.32$, and thus not shown on the graph. Longer residence times mean thicker films for a given Re, so it is expected that the same mechanisms that define lower reaction rates at higher film thicknesses explain the lower reaction rates observed at high HRT. Previous work examining microfluidic photocatalytic reactors has suggested that longer residence times lead to more oxygen starvation of a reaction system [135]. If oxygen availability governs the reaction rate in the IPC system then, this would explain the trends observed.

To understand the broader implications of these results for mass transfer in photocatalytic IPC reactors, an expression to separate the observed reaction rate into an intrinsic and a mass-transfer contribution component can be used [136]:

$$\frac{1}{k^*} = \frac{1}{kK} + \frac{1}{k_m \alpha_v} \tag{3.13}$$

With k^* the observed reaction rate, k the intrinsic maximum reaction rate, K the Langmuir adsorption coefficient, k_m the mass transfer coefficient, and α_v the ratio of the TiO_2 surface area to reactor volume. The first term is the intrinsic reaction rate, governed by surface adsorption and not influenced by mass transfer. K for methylene blue adsorption onto immobilized TiO_2 surfaces has been reported as 6.25 L mol^{-1} [137] and an intrinsic maximum reaction rate, while varying in literature, has been estimated as 40 s^{-1} [138]. The second term describes the influence of mass transfer. α_v for the given system is on the order of 10^3 for a 1-mm-thick flow film. To determine k_m, we can use a relationship between the Sherwood number and k_m [139]:

$$Sh = \frac{k_m h}{D} \tag{3.14}$$

with h the characteristic length, in this case, film thickness, and D the diffusivity of methylene blue in water, 5.7×10^{-10} m^2 s^{-1}. To calculate the Sherwood number, we can use a relationship between the Sherwood Number, Schmidt Number, and Reynolds Number for flow on an inclined plate with surface reaction, adapted from Kulas et al. [140]:

$$Sh = 1.85 \left(\frac{d_e}{L} Re\, Sc\right)^{\frac{1}{3}} \varphi \tag{3.15}$$

with d_e four times the film thickness, or $4h$, and L the plate length. φ is an aspect ratio scaling parameter, with a value of 1 for experimental conditions described. The Schmidt number is the ratio of kinematic viscosity to diffusivity, in this case ~1.5×10^3. For a 1-mm film, with Re 373, we find a value of k_m of 2.27×10^{-5}.

Returning to Eq. 3.12 with these values, we see that the second, mass transfer, term has an order of 10^2, while the first, intrinsic reaction term, has order of 10^{-2}. Thus, in terms of influence on overall reaction rate, we see that the system has outsize dependence on mass transfer. Observed reaction rates are of order $10^{-3} – 10^{-2}$, fitting this range. However, if the system is mass-transfer limited the question of why limited increase in reaction rate was observed with increasing Re remains.

Despite open questions about the influence of instabilities and gas transfer on the overall reaction performance, one conclusion from the above results is that the underlying drivers of reaction rate are not inherent to angle and flow rate. If a change in reaction rate is due to surface instability (e.g. solitary or periodic waves) or oxygen transfer to the catalyst surface, there are several methods of controlling that besides varying the core IPC design parameters. Thus, these results suggest that IPC system designers should resort to operating systems at angles that maximize solar UV capture, and manage mass transfer constraints, should there be any, by controlling aspects of the IPC system besides angle and flow rate (e.g., surface roughness).

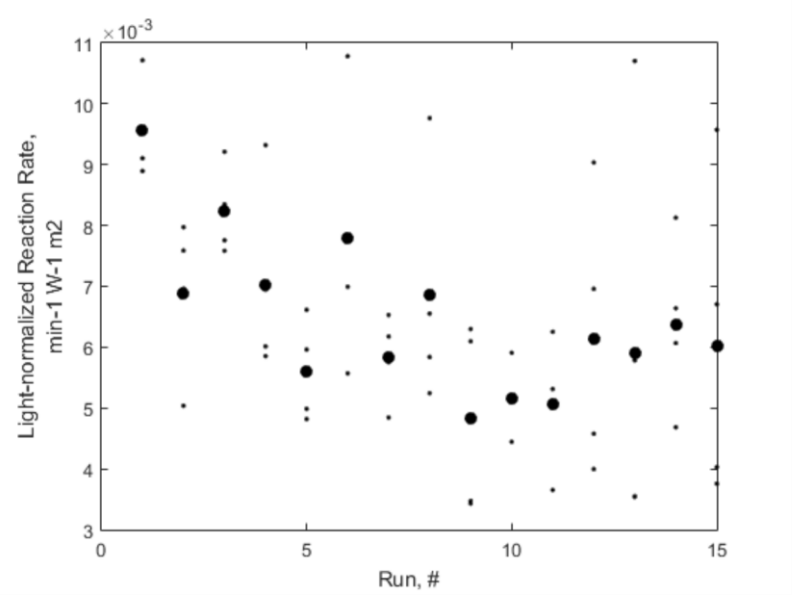

Figure 3.8. Relationship between the experimental run # and the light-normalized reaction rate. While hydrodynamic parameters are not shown in this plot, an apparent trend in average reaction rate (large markers) of decreasing reaction rate over # of runs is evident, despite several individual experiments (small markers) deviating from this trend.

Finally, an analysis of the relationship between reaction rate and run number is shown in Fig. 3.7. Few other studies of photocatalytic reactors systematically study the change in reactor performance with cycle, despite the susceptibility of immobilized TiO_2 coatings to performance degradation over time. Current state-of-the-art approaches to catalyst regeneration include calcination, treatment with H_2O_2, and NaOH [141], all of which may be impractical for IPC applications at scale. Thus, some measure of reduced photocatalytic activity must be expected in real IPC systems. Quantifying the extent of this degradation in the IPC, along with a quantification of the effect of potential in-situ catalyst regeneration approaches, are research opportunities extending from this work.

3.5 Conclusion

Two separate solar photocatalytic inclined plate collectors (IPC) with immobilized TiO_2 were fabricated and their photocatalytic degradation of methylene blue solution under artificial sunlight was characterized. Results indicated that while hydrodynamic conditions could govern reaction rate, and indeed, the overall reaction rate is likely mass-transfer limited, mass transfer was not solely determined by the IPC operating parameters of angle and flow rate. Significant changes in reaction rate were observed with changing Reynolds number and flow film thickness, but these have unclear relationships to underlying mechanisms. To elucidate those mechanisms, and the nature of the photocatalytic reaction's dependence on operating parameters in the IPC, further studies to examine surface flow instabilities and gas transfer are suggested. Finally, despite these

open questions, these results suggest that IPC designers should choose angle to optimize light capture for a given location, and seek to resolve mass transfer considerations using other aspects of IPC design, such as surface roughness.

4. The Vertically Integrated Multistep (VIMS) Reactor for Solar Photocatalytic Water Recycling in Building Facades

4.1 Introduction

In the United States, buildings account for nearly 40% of energy usage, 40% of greenhouse gas emissions, and almost 15% of water usage [142], usage intensities that are echoed globally [143]. With more than 60 million new inhabitants projected to arrive in global cities annually for the forseeable future [144], urban buildings present an urgent opportunity to address global climate change and resource scarcity, and indeed, even yield net benefits [145] [146]. A wide range of building-scale interventions have been successfully to address this opportunity, from efficiency interventions in HVAC control systems [147] to nanotechnology-based electrochromic windows [148]. While much attention focuses on energy consumption in buildings, interventions to increase building water efficiency are of increasing interest, owing to the significant interplay between energy and urban water consumption and end uses [149]–[151].

Among possible building-scale water interventions, onsite recycling of water (See Section 2.4 in this document) could cut building water demand by up to 40%. Several possible building-scale water recycling platforms (See Section 2.4), most promisingly membrane bioreactors, exist, but have shortcomings related to energy consumption [21] and take up substantial internal area, potentially compromising for smaller buildings. To offset energy demand of water treatment systems, powering such systems with solar photovoltaic systems is a promising option [152]. Rooftop-integrated PV systems are a well-characterized commercial technology, but interest is increasing in the façade as a resource for building technologies to both provide PV electricity and building thermal management [153]. Significant work has been devoted to building-integrated photovoltaic (BIPV) systems for application in facades, with dozens of operational systems globally [154], [155]. Extending from BIPV, several approaches to further repurpose façade area for light-driven sustainability applications have been proposed, including solar thermal collection using microfluidics to offset hot water demand and disinfect wastewater [156], photobioreactors to grow algae to create biofuel from wastewater [157], [158], [159] and active shading strategies to minimize building envelope thermal gain [160]. While typical façade-integrated systems are planar, active shading demonstrates advantages of orientations that are not planar to the façade surface. It has been shown in the case of PV applications that optimized 3-D configurations of PV cells can yield substantial gains in light capture and thus, performance [161].

Inspired by these efforts, I propose a façade-integrated solar photocatalytic water recycling system. Using TiO_2-based photocatalysis (See Section 2.3) powered by sunlight, the proposed system is envisioned to recirculate greywater through a reactor

configuration until sufficient treatment is reached. The system is intended to replace the energy-intensive UV treatment that follows filtration for nonpotable reuse applications [61] (see Section 2.2).

The design of the reactor extends from the inclined plate collector (IPC) into a series of sequential IPCs, which allows for tunable reactor parameters that define both hydraulic and light capture performance. Previous proposals have utilized multiple solar photocatalytic IPC's in a sequential cascade design [162], [111], which the inventors argue enhances both oxygen transfer to the photocatalyst surface, encourages mass transfer, and ensures simple construction. However, the linearly sequential design require substantial dimensional area, limiting this approach's relevance in buildings. A reversed-cascade IPC system was presented [119], and substantially reduces the footprint required for the photocatalytic reactor system. However, the proposed cascade system was not experimentally characterized, and required the use of UVC LEDs, limiting its relevance. In none of the above studies was a systematic exploration of how controlling system design parameters influences overall treatment performance conducted.

Here, the proposed system is the Vertically-Integrated Multistep (VIMS) reactor. In this work, I detail the VIMS system, present experimental results and parameter investigations for the degradation of methylene blue under real sunlight conditions in Berkeley, CA, USA. Specific parameter investigations are the step angle and 'step height' – the distance between subsequent coated steps in VIMS. Both parameters underpin the unique tradeoffs inherent in the VIMS design and any cascade photoreactor, in that they govern both hydraulic behavior and light capture performance. Step angle relative to the sun determines the amount of direct sunlight captured, while also determining flow film thickness. Step height governs the level of shadowing depending on solar angle, while also influencing mixing and gas transfer to the system. After a parameter study of these features of VIMS, I present a simple forecast of the potential impact to water consumption the system could have in a real building.

4.2 Materials and Methods

Chemicals & Photocatalyst Immobilization

Reagents were acquired from Sigma-Aldrich unless otherwise noted. Reagent-grade methylene blue (MB) powder was mixed with deionized water to create solutions of 10 or 20 micromolar concentration MB.

Immobilized TiO_2 films were grown according to a procedure outlined in section 3.2. Nanopowder TiO_2 (Evonik, Degussa P-25) was used, with diethanolamine and isopropyl alcohol. Glass slides were procured from Fisher Scientific.

Analytical Methods

A spectrophotometer (DR2400, HACH Company) was used to develop a correlation between MB concentration and absorbance at 665nm. Triplicate samples were used in all instances, and the spectrophotometer blanked against DI water.

Photoreactor Design and Experiments

The VIMS system consists of a sequence of oppositely-oriented inclined plates, to create cascade of water across plates coated with immobilized TiO_2 (Fig. 4.1). Transparent Polymethylmethacrylate (PMMA) was laser-cut to create the front cover of the VIMS system. PMMA is known to absorb substantially in the UV range. The rest of the system (back and side panels) was fabricated from black PMMA via lasercutting, CNC machined from 6061 aluminum (distributor), or 3D-printed from PLA plastic (funnel, steps). Step angle α was controlled by a rotary control system, lasercut from PMMA. Step height *d* was fixed in each reactor. On each step, two TiO_2-coated glass slides were mounted using adhesive, for a step dimension of 25mm x 150mm. This gave the system an overall thickness of 60mm, intended to comply with needed thicknesses of curtain wall systems.

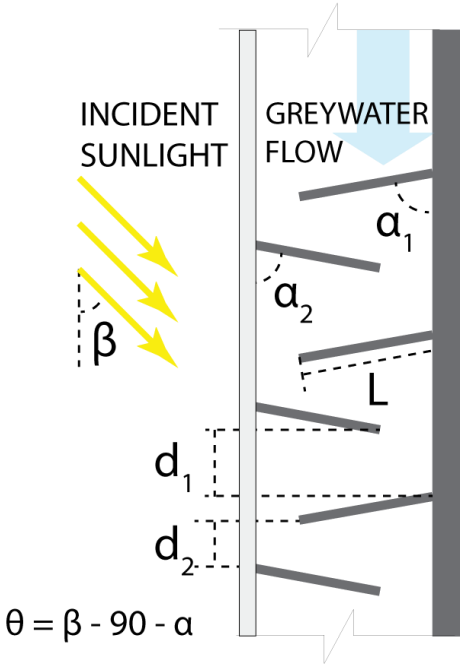

Figure 4.1. VIMS Schematic. A range of design parameters is shown, but the controlled variables in this research are α_1, α_2, and d_1, d_2. β, as a function of real-time solar conditions, varies throughout the experiment. For the experimental conditions investigated, d_1, d_2 are held equal, as are α_1, α_2.

The experimental setup, featuring four separate reactors, can be seen in Fig 4.2 and Fig 4.3. Flow was governed by a peristaltic pump (Cole-Parmer MasterFlex), with flow rate set to 140 mL/min. Each reactor used a separate step height that was fixed, although the step angle was varied for each experiment. As the reactor height was the same across all four reactors, the number of steps per reactor became a function of the step height. Specific combinations of step height and number of steps are shown in Table 4.1.

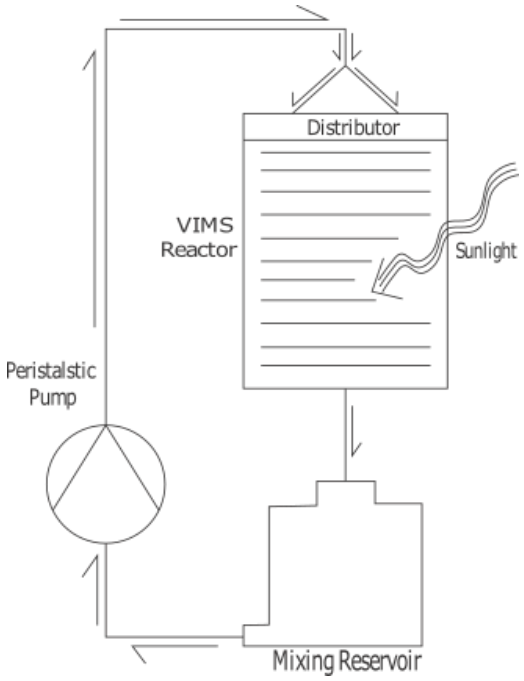

Figure 4.2. Schematic of a single VIMS photoreactor. The peristaltic pump moves MB solution from the continuously stirred reservoir into a distributor, from which it cascades across a sequence of steps.

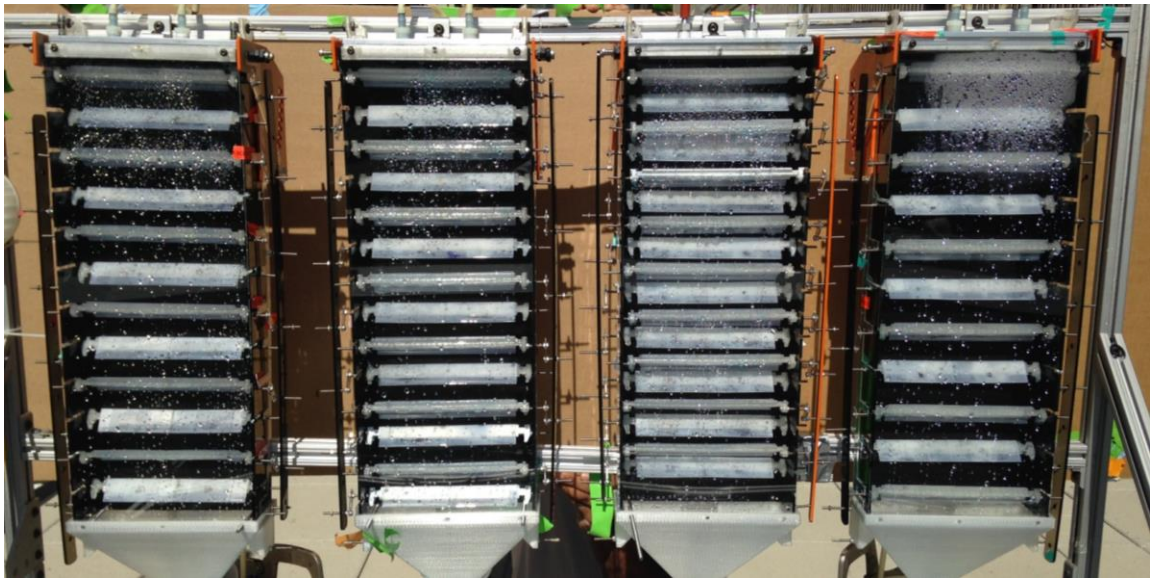

Figure 4.3. VIMS Photoreactor experimental setup in real sunlight conditions. Four separate photoreactors, each with independent reservoirs, distributors, and flow lines, are aligned in parallel on a west-facing rooftop.

Step Height (mm)	Number of Steps / Reactor
25	18
35	14
40	12
45	10

Table 4.1. VIMS Step height combinations with number of steps.

All experiments were carried out at the University of California, Berkeley, CA USA (latitude 37.87^{o}, longitude -122.25^{o}), on a roof top and positioned with southwest-facing orientation (76 ^{o} from S). Experiments were carried out between 1PM and 5PM between February and May 2016. It is noted that location choice has substantial influence on system performance via a variety of factors, including solar resources, heating/cooling demand, and economic impact [163]. In this sense, Berkeley, with a temperate climate profile, produces a vastly different result than, for example, Singapore, an equatorial location with tropical climate.

Solar irradiance was measured by taking an initial spectroradiometry reading of incident light, with the detector lens parallel to the front face of the reactor (StellarNet EPP2000). Spectral range for this instrument was 200 – 1080 nm. Repeated measures of the solar spectrum suggested that the fraction of incoming radiation present as UV was ~4.4%. Solar irradiance with the spectroradiometer was measured at each of the four corners of a 'bounding box' of the front-facing plane of the photoreactors, and averaged to produce an average total spectral irradiance. Real-time solar irradiance was collected using a pyranometer (SPLite2, Kipp & Zonen), also mounted parallel to the front face of the reactor, at 10-second intervals via a multimeter. As this instrument had sensitivity only in the spectral range of 400-1150 nm, UV irradiance was extrapolated based on the fraction of UV measured via spectroradiometry, in these experiments' case, 4.4%.

During the experiment, a 30-minute 'dark' period was enforced by shielding the reactors' front panel with an opaque cover. After 30 minutes had elapsed, the cover was removed and sampling began. Samples were taken at 15 minute intervals for the first half-hour, and then at 30 minute intervals for the remaining reaction period, for a total irradiated experiment time of 120 minutes. Following each experiment, each reactor was flushed with 1L of DI water to desorb any remaining MB.

4.3 Results and Discussion

Reaction Kinetics and Order

As outlined in Section 3.4, the system was described with pseudo-first order kinetics. However, as experiments were conducted under real solar conditions with a transient light source, experimental results needed to be normalized by incident UV light to be

compared meaningfully. To calculate the total average irradiance, the pyranometer-measured irradiance was integrated over the course of each experiment and divided by the experiment time, as per:

$$\overline{E_s} = \frac{\int_{t_i}^{t_f} E_s(t)dt}{(t_f - t_i)} \tag{4.1}$$

with $E_s(t)$ measured at 10s time intervals. An example spectral distribution showing the evolution of the solar spectrum over the course of a single experiment is shown (Fig. 4.4). Average UV irradiance, $\overline{E_{s,UV}}$, is calculated by multiplying the average solar irradiance from Eq. 4.1 by a proportionality factor, in this case, 4.4%. Calculated average UV irradiances are plotted (Fig. 4.5) based on experimental trial; of successful experiments, five trials were qualitatively categorized as 'full sun conditions,' four were 'cloudy', and four were indeterminate – meaning, conditions were dynamic through the course of the experiment. Fig. 4.4 exhibits indeterminate conditions.

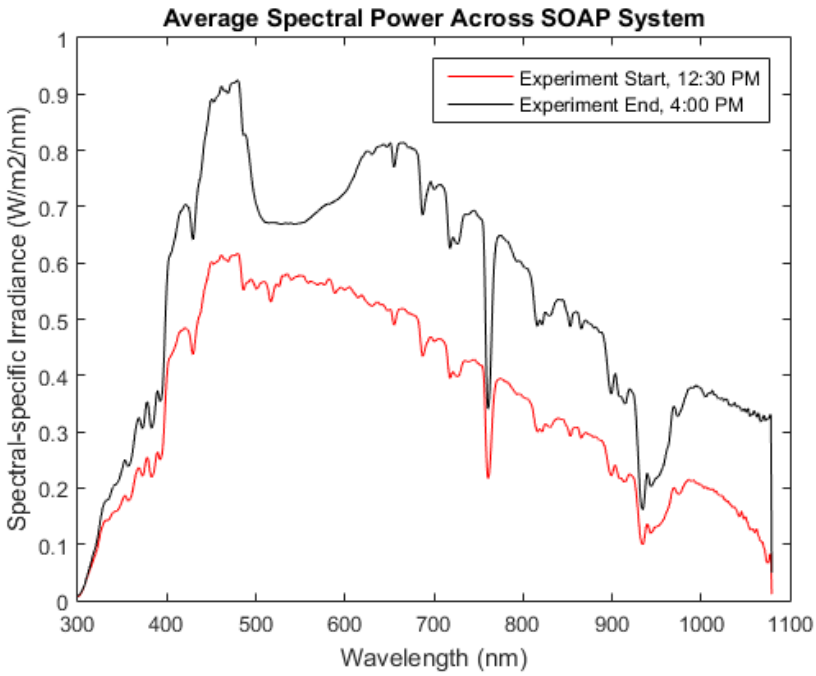

Figure 4.4. Evolution of Solar Spectrum over a VIMS experimental trial. Because of the orientation of the VIMS solar collector as perpendicular to the Earth's surface and oriented westwards, significant increase in solar irradiance is observed towards the end of the experiment, later in the afternoon. As intermittently cloudy conditions were observed during the experiment, these data are labeled indeterminate solar conditions.

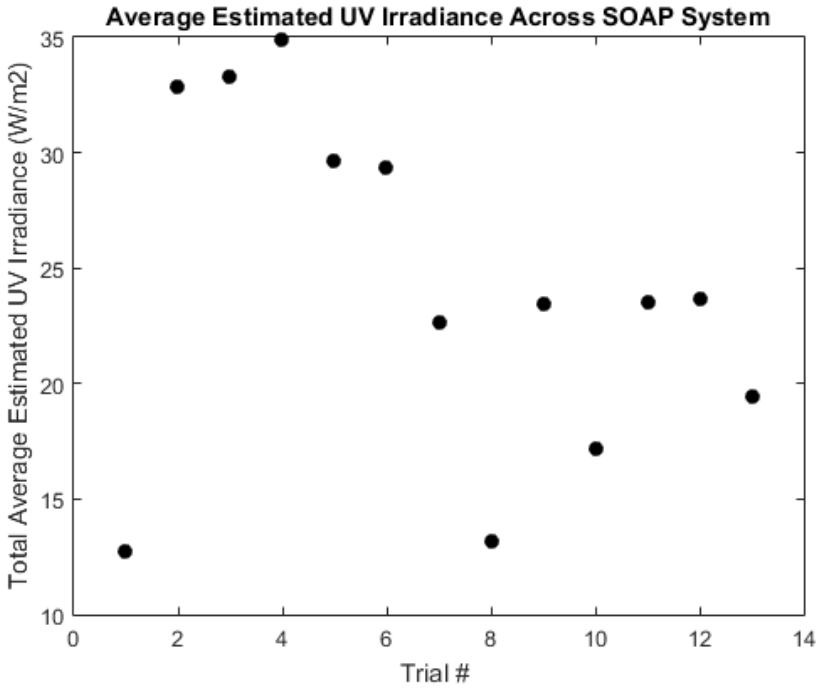

Figure 4.5. Total Average UV Irradiance by Experimental Trial. Different experiment dates experienced substantially different sunlight conditions, owing to overcast skies. As would be expected in a real system, this resulted in a wide range of UV irradiances, plotted here as an average over the experiment time.

Given these results, calculated pseudo-first order reaction rate *k* was normalized first by UV irradiance, as per:

$$k_{UV} = \frac{k}{\overline{E_{s,UV}}} \tag{4.2}$$

To further compare VIMS results across the four photoreactors, reaction rate was further normalized to account for the differing total catalyst area across each photoreactor, owing to the differing number of steps, and by volume, as some photoreactors experienced differential volume loss over the course of the experiment [128]:

$$k_{UV,A,V} = \frac{k_{UV}V}{A_{TiO_2}} \tag{4.2}$$

Thus, the $k_{UV,A,V}$ term allows comparison across separate experimental trials.

Experimental Results

Experimental results (Fig. 4.6) show solar photocatalytic decolorization of methylene blue solution across thirteen different solar conditions (see caption). Pseudo-first order kinetics show strong correlation to the data, and were accepted as appropriately descriptive of the reaction.

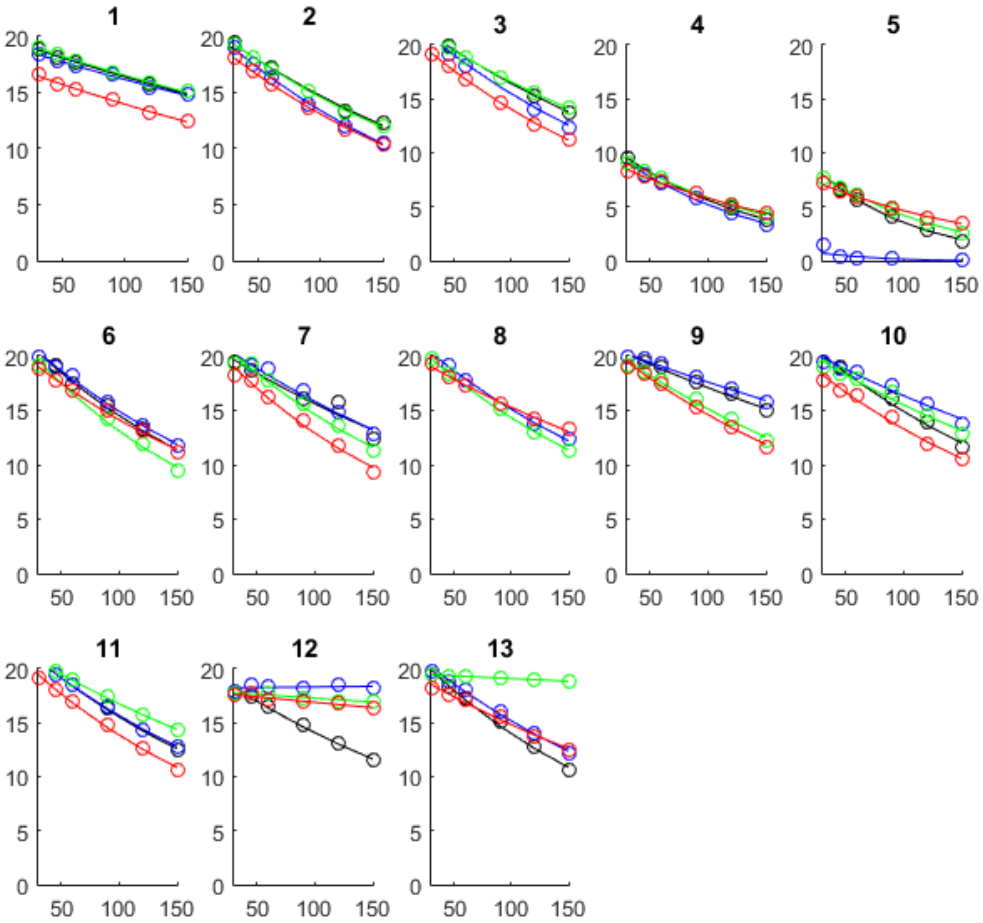

Figure 4.6. Experimental results for VIMS trials under real solar conditions. On each graph, the y-axis represents concentration of MB solution in micromolar, while the x-axis is time in minutes. Data is shown in open circles, and lines represent pseudo-first order fits for the data. Red data indicates 40mm step height; green data represents 35mm step height; blue data, 25mm step height; and black data, 45mm step height. Experiments 12 and 13 contain control experiments: both a dark control, with no exposure of the photoreactor to sunlight, and a no-TiO_2 control, with the photocatalyst-coated surfaces replaced with uncoated glass slides.

Experiments 4 and 5 were performed on solutions at concentration of 10 micromolar. Not shown in this data is the adsorption 'dark' phase of the first 30 minutes. Differences in adsorption performance resulted in slightly different starting concentrations across experiments.

To understand the relationship between VIMS design parameters and overall performance, normalized reaction rate $k_{UV,A,V}$ was plotted against step size (Fig. 4.7) and step angle (Fig. 4.8).

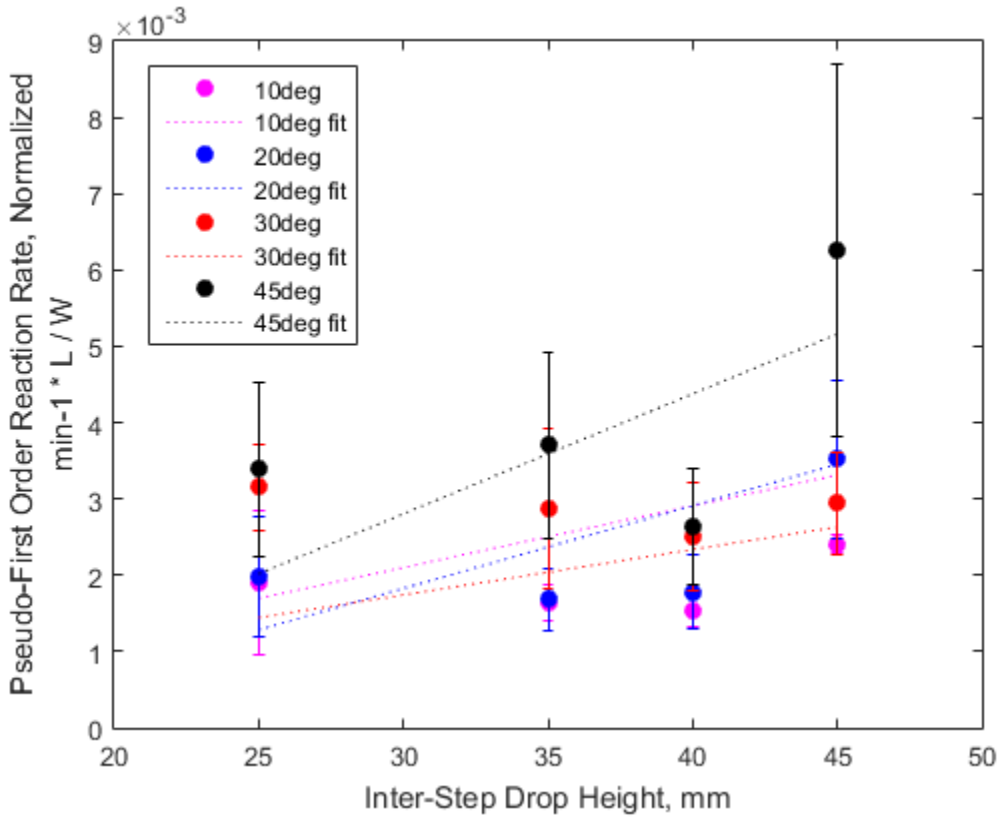

Figure 4.7. Reaction rate $k_{UV,A,V}$ vs. Step Height. Linear best-fit lines are plotted to show trends in the relationship.

A loose correlation of increasing reaction rate with increasing step height is observed. This effect is to be expected, as a forthcoming report on simulations of a similar system by Ross et al. [164] suggests that a larger step separation enhances light capture owing to decreased shadowing by neighboring steps, as at high step separations, there are fewer steps for a given photoreactor height. Thus, because $k_{UV,A,V}$ is normalized by the solar irradiance on the front panel area of the photoreactor, not the light falling on individual

steps, differences in sunlight collection effectiveness within the reactor envelope are not accounted for in normalized reaction rate. Furthermore, while Ross's report does not investigate transient solar conditions, it argues that a similar VIMS system with incident solar irradiance of 60 degrees and step angle of 45 degrees is expected to double its capture of light as step height increases from 20mm to 50mm, primarily owing to a reduction in shadowing. Obviously, the influence of shadowing between steps changes with changing incident angle – as would be observed during the experimental conditions.

However, in the experimental data, a near doubling in $k_{UV,A,V}$ is observed for the VIMS system at step angle 45 degrees as its step height increases from 25 mm to 45 mm. Thus, given the linear relationship between photocatalytic reaction rate and absorbed UV light for intensities in the studied range [75], a doubling in $k_{UV,A,V}$ would be expected, which is borne out in the experimental results for the 45-degree step angle. Other combinations of design parameters, however, deviate substantially from Ross's simulation results. For example, Ross's light capture simulations suggest a near-tripling in light capture for a VIMS system with 10 degree step angle as step height is increased from 20 mm to 50 mm. Experimental results for the 10-degree system, however, exhibit little difference in $k_{UV,A,V}$ as step height is increased. Thus, while light capture governs the underlying photocatalytic reaction linearly, shadowing owing to step density cannot completely explain the observed results.

Other mechanistic factors must be in play to describe VIMS performance. While larger step heights would encourage greater oxygen transfer to water droplets leading to higher dissolved oxygen content in the reactor system [165], and thus, greater availability of electron scavengers in the photocatalytic oxidation of organic compounds, experimental results do not provide evidence that this is happening. Aside from the observed increase in reaction rate with increasing step height for the 45-degree step angle VIMS system, other step angles demonstrate almost negligible increases in $k_{UV,A,V}$ with increasing step height.

It can be observed that when organizing results by step height, and plotting $k_{UV,A,V}$ vs. step angle (Fig. 4.8), VIMS systems with larger step height, that is, the 45 mm step separation, show greater sensitivity to step angle. Extending from Ross's analysis, we hypothesize that at lower step heights, shadowing compromises benefits of increased light capture owing to steeper angles during late-afternoon experiments. Lower step heights do not demonstrate the level of sensitivity of the 45mm system. A careful analysis is needed to quantify the differential effect of the 5mm step height differences on light capture, and compare that differential to the observed reaction rate sensitivity to step angle.

I note that these results coincide nicely with conclusions established in Chapter 3, namely that light capture dominates any hydrodynamic or mass transfer effects of step angle in inclined-flow systems. However, before too many parallels are drawn, it is important to observe that because the 'inclined plate' length in the VIMS system is significantly shorter than that in the experimental IPC of Chapter 3, a fully-developed flow regime

cannot be expected to have developed across each VIMS step. Thus, hydrodynamic considerations will be considerably different than that observed in a system with a fully-developed flow system.

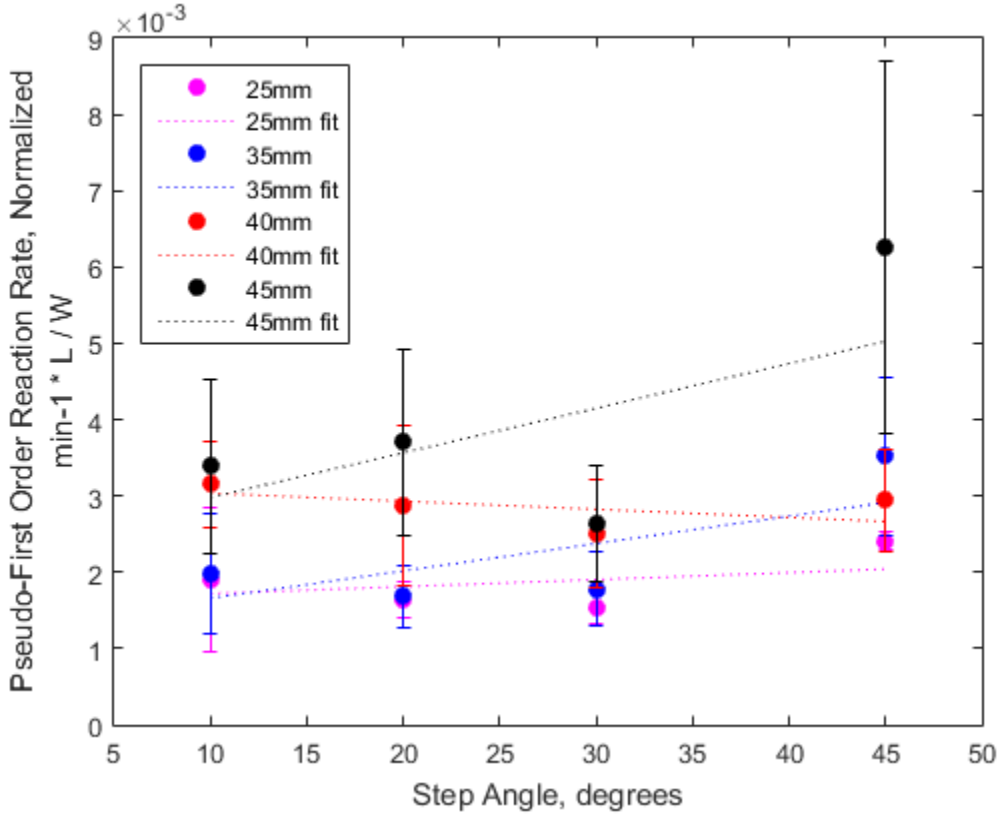

Figure 4.8. Reaction rate $k_{UV,A,V}$ vs. Step Angle. Linear best-fit lines are plotted to show trends in the relationship.

To explore these results further the relationship between the number of steps – not the step height – and the area-, volume-, and UV- normalized reaction rate $k_{UV,A,V}$, and the volume- and UV-normalized reaction rate $k_{UV,V}$:

$$k_{UV,V} = k_{UV}V \tag{4.3}$$

was explored (Fig. 4.9).

As greater illuminated catalyst surface area is known to increase reaction rate, higher reaction rate is expected with an increasing number of steps. When normalizing reaction rate to $k_{UV,A,V}$, the opposite trend is observed – to be expected, since these results are normalized by total photocatalyst area in the reactor. Thus, if one removes the effect of increasing catalyst area, the dominant effect of increasing the number of steps is shadowing in light capture, resulting in lower reaction rates at higher numbers of steps.

However, plotting $k_{UV,V}$ vs. the number of steps – here not normalizing for the total area of catalyst – shows a surprising result, that there is inconclusive dependence of normalized reaction rate on the number of steps. This suggests that for the VIMS system size studied, the addition of catalyst area yields inconclusive increase in reaction performance, and that light capture dominates. This has important implications for design, manufacturing, and costing of VIMS systems, as smaller catalyst area and fewer components would be necessary to realize similar treatment levels of systems featuring larger numbers of steps.

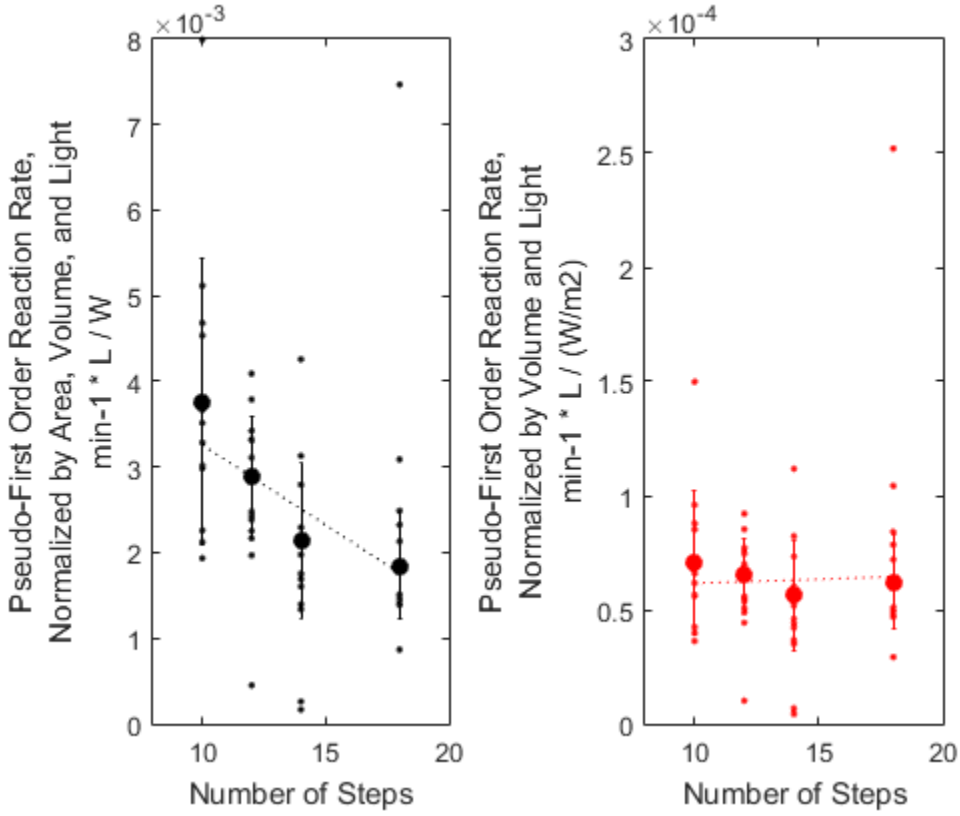

Figure 4.9. Reaction rate vs. Number of Steps. $k_{UV,A,V}$ vs. Number of Steps (left) and $k_{UV,V}$ vs. Number of Steps (right). Linear best-fit lines are plotted to show trends in the relationship.

To extrapolate the performance of a realistic building-scale VIMS system, an areal collector analysis was performed, based on analysis developed in Bolton et al. to quantify the relationship between solar photocatalytic collector area and reaction performance [166], modified by equations presented for scaling to fit pseudo-first order kinetics [167] to explore the relationship between reactor volume, and reaction rate. This analysis was rearranged to calculate the volume of contaminated water treatable given a range of operating parameters:

$$V_s = \frac{k_{UV,V}\, E_{s,UV}\, (\frac{A_c}{A_o})\, t}{\ln(\frac{c_o}{c_f})} \tag{4.4}$$

with $E_{s,UV}$ the average UV irradiance in W/m^2, A_c the scaled-up collector area, in m^2, A_o the experimental collector area, in m^2, t the scaled-up time, in minutes, c_o and c_f the desired methylene blue concentrations at the onset and conclusion of the scaled-up solar exposure, and V_s the treatable volume of water.

To clarify the implications of scale-up, we separate scenarios into sunny and cloudy conditions, with $E_{s,UV}$ of 30 W/m^2 and 15 W/m^2, respectively. This is to illustrate the 'worst case' treatable volume from such a system. A_o for the experimental system is .084 m^2, but for a realistic building façade application, A_c of 9 m^2 is used. t is projected to be 180 minutes, to approximate afternoon sunshine falling on a vertical building-wall, and we select c_o and c_f to represent a 1-natural-log reduction in concentration of pollutant. As $k_{UV,V}$ was demonstrated to vary significantly across experiments, V_s was calculated for each experimentally-determined $k_{UV,V}$ and plotted (Fig. 4.10).

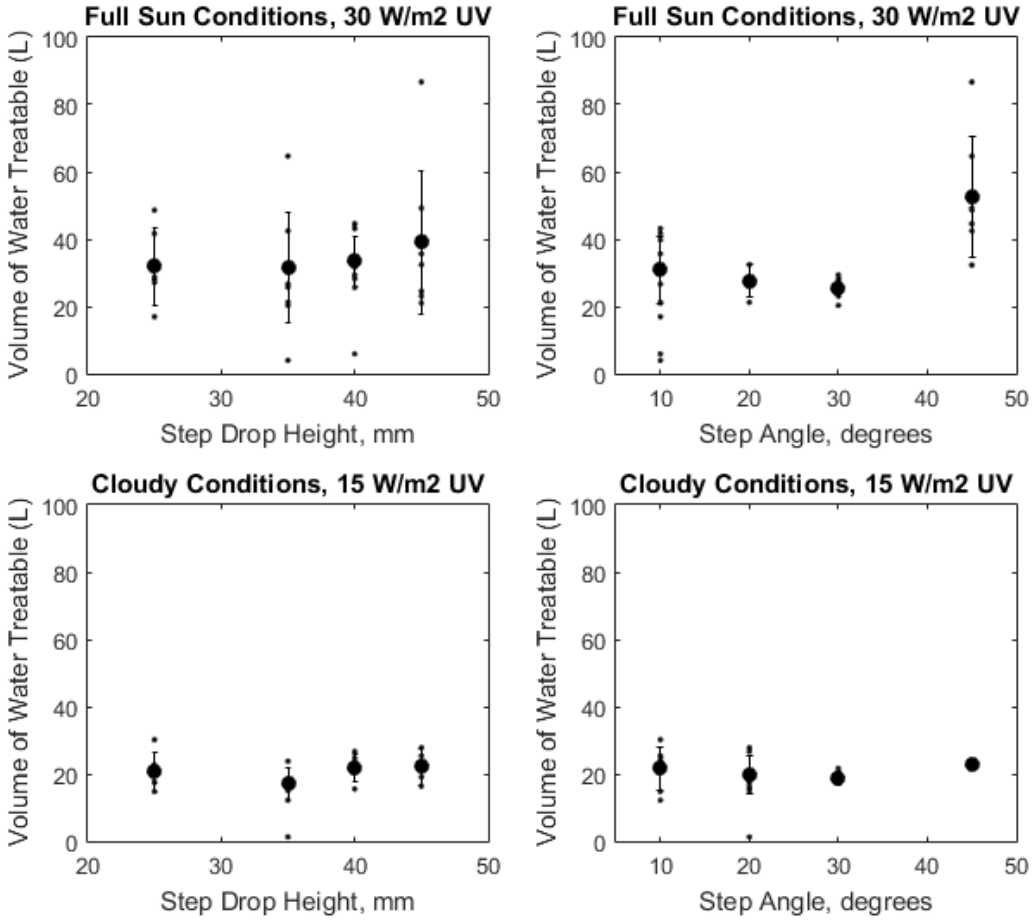

Figure 4.10. Scaling Analysis for a 9m^2 collector. Relationships between step height, step angle, and volume of water treatable to 1-log reduction in methylene blue concentration for sunny and cloudy conditions are plotted. Average data points (large dots) are given error bars showing standard deviation, while individual data points (small dots) are shown.

The projection of V_s shows that step angle and drop height can have substantial effect on treatment performance. However, further work is needed to isolate the effect of step angle and height parameters on overall performance. Perhaps most significantly, the current VIMS system offers relatively poor volumetric treatment when scaled up, with roughly 1-log treatment of 20 L of liquid on cloudy days, and no more than 60L on sunny days. The significant error bounds on results on sunny days indicate that even this performance is highly susceptible to variation. Urban water use exhibits a wide range of demand numbers, although between 60-100L per person per day is largely accepted for multifamily complexes [168]. Given that greywater can be applied to up to 40% of household applications (e.g., toilet flushing), under optimal sun conditions, the best case of the VIMS system could offset nonpotable water demand of up to 2.5 persons.

However, even this result is both optimistic and pessimistic. Even optimistically, a 63% (1-natural log) reduction in MB concentration does not sufficiently demonstrate the inactivation of bacteria necessary to meet stringent nonpotable water re-use requirements. For example, California Title 22 regulations require less than 2.2 CFU / 100mL of coliforms, with raw greywater coliform counts ranging from $10^1 – 10^5$ CFU / 100mL [169]. This implies that up to a 5-$\log_{10}$ reduction in coliform counts could be necessitated in a VIMS system as a prerequisite for treatment, which at current performance rates, would require increased treatment time or area, or decreased treatment volume. While experimental studies that compare methylene blue decolorization to *E. coli* inactivation results vary, a study by van Grieken et al. using immobilized TiO_2 in a fixed-bed reactor illuminated with a UV-A lamp showed that a 63% decolorization of methylene blue corresponded to a 4-log inactivation of *E. coli* [170]. While van Grieken's results may be encouraging, *E. coli* inaction must be independently verified for the studied system to be conclusive.

There is significant reason to expect that these performance indicators underpredict possible VIMS treatment, however. The front cover material used was conventional PMMA, selected for its high optical transparency, strength, and ease of fabrication. However, conventional PMMA is known to absorb significant fractions of UV light, although it is significantly more UV transparent than other competing transparent plastics, such as polycarbonate (which absorbs heavily across the entire UV-spectrum). UV-transmitting PMMA, made by changing polymer additives, is commercially available, but was unavailable in these experiments. Based on spectroradiometry, it was determined that up to 54% of incoming solar UV energy was absorbed by the front cover. Given the linear relationship between UV light and photocatalytic reaction performance, by selecting a UV-transmitting acrylic cover that has transmittance of 90% in the UV range, our system could treat up to 100L of water at $9m^2$, offsetting the nonpotable water needs of at least four individuals. At the time of experimental design and experiments, a cost-effective option was not available; subsequently, however, SolAcryl Super UV-Transmitting Acrylic was identified and used in later experiments (see Chapter 5). In future work on VIMS, this material will be sourced.

As this research has shown, future research must focus on augmenting experimental results with understanding of maximizing light capture, in three particular areas. First, careful synthesis of light capture simulations with experimental results must yield a clearer design criteria for optimization of such systems. Similar to work in the PV field, a clear correlation between global location and VIMS design parameters and orientation must be established. Second, selection of materials must be made to ensure maximum light transmittance. This has two implications. In collector cover materials, this means the aforementioned selection of UV-transmitting acrylic or the use of materials like quartz or borosilicate glasses, prized for their excellent UV transmittance. In photocatalyst materials, it implies choice of photocatalyst with a band gap engineered to accept lower-energy photons, and thus, more of the solar spectrum. Such photocatalysts, however, are still being proven in laboratory conditions and their reliability remains unknown. Finally,

reimagining of the VIMS system to accommodate both the lessons from this research and the performance demands of successfully treating real wastewater, to achieve demonstrable 5-log pathogen reduction among other metrics, is necessary.

Furthermore, it is noted that in this research, scale-up calculations do not account for solar dynamics and specific location, and further analysis using best practices from solar modeling and the building science field, such as EnergyPlus or TRNSYS, is needed as a next step [171], [172].

Thus, while the VIMS system is not viable in its current experimental form, with careful materials selection and further optimization of orientation and design parameters, there is significant promise of creating global impact through a building façade-integrated water recycling system.

4.4 Conclusions

In this work, a building façade-integrated solar photocatalytic water recycling system was proposed, fabricated at laboratory scale, and characterized under real solar conditions in Berkeley, CA. Results indicated that light capture closely governed system performance, potentially even more so than photocatalyst surface area, and optimal design parameters were those which minimized shadowing and most oriented VIMS catalyst-coated surfaces towards the sun for direct light capture.

While current treatment performance is insufficient for real building-scale impact, several strategies for maximizing VIMS performance are proposed. First, a synthesis of solar capture modeling, based on an accepted repository of solar data such as EnergyPlus, with reactor design is needed to optimize VIMS system performance based on time, location, and orientation. Second, materials selection for both the VIMS system construction – specifically, highly UV-transmitting cover materials – and the photocatalyst coating – specifically photocatalysts excitable by visible-light photons – can yield significant improvement in VIMS performance. Third, experiments with real greywater and real *E. coli* inactivation are mandatory to drive iteration of system design for full proof-of-concept. These further research directions, combined with the presented research results, suggest the potential of future façade-integrated water treatment systems.

5. Hybrid Solar Photocatalytic Water Treatment and Solar Thermal Gain (PC-T) for Sustainable Buildings

5.1 Introduction

As described in Section 4.2, the promise and opportunity of building-integrated systems to address resource scarcity and improve urban sustainability is substantial: globally, 40% of energy and 15% of water is consumed in buildings [143]. This opportunity is borne out by the vast range of building-scale interventions deployed to improve the efficiency and quality of energy, water, and air in the urban environment – interventions that distinguish 'green buildings' [173], [174]. While rooftop solar photovoltaic (PV) installations are perhaps the most recognizable such intervention, significant potential in building-integrated systems lies in the building envelope, and specifically, the façade.

The building envelope façade acts as an interfacial layer between the building and environment [175], [176], and plays an outsize role in determining key operating parameters for the building, especially lighting and thermal management [177], representing correspondingly significant construction cost and complexity as a result [178] As described in Section 4.2, the façade has attracted a wide range of proposed interventions in pursuit of sustainability and occupant comfort. One of the earliest technology interventions was the ventilated double-skin facade to maximize daylight while controlling temperature, first proposed in the 1930s by Le Corbusier [179] and an active area of applied research today [180]. More recently-proposed technological façade interventions include phase-change thermal insulation based on advanced polymeric materials [181] and algal biofuel-producing photobioreactors for façade-integration [182]. The field of solar thermal facades (STFs) extends on both of these research directions to explore facades that optimally capture solar energy as heat and light for different energy-offset purposes [183] [184]. Such technologies are often intricately integrated with other building systems to best realize whole-system sustainability.

Among façade integrations, building-integrated photovoltaics (BIPV), as previously described, have received significant interest. They are distinguished from traditional rooftop solar PV by their direct integration into a building envelope, for aesthetic or structural reasons [185]. Façade-integrated PV, typically amorphous silicon semiconductor panels, are exposed to less direct sunlight than rooftops and are most appropriate for northern or southern latitudes [186]. However, they offer the opportunity to generate electricity with minimal marginal cost over standard building materials [187]. A key challenge in successfully operating BIPV systems in facades is thermal management, as temperature is crucially important to determining PV electrical efficiency [188]. Efforts to manage temperature in façade-integrated PV have included exposure to ambient air, which is recycled to help offset HVAC load [189], to forced

flow of water over the façade-integrated PV, which is claimed to improve overall electrical yield by 9% [190].

Understanding the need to couple PV light capture with cooling, hybrid photovoltaic-thermal (PV-T) systems have been intentionally engineered to capture heat that would normally be wasted in PV systems. As most commercial PV systems demonstrate 4-17% efficiency, more than 50% of solar spectral energy is lost. By capturing this excess spectral energy in the form of thermal gain of a working medium, to be subsequently used to offset building thermal demand, PV-T engineers can maximize overall system efficiency [191]. Since the first experimental proofs-of-concept of the PV-T system in the late 1970's [192], [193], numerous studies have been produced to characterize PV-T systems, and several functioning full-scale installations have been deployed. These efforts are covered in detail in a recent review by Yang and Athienitis [194]. Several PV-T systems have been characterized in façade-amenable configurations, with flat-panel configurations using air [195] or water [196] as a working fluid, and several designs using motorized active elements to maximize solar PV output and thermal gain have been proposed [197], [198]. While thermal absorber configuration varies substantially based on the overall PV-T system design, flat plate collectors typically use tubing thermally bonded under solar PV cells and embedded in insulation. Beyond electricity and hot water production, façade-integrated PV-T systems using water as a working fluid have great potential for acting as insulation for the building envelope, broadening the potential impact of PV-T systems [199]. Innovation around materials, assembly, and operation continue to drive improvements in system efficiencies [200]. However, while PV-T systems hold great promise to address building energy needs through offsetting HVAC and electricity demand, they can have little direct effect on water consumption in buildings.

Extending on the work of the PV-T community to address building-scale water demand, we propose to simultaneously use solar photocatalysis and solar thermal gain in the façade envelope, developing what we call solar photocatalytic-thermal (PC-T) systems. Photocatalytic water treatment, as described in Section 2.2, is the absorption of a photon with energy greater than the band gap of a semiconductor photocatalyst, separating an electron-hole pair. The electron and hole subsequently produce reactive oxygen species to destroy pollutants, or the hole directly oxidizes pollutants [75]. While many photocatalysts are under study, solar photocatalysis via titanium dioxide (TiO_2) is the most widely used and inexpensive. Its main drawback is that it is only active under UV light, and under ideal solar conditions will have ~4-5 % efficiency – losing 95% of incident solar energy as waste heat (Fig. 5.1). Thus, there is significant opportunity to engineering photocatalytic treatment systems to capture this waste heat to improve overall system efficiency. More promisingly, at temperatures up to approximately 80 C, the photocatalytic reaction rate is well known to increase with increasing temperature [75]. Thus, capturing otherwise-waste heat directly in the reaction medium can serve to both enhance the reaction performance and potentially offset broader building energy needs.

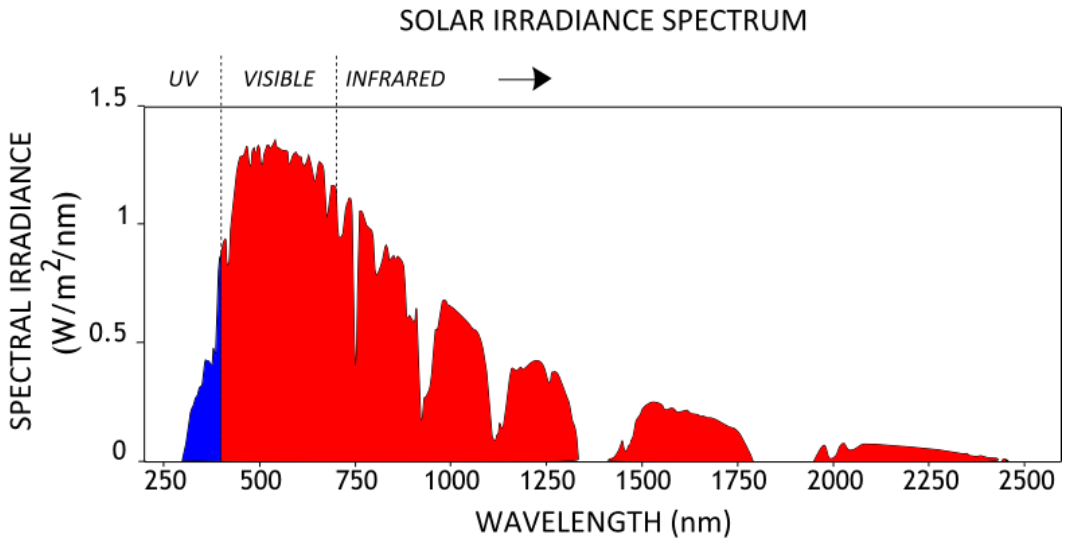

Figure 5.1. Comparative fractions of solar spectrum. Only UV light (blue region) is available to drive photocatalysis in TiO_2-based systems, leaving the vast majority of sunlight wasted (red region). Thermally harvesting this portion of sunlight could yield substantial improvements in overall system efficiency.

Current work in developing photocatalytic systems has proven that solar thermal collection enhances reaction rate substantially. Hashemi et al. showed that by designing a batch TiO_2 microreactor to absorb rather than reflect or scatter visible and infrared sunlight, they could enhance the net photocatalytic decolorization of methylene blue by 82% [201]. The authors argue that such enhancement is due to the operating temperature of the absorbing reactor increasing to ~45 C during the course of the experiment. Wang et al. reported an up to 40% thermal enhancement in photocatalytic decolorization of methylene blue in a continuous-flow $BiVO_4$ microreactor under a blue-UV LED array [202]. The thermal enhancement roughly correlates to a heightened temperature of 30^o C, as opposed to room temperature, 20^o C. Thus, while close synergy between photocatalytic and thermal performance is demonstrated, the combined efficiencies of the process remain uncharacterized.

Façade-integrated systems for water treatment are a promising direction of research, as pioneered by Gutierrez [203] and Lee et al. [156]. In Lee's work, the research team described photothermal disinfection of bacteria coupled to solar thermal gain using a concentrating hemispheric microlens array for integration in building facades. Lee's work, besides demonstrating the high thermal efficiencies possible (reported to be 70%) in uninsulated systems, underlines the possibility of solar pasteurization of pathogens in wastewater, without using photocatalysts. While not directly suggesting façade integration, Liu et al. proposed combining solar thermal phase change materials with photocatalytic graphene-TiO_2 microspheres to simultaneously treat water and dynamically capture and release

heat in building envelopes using a single material [204]. Liu's work highlights the promise of multifunctional building envelope systems that can simultaneously offset water and energy demand.

In this work, we extend on Liu and Lee's innovations to realize a façade-integrated system for hybrid PC-T operation. The system is intended to, at scale, heat and treat building wastewater synergistically, offsetting building energy demand and water consumption. Solar thermal collection heats up greywater from a building in a photoreactor. This enhances photocatalytic reaction temperature, leading to greater water treatment performance. Treated greywater leaves the system with an elevated temperature, where the heat latent in it could be used to offset building energy demand in various ways, such as heat exchange for a water heater or direct space heating via hydronics.

We examine three systems: a simple black absorber-backed flat panel control; a photocatalyst-backed flat panel; and a photocatalytic reactor configuration, the vertically-integrated multistep (VIMS) reactor (see Chapter 4). Prototype systems were fabricated at laboratory and subpilot scales to characterize overall photocatalytic and thermal performance. While thermal and photocatalytic efficiencies remain relatively low, we suggest directions for future optimization to realize more effective PC-T systems.

5.2 Materials and Methods

Chemicals & Photocatalyst Immobilization

Reagents were acquired from Sigma-Aldrich unless otherwise noted. Reagent-grade methylene blue (MB) powder was mixed with deionized water to create solutions of 20 micromolar concentration MB.

Immobilized TiO_2 films were grown on glass slides according to a procedure outlined in section 3.2. Nanopowder TiO_2 (Evonik, Degussa P-25) was used, with diethanolamine and isopropyl alcohol. Glass slides were procured from Fisher Scientific.

For subpilot-scale experiments, as the dimensions of photocatalyst coating required were beyond the capacity of the laboratory, a commercially available TiO_2-coated panel was procured (Reynobond EcoClean, Alcoa). The commercially-coated panel consisted of aluminum sheet coated with nanostructured TiO_2 rated to photocatalytically degrade atmospheric pollutants with a polycarbonate backing.

Analytical Methods

A spectrophotometer (DR2400, HACH Company) was used to develop a correlation between MB concentration and absorbance at 665nm. Triplicate samples were used in all instances, and the spectrophotometer blanked against DI water.

Photoreactor Design and Experiments

At both subpilot and laboratory scales, experimental protocols were based on AHSRAE 93-2010 [205] for open-loop steady-state characterization of solar thermal collectors. While a separate testing architecture based on the European EN 12975:2000 standard exists, the ASHRAE standard is chosen for its wide adoption in the USA. It is also noted that steady state models are conservative in evaluating overall thermal energy gained, compared to quasi-static approaches [206]. Thus, the ASHRAE procedures have been applied in this work. Details on procedures for each scale of experiment are below. The general layout of the three reactor concepts characterized in this work are shown in Fig. 5.2, and a general experimental schematic for a single reactor is shown in Fig. 5.3.

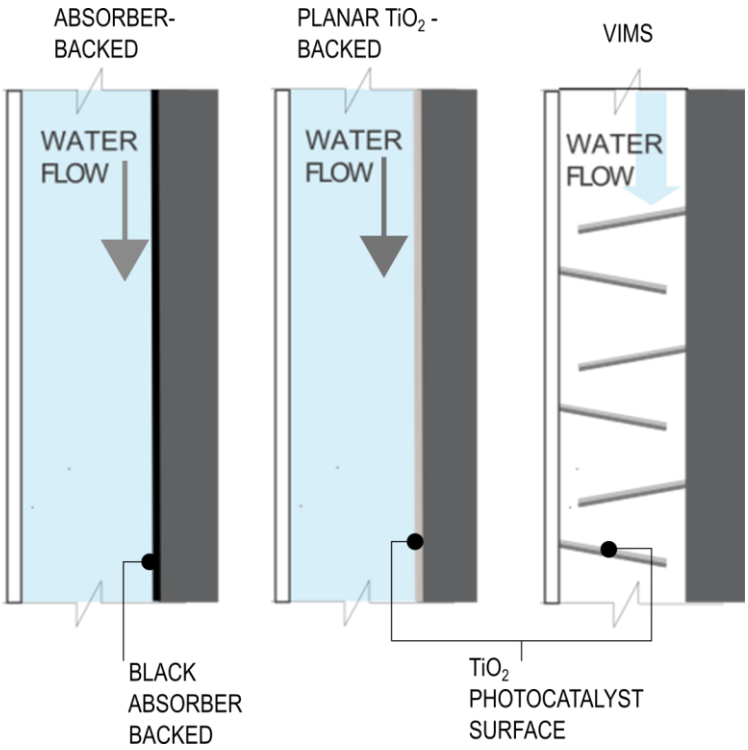

Figure 5.2. Reactor concepts experimentally characterized in this work. The black absorber-backed reactor, at left, includes no photocatalyst, while the planar TiO_2-backed and VIMS systems do include photocatalyst.

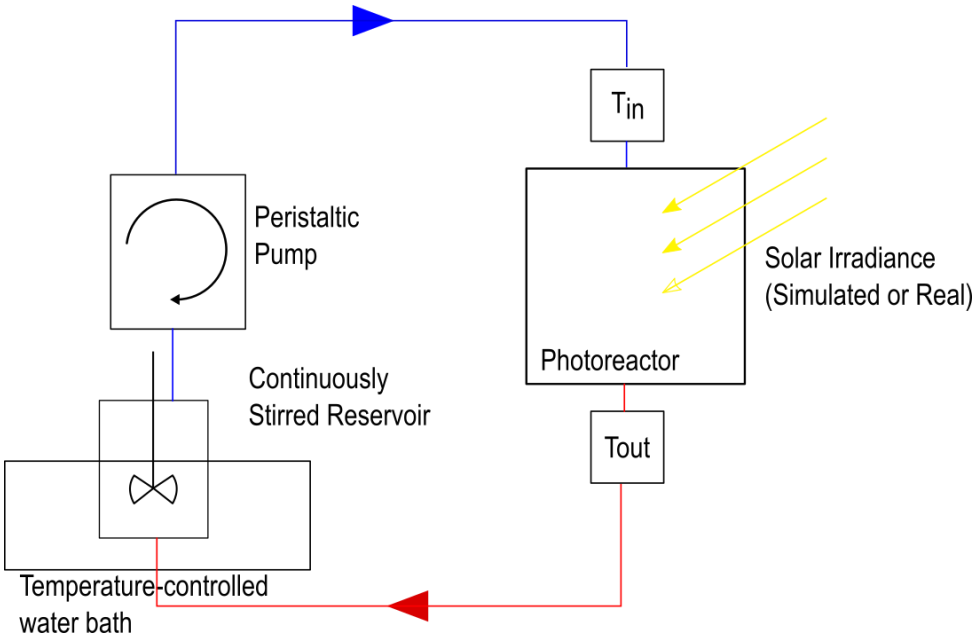

Figure 5.3. Solar PC-T experimental schematic. While the schematic shows a single photoreactor, real experiments consist of two to three reactors: two photoreactors at the subpilot scale, and three photoreactors at the laboratory scale.

Photoreactor Design and Experimental Protocol: Subpilot Scale

The black absorber, photocatalyst-backed, and VIMS systems were all constructed out of CNC-machined 6061 Aluminum. Front covers for each system consisted of PMMA sheet lasercut to fit the dimensions of the reactors, which exhibits 40% transparency in the UV region. Total collector area for each of the subpilot systems was 0.25 m^2, with collector dimensions of 50cm x 50cm. The depth of each panel was 2cm, for a total enclosed volume of 5L.

For the black absorber-backed system, black PMMA was bonded to the rear of the reactor. For the photocatalyst-backed system, a commercially-coated TiO_2 sheet (Reynobond EcoClean) was bonded to the back of the reactor. For the VIMS system, a cartridge design with each inclined step at 10 degrees from the horizontal was inserted into the reactor.

During operation, the absorber-backed and commercially-coated systems were filled with methylene blue solution, while the VIMS reactor accumulated minimal volume, involving thin film flow along inclined photocatalytic surfaces.

Subpilot reactors were setup on a south-facing building rooftop in Berkeley CA (10 ^{o} of S). 17.5 L of methylene blue solution of concentration 15-20 micromolar was used as the medium. Solar irradiance data was collected using a spectroradiometer (StellarNet

EPP2000) and a pyranometer (Kipp Zonen SPLite2). Flow rate was gravity driven, and ranged between .010 and .011 kg/s, or between .04 and .044 kg/(s $m^2_{collector}$). Recirculation of working fluid was driven by a peristaltic pump (Cole-Parmer MasterFlex). An example experimental setup in operation is shown in Fig. 5.4 and Fig. 5.5.

Figure 5.4. Solar PC-T experiments under real solar conditions at subpilot scale. Here, two photoreactors, VIMS (left) and the Planar TiO_2 (right) are in operation during a rooftop experiment in Berkeley, CA.

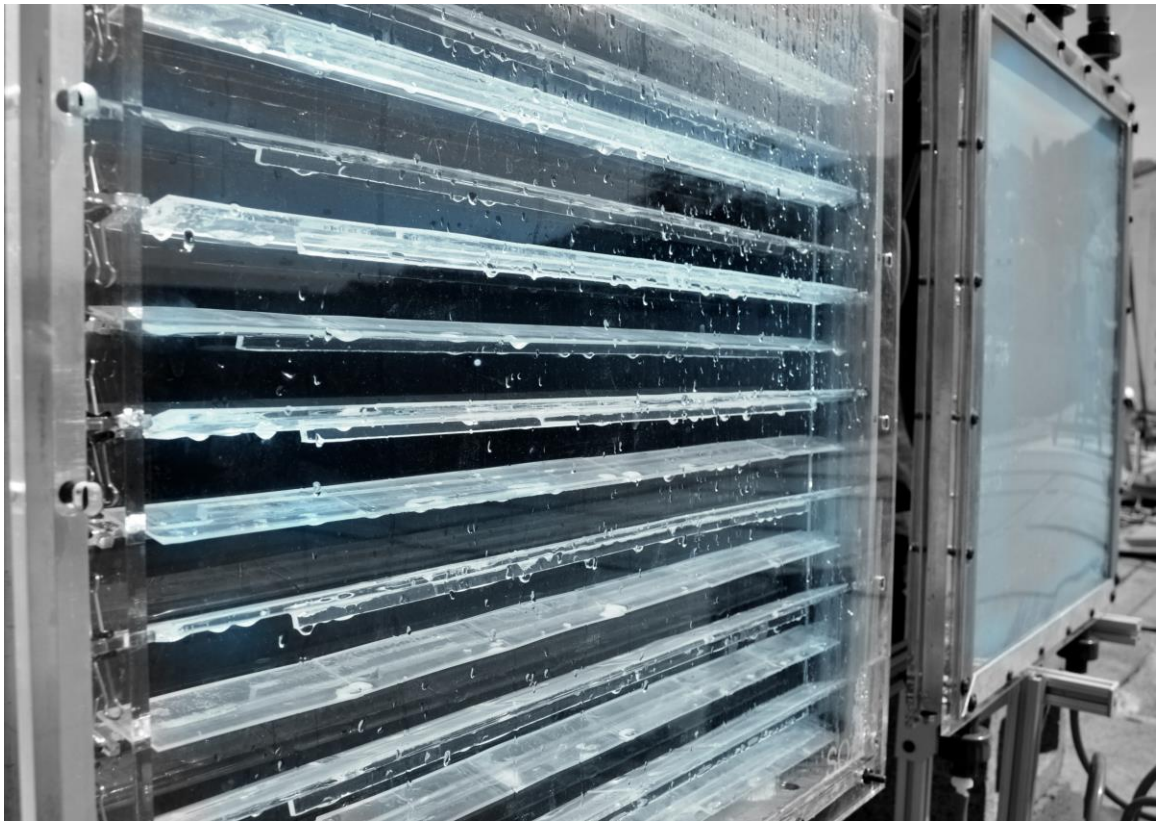

Figure 5.5. Close view of VIMS and Planar TiO_2 system. VIMS (left) and the Planar TiO_2 (right) are in operation during a rooftop experiment in Berkeley, CA, showing methylene blue flow pattern in VIMS.

To measure thermal efficiencies, input, output, and ambient temperatures were measured using wireless thermal data loggers (HOBOWare), and logged at 10s intervals. Input temperatures were controlled by a heater/chiller (ANOVA R10) set up in a heat exchange loop with the working fluid. The instantaneous thermal efficiency η_g is described in Eq. 5.1 & 5.2:

$$\eta_g = \left(\frac{A_a}{A_g}\right) F_R \left[(\tau\alpha)_e - U_L \frac{(t_{f,i} - t_a)}{G_t}\right] \tag{5.1}$$

$$\eta_g = \left(\dot{m} C_p (t_{f,e} - t_{f,i})/A_g G_t\right) \tag{5.2}$$

with A_g the collector area, G_t, the irradiance, m the mass flow rate of the working fluid, C_p the specific heat of the working fluid, and $t_{f,e}$ and $t_{f,i}$ the steady-state outlet and inlet temperatures, respectively. In equation 5.1., F_R is the heat removal factor, U_L is the loss

coefficient representing environmental losses during collector operation, and $\tau\alpha_e$the transmissivity and absorption of front cover material.

As the goal of collector characterization is to relate overall collector thermal efficiency to variables that can be predicted based on historical or simulation data – inlet temperature, ambient temperature, and irradiance – expression 5.1 can be reformulated as a linear equation with one independent variable, as follows:

$$U = F_r U_L (\frac{A_a}{A_g}) \tag{5.3}$$

$$\eta_g = U\left(\left(t_{f,i} - t_a\right)/G_t\right) + b \tag{5.4}$$

with the $\left(t_{f,i} - t_a\right)/G_t$ term acting as the independent variable. By fitting experimental data to this equation, estimates of the net loss term *U* can be made, and used to predict collector performance under a broader range of solar and thermal conditions.

To measure photocatalytic oxidation of methylene blue solution, triplicate 5mL samples of working fluid were taken at 10-minute intervals following a 20-minute no-sampling period, to control for the effect of adsorption in photocatalytic reaction rate. Samples were analyzed in a spectrophotometer (HACH DR2400) to measure absorption at the 665 nm wavelength. Absorption values were used to develop a pseudo first-order photocatalytic rate, as described in Section 2.3.

Photoreactor Design and Experiments: Laboratory Scale

For the laboratory-scale experiments, the black absorber, photocatalyst-backed, and VIMS systems were all constructed out of CNC-machined 6061 Aluminum. Front covers for each system consisted of specialized UV-transmitting PMMA sheet (Solacryl, Spartech Polycast) at 1/8" thickness, lasercut to fit the dimensions of the reactors. This cover material exhibits >70% transparency in the UV region. Total collector area for each of the laboratory systems was .0155 m^2, with collector dimensions of 3 in x 8 in. The depths of the absorber- and TiO_2-backed panels were both 5 mm, while the VIMS system had a depth of 40mm to accommodate the VIMS cartridge (see below). All reactors were sealed with an o-ring clamped between the PMMA cover and aluminum body. Reactors were mounted in building-grade rigid closed-cell expanded polystyrene foam insulation (InsulFoam R-Tech) with an R-Value of 5.78. CNC machining was used to create close-fit pockets in the insulation for each reactor, ensuring maximal contact between the insulation and aluminum surface. A fan was mounted and run to ensure air flow of 1-2 m/s across the front cover of each reactor.

For the black absorber-backed system, black PMMA was bonded to the rear of the reactor. For the photocatalyst-backed system, glass slides coated with immobilized TiO_2

films were mounted in a planar configuration to cover the entire back surface. For the VIMS system, a cartridge design with each inclined step at 15 degrees from the horizontal was inserted into the reactor, with each step including a TiO_2-coated glass slide. For both TiO_2 systems, the coating procedure was as that in Section 3.2. The experimental setup for laboratory-scale work is shown in Fig. 5.6.

Figure 5.6. Solar PC-T experiments under simulated solar conditions at laboratory scale. Here, three photoreactors, Planar TiO_2 (left), VIMS (center), and Absorber-backed (right) are in operation under simulated solar irradiance in a laboratory setting. All three reactors are housed in a tight-fit insulation manifold.

As in the subpilot scale experiments, during operation, the absorber- and TiO_2-backed systems were filled with solution during operation. The VIMS system was subject to thin film flow across its photocatalytic surfaces.

Laboratory experiments were conducted under a xenon-arc lamp solar simulator (ATLAS SunTest XLS+) angled at 55 degrees from the horizontal, to simulate afternoon solar conditions on a west-facing façade. A volume of 200 mL of methylene blue solution of concentration 20 micromolar was used as the medium. Solar irradiance data was collected using a spectroradiometer (StellarNet EPP2000). As the arc lamp outputs a spatially varying irradiance field, especially owing to the angle of inclination, irradiance

was measured at 9 points across each reactor, and integrated to develop an average W/m^2 irradiance for each reactor.

Flow rate was driven by a peristaltic pump (Cole-Parmer MasterFlex). Due to significant differences in hydraulic resistance between the three reactors, the mass flow rates for each were somewhat different. The black absorber-backed system had a mass flow rate of 0.0022 kg/s, or normalized for collector area, 0.1398 kg/(s m^2); the TiO_2-backed system had a mass flow rate of 0.0018 kg/s, or 0.1161 kg/(s m^2); and the VIMS system had a mass flow rate of 0.0026 kg/s, or 0.1677 kg/(s m^2).

To measure thermal efficiencies, input, output, and ambient temperatures were measured using platinum resistance temperature detectors (ProtoVoltaics PT100) connected to a microprocessor (Arduino) with 24-bit analog-to-digital converter (ProtoVoltaics RTD). A custom setup using RTD's was selected for fast and repeatable temperature measurement. Temperature was measured and logged at 6-second intervals. Input temperatures were controlled by a heater/chiller (ANOVA R10) which supplied a water bath, in which recirculating working fluid was returned. This ensure a consistent steady-state inlet temperature for a given experiment. The experiment was run with collector area covered by aluminum foil for 30 minutes to allow the system temperature to increase by any external effects, and to control for adsorption (see below).

To measure photocatalytic reaction rate, triplicate samples of 3.5 mL were taken at 30-minute intervals. During the first 30-minute period, the collector area was blocked by aluminum foil to create 'dark' conditions for the reaction, ensuring that adsorption of dye onto the TiO_2 surface would not affect overall photocatalytic reaction performance. Afterwards, the foil was removed, and samples were taken at 15-minute intervals for the first hour of the experiment, and 30-minute intervals thereafter. Sample absorbance at 665nm was measured in a spectrophotometer, and then samples were returned to the mixing reservoir. Absorbances were used to calculate concentrations, which were formed the bases of pseudo-first order reaction rate calculations (see Chapter 3).

5.3 Results and Discussion

Outdoor Experiments

Outdoor experiments yielded data with very high error and noise, from which it was difficult to develop high-confidence conclusions (Fig. 5.7). The black absorber-backed panel, Fig. 5.7a, demonstrated thermal efficiencies between near-zero and 0.4, and, as there was no photocatalyst present, produced no photocatalytic reaction.

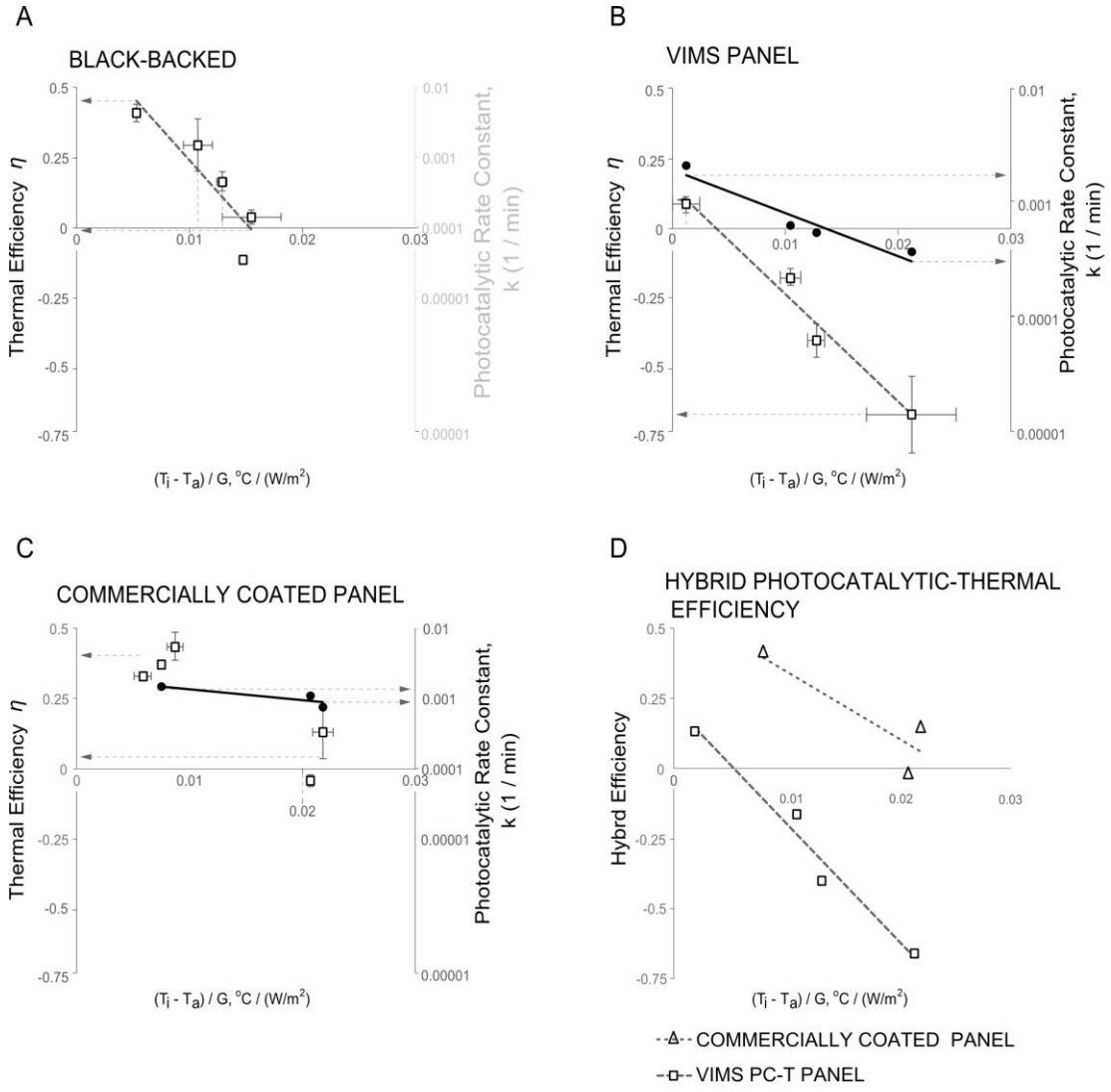

Figure 5.7. Thermal efficiencies, photocatalytic performance, and hybrid efficiency of PC-T systems. Thermal and photocatalytic performance for each panel design (a-c) are presented. Dashed lines represent thermal efficiency linear fits, while solid lines represent photocatalytic reaction rate constant for methylene blue degradation. A hybrid efficiency term is proposed (Eq. 3) and applied to each reactor (d), indicating that the commercially coated design offers the most promising PC-T performance.

The VIMS system in the outdoor configuration demonstrated poor thermal efficiencies, between -0.75 and 0.125 (Fig. 5.7b). These results suggests that for the majority of inlet temperatures, ambient, and solar conditions, incoming methylene blue leaves the system at a cooler temperature than which it enters. Thus, VIMS' design is quite unsatisfactory

as a system for solar thermal gain. However, as it involves photocatalyst on each step surface, degradation of methylene blue dye was demonstrated, interestingly with a declining relationship between photocatalytic reaction rate and increasing (T_i - T_{amb}) / G term. As increasing T_i would indicate a higher reaction temperature, and thus, a higher reaction rate, this result is driven by ambient temperature, T_a, and G, solar irradiance. Increased solar irradiance has a linear relationship with photocatalytic reaction rate, and thus, higher values of the x-coordinate suggest lower light intensities.

The commercially-coated TiO_2 panel (Fig. 5.7c) showed consistently positive thermal efficiencies, ranging from near-zero to 0.5. The clustering of data in the plot makes the thermal results poor grounds for observing a trend. The commercially-coated panel showed photocatalytic reaction performance, with less sensitivity to the x-coordinate – values were consistently near 0.001 min^{-1}.

In an attempt to evaluate the effectiveness of both operating modes – thermal and photocatalytic – with a single term, a 'hybrid efficiency' is developed. This is inspired by the PV-T community, wherein multiple approaches have been developed combine two disparate outputs – thermal energy and electrical energy – into a single numerical valuable. Notable work has quantified hybrid performance with a variety of metrics, from economic or environmental value [207] to exergy [208]. The purpose of our hybrid efficiency term is not to necessarily assign value, but to simply quantify and compare PC-T systems. Accordingly, as a first step, based on an efficiency approach [209], we propose a hybrid efficiency:

$$\eta_{hybrid} = \eta_{thermal} + C_k * k_{photocatalytic} \tag{5.4}$$

With $\eta_{thermal}$ the calculated thermal efficiency, $k_{photocatalytic}$ the pseudo-first order reaction rate, and C_k a scaling parameter to bring the two values into the same order of magnitude. Given that thermal efficiencies will operate between 0 and 1, C_k is here set to a value of 500 based on the range of $k_{photocatalytic}$ we reported. This value of C_k is acknowledged as somewhat arbitrary, a more thorough argument for hybrid efficiency, grounded perhaps in economic impact or exergy, would be better-suited to this evaluation. Because the nature of quantifying the comparative exergy of clean water and hot water makes little sense, a detailed economic analysis is required.

Nonetheless, we use Eq. 5.4 to describe hybrid performance of the system (Fig. 3d). Based on our proposed model, we see that the commercially coated system is categorically more efficient than VIMS across the range of studied x-coordinates.

The level of data uncertainty and the generally poor performance of the systems as thermal collectors – dedicated solar thermal collectors can operate in the 0.8 – 0.9 range, and hybrid PV-T systems can demonstrate thermal efficiencies above 0.7 – suggest that significantly more work is needed in terms of design and optimization to achieve meaningful impact through PC-T systems.

Given the significant error, several research and development opportunities were identified from these results within the flat-panel (e.g. non-concentrating) geometry. First, a front cover panel material that consists of UV-transmitting plastic is essential. Minimal transmission of UV, of roughly 40%, was observed in the experimental system. Replacing that with commercially-available UV-transmitting plastic, which can transmit 70-80% of UV light, could double photocatalytic reaction rate and reveal more meaningful trends.

Second, insulation of the entire system is essential, and realistic. Real solar thermal collection systems are heavily insulated, as would be any system embedded in a building envelope. Exposure to real solar conditions in an outdoor environment introduced significant losses and sensitivities that may have compromised some experimental data, and certainly limited the thermal efficiency potential of the prototype systems. Insulation here means both building insulation to surround the non-collecting surfaces of the reactor, minimizing radiative loss beyond the cover, but also front cover insulation, such as a double glazing or double-panel with vacuum gap [23]. Approaches to front cover insulation, however, need to be carefully characterized to ensure they do not adversely affect light transmission for photocatalytic water treatment.

Third, characterizing the system in a more tightly controlled context, with consistent environmental losses, is necessary to get a clearer understanding of the system's properties.

Laboratory Experiments

Several of the shortcomings of the subpilot-scale outdoor experiment were addressed in the design of the laboratory experiments. Insulation, UV-transmitting plastic, and consistent irradiance and environmental conditions were all realized (see Section 5.3).

For clarity of review, photocatalytic treatment performance has been separated from thermal results in the follow analysis. Thermal efficiencies (Fig. 5.8) are developed for each PC-T system. There are several salient observations from these data. First is the observation that the black absorber and planar TiO_2 perform similarly in terms of thermal efficiency for given experimental conditions. We observed both systems to have peak thermal efficiencies of roughly 0.75. This has an interesting implication for PC-T system design, as it implies that the TiO_2 surface and methylene blue liquid column are as effective at absorbing light as thermal energy as the black PMMA backing and blue liquid column. This is surprising, as the TiO_2 surface is bright white in color, suggesting high levels of light scattering. Aside from the backing material and some slight hydraulic differences, the absorber and planar TiO_2 systems are identical.

Second is the poor thermal performance of the VIMS system, as in the outdoor pilot experiments. This is borne out by the data, which largely show the VIMS system having negative efficiency (cooling influent water) except when the

abscissa value is less than zero – meaning that the ambient temperature is greater than the input temperature, and thus not a useful test case for the system. These results indicate that while VIMS performs poorly as a hybrid PC-T system, the planar TiO_2 and black absorber show promising performance. VIMS demonstrates high losses (as approximated by the slope of the linear best-fit line), suggesting that this performance continues under conditions corresponded to greater abscissa values. The planar TiO_2 and black absorber systems show markedly less dramatic slopes, suggesting their system losses are much lower than that seen in VIMS.

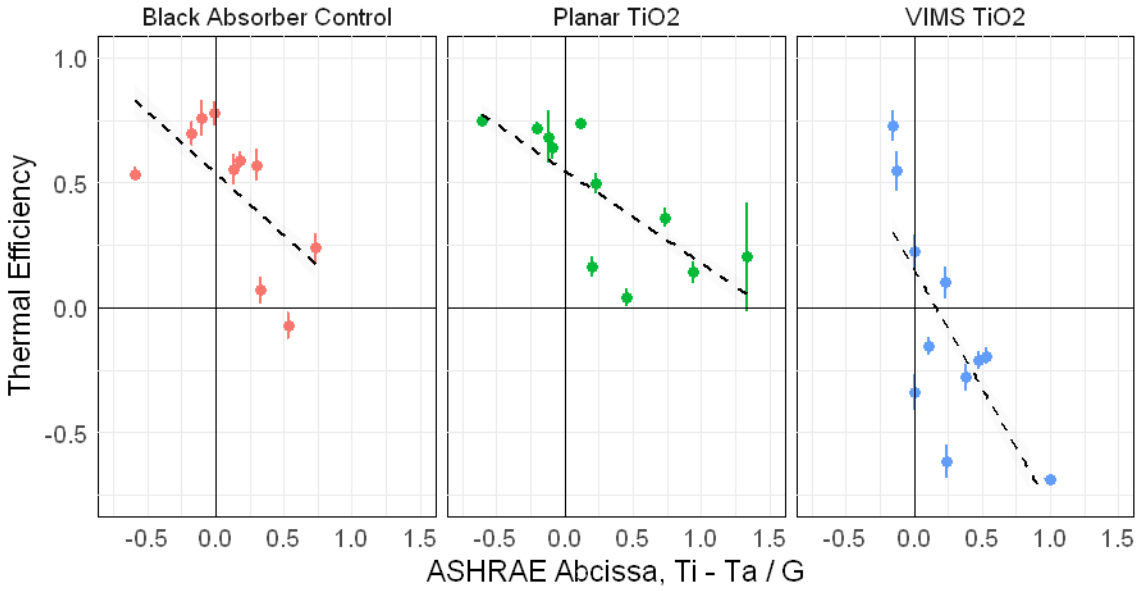

Figure 5.8. Thermal efficiencies plotted against the ASHRAE abscissa term. Thermal performances for each panel design are presented. Dashed lines represent thermal efficiency linear fits.

Photocatalytic reaction rate is shown to have a roughly linear relationship with the ASHRAE abscissa term (Fig. 5.9). As these experiments were conducted under constant irradiance for each reactor, the key parameter governing the increasing ASHRAE abscissa term will be T_i, the steady-state inlet temperature (Fig. 5.10). Together, these trends agree well with established photocatalytic reaction engineering principles, in that an elevated reaction temperature yields elevated reaction rate. While the VIMS system demonstrates higher overall average reaction rate, and greater sensitivity to the ASHRAE abscissa value, the planar TiO_2 system demonstrates comparable reaction rates across abscissa values, with less sensitivity to ASHRAE abcissa. As expected, the black absorber system demonstrated no photocatalytic reaction, as there was no photocatalyst present.

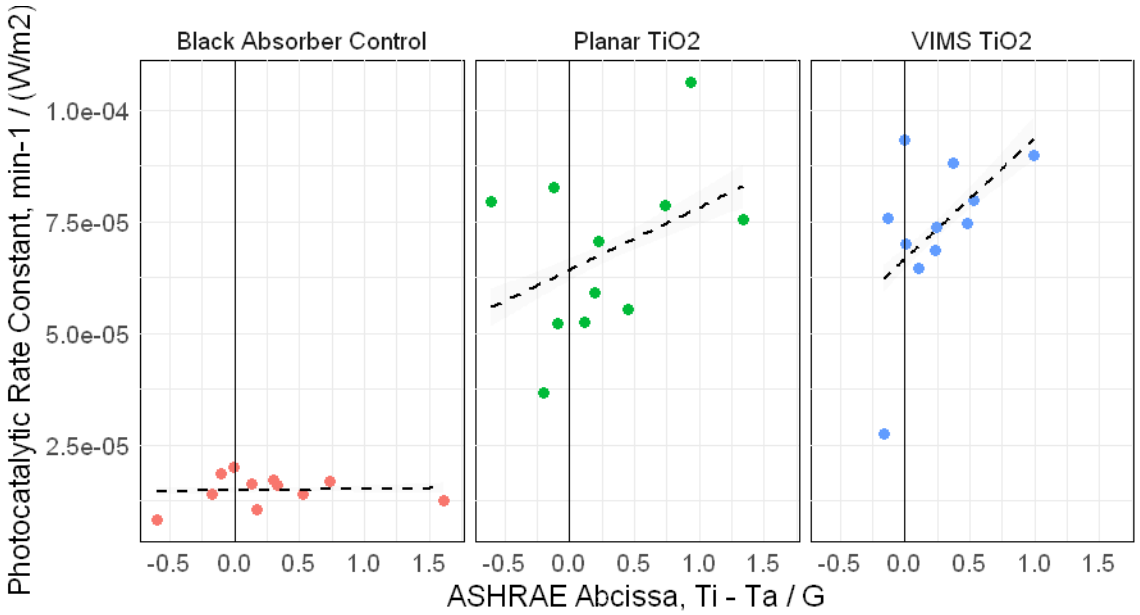

Figure 5.9. Irradiance-normalized Photocatalytic rate constants plotted against the ASHRAE abscissa term. Photocatalytic rate constants are plotted against the ASHRAE Abcissa term. Dashed lines represent linear fit to photocatalytic rate constant.

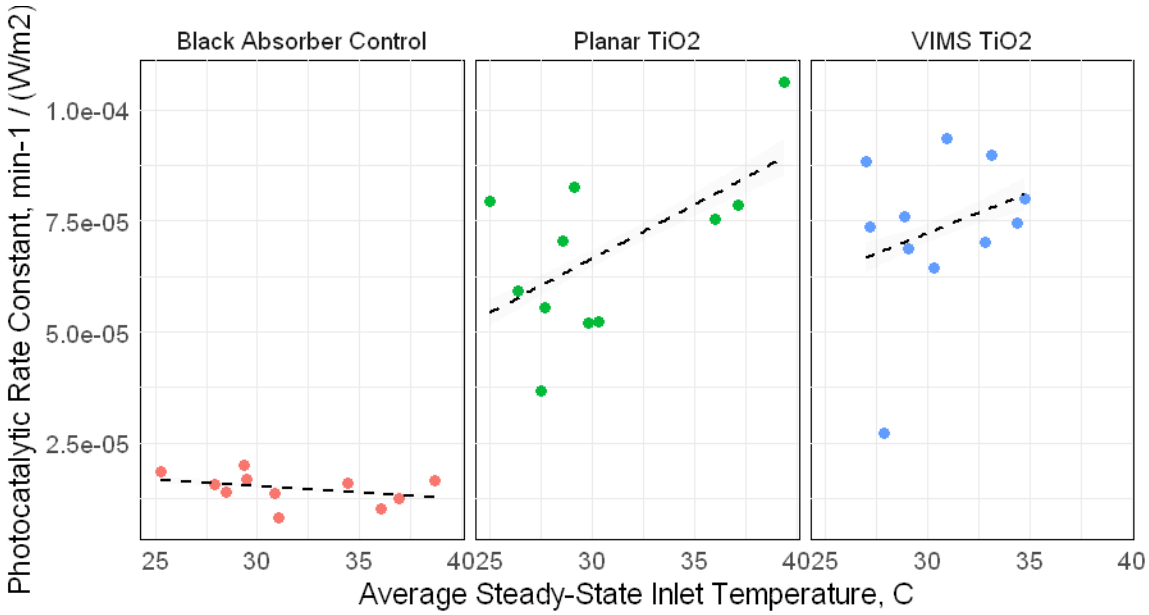

Figure 5.10. Irradiance-normalized photocatalytic rate constants plotted against the average steady-state inlet temperature.
Photocatalytic rate constants are plotted against the inlet temperature. Dashed lines represent linear fit to photocatalytic rate constant.

Most striking about the results of the photocatalytic reaction performance and thermal efficiency is their demonstration of opposite trends. While photocatalytic rate constants increase with increase ASHRAE abscissa values, thermal efficiency decreases. This suggests a fundamental trade-off between these two parameters, an observation which makes mechanistic sense. Thermal efficiency is a measure of the system's ability to absorb energy in the form of a temperature increase in the working fluid, relative to the input irradiance energy. This is enhanced at lower inlet temperatures relative to ambient conditions – the system is more likely to absorb energy due to minimal losses. At temperatures $T_i > T_a$, the system is more likely to experience losses to the environment. Photocatalytic reaction rate, however, is dependent solely on input temperature. Thus, plotting photocatalytic reaction rate versus thermal efficiency (Fig. 5.11) reveals a roughly linearly-descending relationship between the two. This makes the principle of hybrid PC-T operation more complicated, as system operators and designers must trade-off between maximizing thermal gain and achieving photocatalytic treatment in their choice of system.

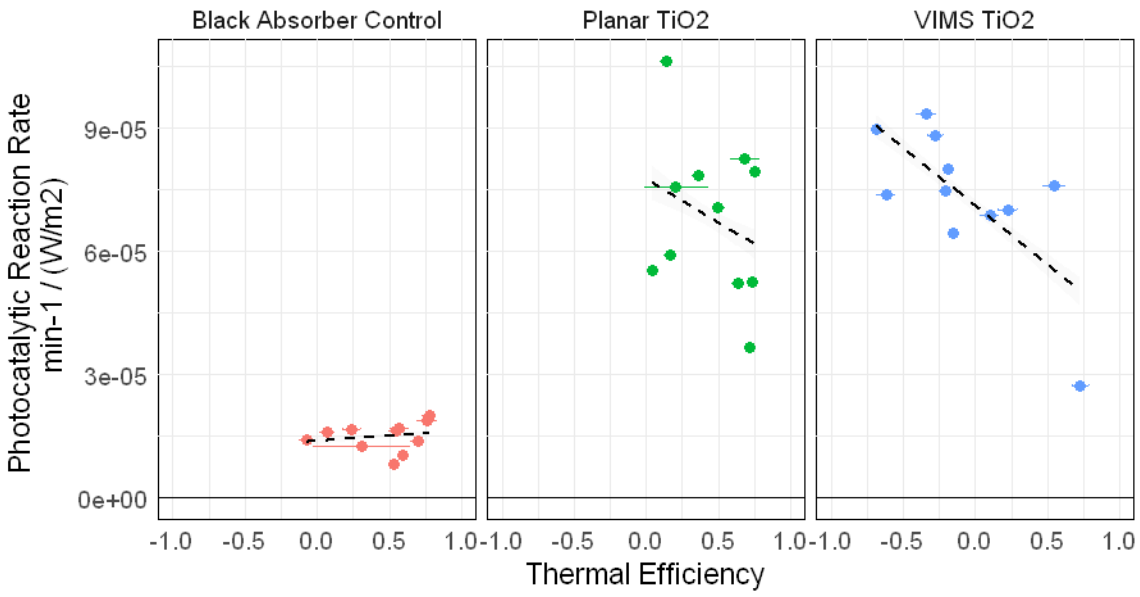

Figure 5.11. Irradiance-normalized photocatalytic reaction rate plotted versus thermal efficiency. Dashed lines indicate a linear fit.

This tradeoff is already substantially constrained by realistic operating temperatures of a greywater treatment system. While domestic water use temperatures destined for greywater range between 35° and 45° C for bathroom water, and up to 70° C for laundry water [210], by the time usage has occurred, the greywater temperature can drop between 0-8° C, depending on the use [211]. Assuming a 4° C temperature drop, operating temperatures for greywater systems will be, at a minimum, ~30° C. This suggests that in the context of these experimental results, reaction temperatures will be high. The challenge will be in achieving incremental heat gain above a relatively high working fluid input temperature. As observed from Fig. 5.7, systems report their lowest thermal efficiencies at the highest operating temperatures, and this trend is further explicated by the observed low temperature increase at higher operating temperatures, Fig. 5.12. This suggests that losses in the system need to be much more tightly managed, as will be discussed at the end of this section: heat transfer away from the working fluid temperature outweighs the energy gained by solar irradiance.

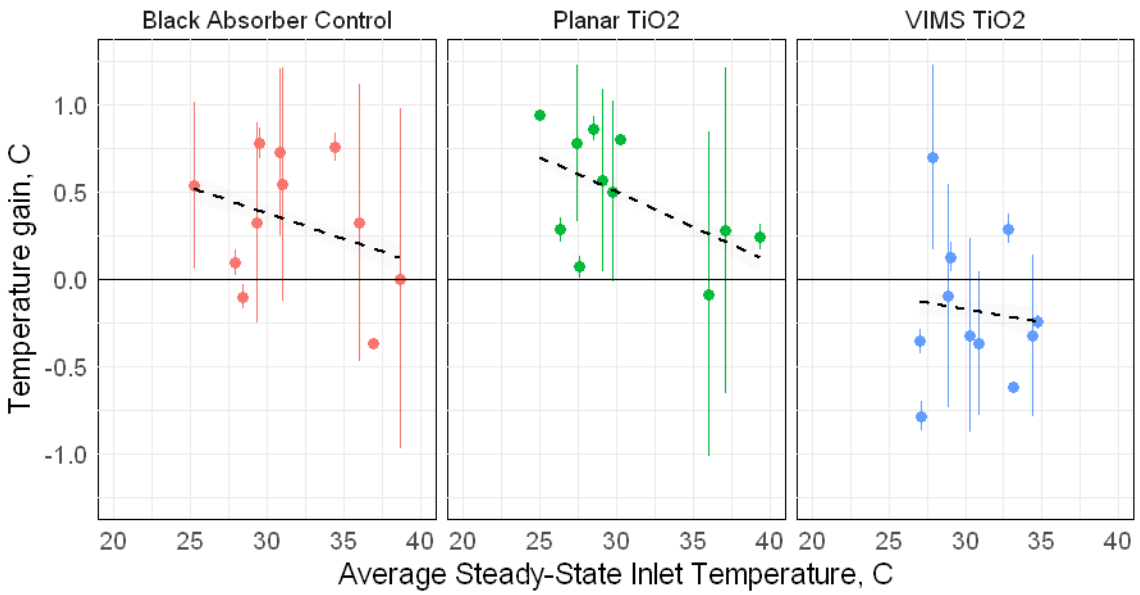

Figure 5.12. Temperature gain plotted versus steady-state inlet temperature. Net temperature gain across the photoreactor are plotted versus average steady-state inlet temperature.

These results thus indicate that simultaneous realization of solar thermal collection and solar photocatalysis is possible. Furthermore, as would be expected, we see a clear trend of thermally enhanced photocatalysis: at higher temperatures, there is a significantly enhanced photocatalytic reaction rate. Rather than extending on previous analyses on thermally-enhanced photocatalysis to establish a clear operating guide for hybrid PC-T operation, these findings complicate the realization of a hybrid PC-T system, as thermal efficiency and photocatalytic reaction rate are revealed to operate in opposition.

Thus, several further research directions are proposed from these findings. First, thermal performance needs to be enhanced, beginning with insulation of the entire PC-T system. As mentioned previously, vacuum-gap insulation for the front cover [23], along with careful analysis of the implication of such insulation for light capture in the system, is essential. Similarly, maximally-performing insulation of other surfaces of the system are crucial, although under certain climactic conditions, it may be beneficial to have good heat exchange between PC-T systems and the building envelope to provide heat transfer away from the building interior. These will help minimize system losses observed in these experiments.

If insulation helps decrease system losses, a secondary approach to enhancing thermal performance is to increase in the incident radiation on the system. Characterizing a compound parabolic collector (CPC) photoreactor for simultaneous thermal gain and treatment would provide a valuable benchmark for such systems. Lee's work [156] shows the promised thermal enhancement of a hemispherical microlens array, which points to

the range of possibilities for concentrating solar irradiance to enhance thermal performance in façade-integrated systems.

Extending on thermal performance, it is important to note that in the U.S. re-use regulations are predicated on coliform bacteria counts [61]. Solar thermal pasteurization offers an approach to inactivate bacteria present in greywater, potentially in a continuous flow operating mode [212]. With further thermal performance enhancement, a PC-T system could reach appropriate temperatures for sufficient time for pasteurization, while simultaneously destroying pollutants through photocatalysis.

Second, photocatalytic water treatment performance can be enhanced in several ways. As these experimental results show minimal process intensification owing to the VIMS design, a planar-TiO_2 system could be considered a baseline for such systems. Proposed reactor designs to intensify reaction rate through enhanced light capture, such as a fiber optic cable-based system [213], could be revisited with a lens for hybrid PC-T performance. Another approach would be to integrate advanced photocatalysts, engineered to drive photocatalysis under a broader range wavelengths of light (e.g., visible) [87] [214]. As in any photocatalytic reactor system, enhancing light transport and broadening the photocatalyst's light activation spectrum would lead to more successful PC-T systems.

Third, a careful understanding of some of the tradeoffs inherent in a PC-T system on an annualized and localized basis is needed. Tradeoffs in PC-T operation will exist because of the inherent variability of several key operating parameters: ambient temperature, solar irradiance, and environmental losses. All vary substantially with time and location, and thus, the annualized and localized performance of such systems must be carefully understood.

Finally, as proposed by Coventry [207], a net economic analysis that quantifies the value of domestic hot water and water treated to nonpotable re-use standards is needed. A true levelized cost analysis is complicated by the fact that capital and installation costs for a façade-integrated system are difficult to estimate. Nonetheless, a rigorous study of the net value created by a hybrid PC-T system, beyond metrics of water treatment and thermal efficiency, is needed.

5.4 Conclusions

In this work, the first characterization a hybrid solar PC-T system for simultaneous greywater treatment and solar thermal collection is reported. Experimental studies of immobilized TiO_2-based PC-T photoreactors in bulk flow and thin film cascade configurations were performed, and compared to a control black-absorber based system. Characterizatoin was performed in both outdoor sunlight conditions, and under simulated solar light. Results indicate that there is an inherent tradeoff between photocatalytic reaction performance and overall thermal efficiency of the system. This tradeoff is driven by the thermal enhancement of photocatalysis, which is dependent on steady-state working fluid temperature, and the sensitivity of thermal efficiency to heat transfer losses

to the environment, which are exacerbated by higher operating temperatures. Thus, while synergistic heating and treating of water is realized here, this work highlights research opportunities to identify an optimal operating profile for PC-T systems.

6. Conclusions & Future Research Directions

Water scarcity, already a reality in many local regions of the world, will become a global challenge by 2050, with substantial populations unable to access sufficient water. Solutions to address water scarcity, however, must do so under the parallel driving forces of urban population growth, climate change, and the food-energy-water nexus. Significant effort has been invested in developing frameworks for future water systems - David Sedlak calls this 'Water 4.0,' and Peter Gleick refers to it as the 'Soft Path' [17] – but regardless of the specific framework, future interventions and solutions to water scarcity must be sensitive to the driving forces that accompany it.

This thesis has proposed one solution to help offset challenges: building façade-integrated systems for solar photocatalytic greywater recycling and solar thermal gain. The proposed system decentralizes water recycling to the building scale, uses solar energy for operation, and promises to offset the energy demand of the building. This chapter summarizes the key findings of the dissertation and proposes future research opportunities for each key research activity.

6.1 Summary

To realize a façade-integrated solar photocatalytic water recycling and solar thermal gain system, several findings were needed. First, a careful understanding of the optical properties of the greywater matrix were necessary in order to optimize photo-dependent treatment methods, like photocatalysis. Second, an understanding of the relationship between hydrodynamics, solar irradiation, and system design parameters, as described by the inclined plate reactor, were prerequisite to designing an effective treatment system. Third, a new reactor concept that could integrate easily with the constraints of the building façade – specifically, a thin profile and vertical orientation - was required. Fourth, and finally, the relationship between simultaneous solar thermal collector efficiency and solar photocatalytic treatment was a substantial unknown, and required characterization. This dissertation aimed to offer new insight and experimental research findings to resolve all of these requirements.

In Chapter 2, I showed that greywater exhibits high absorbance in the UVA/B range but low absorbance per mg/L COD or soluble COD. This diverged significantly from the optical characteristics of many published synthetic greywater recipes, which were characterized in this chapter. These results underlined that careful consideration of optical path length in photodependent treatment methods is crucial in recycling domestic greywaters, and have significant implications for the design of photo-dependent treatment reactors.

In Chapter 3, I experimentally showed that inclined plate photocatalytic reactor performance, as described by decolorization of methylene blue under simulated sunlight, is governed by light intensity and light capture rather than hydrodynamics and mass transfer. This is despite the fact that two are tightly coupled through the design parameter

of inclination angle. This result suggests that photocatalytic reactor designers must give light transmission and capture a significant premium in the consideration of their system design.

In Chapter 4, I proposed a new photocatalytic reactor design concept, the vertically integrated multistep (VIMS) reactor, to realize water re-use within the envelope of the building façade. VIMS, essentially a sequential series of inclined plates, was shown to effectively decolorize methylene blue under real solar conditions in Berkeley, CA. Based on solar photocatalytic reactor modeling, I showed that a $9m^2$-scale VIMS system could treat up to 60L of methylene blue solution per day, although performance is highly sensitive to variations in solar intensity, and the proxy of methylene blue for greywater requires further validation.

In Chapter 5, I experimentally characterized simultaneous solar photocatalytic water treatment and solar thermal gain in the VIMS system and a simple flat-plate façade collector. These results are the first demonstration of simultaneous solar thermal collection and solar photocatalysis, and show that the relationship between the two phenomena is inverse. However, given the temperature profile of typical domestic greywater, there is strong potential for synergy between energy capture from sunlight and greywater, and greywater re-use.

6.2 Future Research Directions

This dissertation intended to fill key gaps in knowledge necessary to realize a façade-integrated solar photocatalytic water recycling and solar thermal gain system. Along the way, several research questions arose that could not be resolved in the scope of the dissertation work, and were deemed important for furthering the specific field assessed in each chapter. These included, for example, understanding the relationship between surface waves, aeration, and reaction performance in an inclined plate reactor. Such questions that extend immediately from the completed research are described at the conclusion of each chapter.

Several larger questions beyond the immediate research results from each chapter invite deeper inquiry, and three of these questions are the focus of this section.

6.2.1 Technoeconomic and Spatial Analyses of Photocatalytic-Thermal and Building Façade Systems

This thesis has focused on technology development for the built environment, with some implications for impact at the building-scale. Unanswered, however, are broader questions about the potential local, regional, national, and global impacts of such a technology, benchmarked against existing solutions to energy and water challenges. Thus, technoeconomic and spatial analyses of the performance of solar photocatalytic-thermal systems are necessary. This is all the more crucial as city block-scale wastewater

thermal harvesting and building-scale water recycling enter commercial deployment. A framework to clarify when and where photocatalytic-thermal technology can make a difference is essential.

6.2.2 Building-Integrated Platforms for Advanced Materials and Functionalities

This thesis has been focused on using conventional, readily available titanium dioxide nanomaterials deployable with room-temperature methods (as opposed to cleanroom approaches). This approach came with the tradeoff that efficiencies of TiO_2 photocatalysts are very low, owing to the wide band gap of the semiconductor. As rapid advances in materials science continue, however, large numbers of new photocatalysts, coating methodologies, and other innovations are being reported. The system described in this thesis is an ideal platform for integrating water and energy technologies into the built environment, and can be viewed generally as a carrier of materials technology.

This lends itself to two evident research directions. The first is to understand the performance and opportunities presented by novel photocatalysts into solar-photocatalytic systems. Particularly exciting is the possibility of coupling bandgap-engineered photocatalysts that accept visible light with tunable plasmonic materials that can lead to selective heating – involving specialized materials to more effectively drive water treatment and water heating.

The second is to explore what other types of technologies can be advantageously integrated into panelized systems for building facades. There are myriad possibilities, and some examples include dye-sensitized solar cells, microbial bioreactors for various sustainability applications, and engineered hydroponics or living walls. This thesis has shown the potential of building-façade integrated systems for realizing a more sustainable environment; further research can investigate how a platform like this could be extended into other functionalities.

6.2.3 Design Integration for the Building Scale

Significant research opportunity remains around the architectural and urban integration of such systems. This thesis used the constraints of the building façade to design the system and consider inputs and outputs, but stopped short of integrating such systems into the larger building. Four research areas present promising directions of inquiry here.

First, understanding the opportunities and tradeoffs of integration at the building-scale – for example, considering the energy and cost implications of dual-piping a building, pumping water throughout a high-rise, and other integration and operational questions – are crucial to move forward.

Second, control strategies to include water recycling systems into a larger building management system are necessary, as emergent benefits to sustainability could arise from controlling energy, HVAC, lighting, and other building systems in tandem.

Third, a coupling of other key solar-dependent building systems with the proposed platform offers significant opportunities for further research. For example, coupling daylighting, insulation / HVAC, or other building functions with the proposed façade-integrated photocatalytic-thermal system could enable a more favorable case for building integration.

Fourth, a key part of integration not yet considered is architectural design integration – the implications of a panelized façade system for overall building appearance and design. A research investigation with architectural designers to revisit the shape and design constraints of the photocatalytic-thermal system would lead to system that is more favorably integrated with designers' workflow – and ultimately, could be adopted not just for its desirable performance, but its desirable aesthetics, as well.

Fifth, and cutting across all research directions mentioned thus far, are the close adoption of multi-scalar simulation and modeling tools in the design and development of novel building systems. While the building science field has been a ready adopter of advanced simulation software, often times this modeling exists solely at the building scale. To truly advance the field into new areas of impact, simulations of nano-scale phenomena must be coupled up to regional-level implications, and simulation and modeling can move from analytical tools to act as decision support and direction for policy and implementation.

Sixth, and finally, a framework for unifying design and research and development practices across the nascent building science and engineering research community is necessary. As the field expands from interventions in control strategies and building simulation to include the design and development and characterization of novel research-based systems, best practices for collaboration between architectural designers, engineering designers, and scientific researchers should be explored and established.

References

[1] K. Watkins, “Human Development Report 2006 - Beyond scarcity: Power, poverty and the global water crisis,” 2006.

[2] UNESCO, “The United Nations World Water Development Report 2017. Wastewater. The Untapped Resource.,” 2017.

[3] 2030 Water Resources Group, “Charting Our Water Future,” 2009.

[4] S. L. Postel, “Entering an Era of Water Scarcity : The Challenges Ahead,” vol. 10, no. 4, pp. 941–948, 2015.

[5] M. Tran, E. Koncagul, and R. Connor, “Water and jobs: facts and figures,” 2016.

[6] F. R. Rijsberman, “Water scarcity: Fact or fiction?,” *Agric. Water Manag.*, vol. 80, no. 1–3 SPEC. ISS., pp. 5–22, 2006.

[7] T. P. Barnett, J. C. Adam, and D. P. Lettenmaier, “Potential impacts of a warming climate on water availability in snow-dominated regions,” *Nature*, vol. 438, no. 7066, pp. 303–309, 2005.

[8] A. Hunt and P. Watkiss, “Climate change impacts and adaptation in cities: A review of the literature,” *Clim. Change*, vol. 104, no. 1, pp. 13–49, 2011.

[9] World Bank, “Fossil Fuel Energy Consumption,” 2017.

[10] J. A. Elias-Maxil, J. P. Van Der Hoek, J. Hofman, and L. Rietveld, “Energy in the urban water cycle: Actions to reduce the total expenditure of fossil fuels with emphasis on heat reclamation from urban water,” *Renew. Sustain. Energy Rev.*, vol. 30, pp. 808–820, 2014.

[11] G. T. Daigger, “Evolving Urban Water and Residuals Management Paradigms: Water Reclamation and Reuse, Decentralization, Resource Recovery,” in *Proceedings of the Water Environment Federation, October 2008*, 2008, vol. 2008, no. 15, pp. 1537–1565.

[12] A. Siddiqi and L. D. Anadon, “The water-energy nexus in Middle East and North Africa,” *Energy Policy*, vol. 39, no. 8, pp. 4529–4540, 2011.

[13] R. Wilkinson, G. Wolff, W. Kost, and R. Schwom, “An Analysis of the Energy Intensity of Water in California: Providing a Basis for Quantification of Energy Savings from Water System Improvements,” *ACEEE Summer Study Energy Effic. Build.*, vol. 12, no. Wilkinson 2000, pp. 123–133, 2006.

[14] K. Hussey and J. Pittock, “The energy-water nexus: Managing the links between energy and water for a sustainable future,” *Ecol. Soc.*, vol. 17, no. 1, 2012.

[15] C. J. Vörösmarty, C. J. Vo, and P. Green, “Global Water Resources : Vulnerability from Climate Change and Population Growth,” *Science (80-.).*, vol. 289, pp. 284–289, 2000.

[16] R. I. McDonald, P. Green, D. Balk, B. M. Fekete, C. Revenga, M. Todd, and M. Montgomery, “Urban growth, climate change, and freshwater availability,” *Proc. Natl. Acad. Sci.*, vol. 108, no. 15, pp. 6312–6317, 2011.

[17] P. H. Gleick, “Global freshwater resources: soft-path solutions for the 21st century,” *Science (80-.).*, vol. 302, no. 5650, pp. 1524–1528, 2003.

[18] N. L. Poff, C. M. Brown, T. E. Grantham, J. H. Matthews, M. A. Palmer, C. M. Spence, R. L. Wilby, M. Haasnoot, G. F. Mendoza, K. C. Dominique, and A. Baeza, “Sustainable water management under future uncertainty with eco-engineering decision scaling,” *Nat. Clim. Chang.*, vol. 6, no. 1, pp. 25–34, 2016.

[19] A. Ansar, B. Flyvbjerg, A. Budzier, and D. Lunn, “Should we build more large dams? The actual costs of hydropower megaproject development,” *Energy Policy*, vol. 69, pp. 43–56, 2014.
[20] OECD, *Water and Climate Change Adaptation: Policies to Navigate Uncharted Waters*. 2013.
[21] O. Kavvada, A. Horvath, J. R. Stokes-Draut, T. P. Hendrickson, W. A. Eisenstein, and K. L. Nelson, “Assessing Location and Scale of Urban Nonpotable Water Reuse Systems for Life-Cycle Energy Consumption and Greenhouse Gas Emissions,” *Environ. Sci. Technol.*, vol. 50, no. 24, pp. 13184–13194, 2016.
[22] S. A. Kalogirou, “Seawater desalination using renewable energy sources,” *Prog. Energy Combust. Sci.*, vol. 31, no. 3, pp. 242–281, 2005.
[23] S. A. Kalogirou, “Solar thermal collectors and applications,” *Prog. Energy Combust. Sci.*, vol. 30, no. 3, pp. 231–295, 2004.
[24] E. Schroeder, G. Tchobanoglous, H. L. Leverenz, and T. Asano, “Direct Potable Reuse: Supplies, Agriculture, the Environment, and Energy Conservation,” 2012.
[25] E. Friedler and M. Hadari, “Economic feasibility of on-site greywater reuse in multi-storey buildings,” *Desalination*, vol. 190, no. 1–3, pp. 221–234, 2006.
[26] R. Sitzenfrei, S. Hillebrand, and W. Rauch, “Investigating the interactions of decentralized and centralized wastewater heat recovery systems,” *Water Sci. Technol.*, vol. 75, no. 5, pp. 1243–1250, 2017.
[27] “When Being Clean Means Getting Dirty – Bloomberg.” [Online]. Available: https://www.bloomberg.com/news/videos/2016-12-06/when-being-clean-means-getting-dirty. [Accessed: 19-Dec-2017].
[28] “News | ORBITAL SYSTEMS.” [Online]. Available: https://orbital-systems.com/news/. [Accessed: 19-Dec-2017].
[29] D. Saurí, “Water Conservation: Theory and Evidence in Urban Areas of the Developed World,” *Annu. Rev. Environ. Resour.*, vol. 38, no. 1, pp. 227–248, 2013.
[30] R. R. Brown, N. Keath, and T. H. F. Wong, “Urban water management in cities: historical, current and future regimes,” *Water Sci. Technol.*, vol. 59, no. 5, pp. 847–855, 2009.
[31] M. Lafforgue and V. Lenouvel, “Closing the urban water loop: lessons from Singapore and Windhoek,” *Environ. Sci. Water Res. Technol.*, vol. 1, no. 5, pp. 622–631, 2015.
[32] P. Kehoe, S. Rhodes, and J. Scarpulla, “Re-Thinking Water Sources : Regulatory Blueprints for Non-Potable Water Use,” in *Proceedings of the Water Environment Federation, WEFTEC 2014*, 2014, pp. 730–743.
[33] D. L. Sedlak, *Water 4.0 : the past, present, and future of the world’s most vital resource*. Yale University Press, 2014.
[34] D. Christova-Boal, R. E. Eden, and S. McFarlane, “Investigation into greywater reuse for urban residential properties,” *Desalination*, vol. 106, no. 1–3, pp. 391–397, 1996.
[35] L. Hernández Leal, H. Temmink, G. Zeeman, and C. J. N. Buisman, “Characterization and anaerobic biodegradability of grey water,” *Desalination*, vol. 270, no. 1–3, pp. 111–115, 2011.
[36] A. Morel and S. Diener, “Greywater Management in Low and Middle-Income

Countries," 2006.
[37] Z. L. T. Yu, A. Rahardianto, J. R. DeShazo, M. K. Stenstrom, and Y. Cohen, "Critical Review: Regulatory Incentives and Impediments for Onsite Graywater Reuse in the United States," *Water Environ. Res.*, vol. 85, no. 7, pp. 650–662, 2013.
[38] M. Pidou, L. Avery, T. Stephenson, P. Jeffrey, S. A. Parsons, S. Liu, F. A. Memon, and B. Jefferson, "Chemical solutions for greywater recycling," *Chemosphere*, vol. 71, no. 1, pp. 147–155, 2008.
[39] E. Friedler, R. Kovalio, and N. I. Galil, "On-site greywater treatment and reuse in multi-storey buildings," *Water Sci. Technol.*, vol. 51, no. 10, pp. 187–194, 2005.
[40] Y. Boyjoo, V. K. Pareek, and M. Ang, "A review of greywater characteristics and treatment processes," *Water Sci. Technol.*, vol. 67, no. 7, pp. 1403–1424, 2013.
[41] B. Jefferson, A. Laine, S. Parsons, T. Stephenson, and S. Judd, "1999 - Jefferson - Urban Water - Technologies for domestic water recycling.pdf," *Urban Water*, vol. 1, pp. 285–292, 1999.
[42] F. Li, K. Wichmann, and R. Otterpohl, "Review of the technological approaches for grey water treatment and reuses," *Sci. Total Environ.*, vol. 407, no. 11, pp. 3439–3449, May 2009.
[43] E. Eriksson, K. Auffarth, M. Henze, and A. Ledin, "Characteristics of grey wastewater," *Urban Water*, vol. 4, no. 1, pp. 85–104, Mar. 2002.
[44] E. Eriksson, K. Auffarth, A. M. Eilersen, M. Henze, and A. Ledin, "Household chemicals and personal care products as sources for xenobiotic organic compounds in grey wastewater," *Water SA*, vol. 29, no. 2, pp. 135–146, 2003.
[45] R. Etchepare and J. P. van der Hoek, "Health risk assessment of organic micropollutants in greywater for potable reuse," *Water Res.*, vol. 72, pp. 186–198, Apr. 2015.
[46] J. P. van der Hoek, J. L. Izar Tenorio, C. Hellinga, J. B. van Lier, and A. J. M. van Wijk, "Green Village Delft – integration of an autarkic water supply in a local sustainable energy system," *J. Water Reuse Desalin.*, vol. 4, no. 3, p. 154, 2014.
[47] T. Asano, *Water reuse : issues, technologies, and applications*. McGraw-Hill, 2007.
[48] US-EPA, "Guidelines for Water Reuse 2012," no. September, 2012.
[49] The California Water Boards, "State Water Resources Control Board Regulations Related to Recycled Water," pp. 1–81, 2015.
[50] F. Masi, B. El Hamouri, H. Abdel Shafi, A. Baban, A. Ghrabi, and M. Regelsberger, "Treatment of segregated black/grey domestic wastewater using constructed wetlands in the Mediterranean basin: The zer0-m experience," *Water Sci. Technol.*, vol. 61, no. 1, pp. 97–105, 2010.
[51] F. Hourlier, A. Masse, P. Jaouen, A. Lakel, C. Gerente, C. Faur, and P. Le Cloirec, "Formulation of synthetic greywater as an evaluation tool for wastewater recycling technologies.," *Environ. Technol.*, vol. 31, no. 2, pp. 215–223, 2010.
[52] J. Y. C. Leong, K. S. Oh, P. E. Poh, and M. N. Chong, "Prospects of hybrid rainwater-greywater decentralised system for water recycling and reuse: A review," *J. Clean. Prod.*, vol. 142, pp. 3014–3027, 2017.
[53] E. Wanjiru and X. Xia, "Optimal energy-water management in urban residential buildings through grey water recycling," *Sustain. Cities Soc.*, vol. 32, no. May, pp.

654–668, 2017.
[54] E. Lohan, P. a Muñoz, G. Salthouse, C. Fisher, and K. R. Black, “Performance of Decentralized Wastewater Systems for Green Building Projects in North America and Australia,” pp. 1–11.
[55] E. Atasoy, S. Murat, A. Baban, and M. Tiris, “Membrane bioreactor (MBR) treatment of segregated household wastewater for reuse,” *Clean - Soil, Air, Water*, vol. 35, no. 5, pp. 465–472, 2007.
[56] N. Atanasova, M. Dalmau, J. Comas, M. Poch, I. Rodriguez-Roda, and G. Buttiglieri, “Optimized MBR for greywater reuse systems in hotel facilities,” *J. Environ. Manage.*, vol. 193, pp. 503–511, 2017.
[57] “Commercial buildings and multiple dwellings – one recycling solution .”
[58] “Greywater Systems | AquacellAquacell.” [Online]. Available: http://aquacell.com.au/services/systems/greywater/. [Accessed: 17-Jul-2017].
[59] S. De Gisi, P. Casella, M. Notarnicola, and R. Farina, “Grey water in buildings: a mini-review of guidelines, technologies and case studies,” *Civ. Eng. Environ. Syst.*, vol. 33, no. 1, pp. 35–54, 2016.
[60] Aquacell., “Aquacell G20: 181 Fremont St, San Francisco CA.,” *www.aquacell.us*.
[61] S. E. Beck, R. A. Rodríguez, A. Salveson, N. Goel, S. Rhodes, P. Kehoe, and K. G. Linden, “Disinfection Methods for Treating Low TOC, Light Graywater to California Title 22 Water Reuse Standards,” *J. Environ. Eng.*, vol. 139, no. 9, pp. 1137–1145, 2013.
[62] E. Huber and M. Frost, “Light scattering by small particles,” *J. Water Supply Res. Technol. - Aqua*, vol. 47, no. 2, pp. 87–94, 1998.
[63] J. Christensen and K. Linden, “How Particles Affect UV Light in the UV Disinfection of Unfiltered Drinking Water,” *J. Am. Waterworks Assoc.*, vol. 95, no. 4, pp. 179–189, 2003.
[64] R. a Fenner and K. Komvuschara, “A New Kinetic Model for Ultraviolet Disinfection of Greywater,” *J. Environ. Eng.*, vol. 131, no. 6, pp. 850–864, 2005.
[65] M. Sanchez, M. J. Rivero, and I. Ortiz, “Photocatalytic oxidation of grey water over titanium dioxide suspensions,” *Desalination*, vol. 262, no. 1–3, pp. 141–146, 2010.
[66] W. H. Chin, F. A. Roddick, and J. L. Harris, “Greywater treatment by UVC/H2O2,” *Water Res.*, vol. 43, no. 16, pp. 3940–3947, 2009.
[67] S. Surendran and A. Wheatley, “Grey-Water Reclamation for Non-Potable Re-Use,” *Water Environ. J.*, no. 16, 1998.
[68] Statista, “U.S. Population: Which Brands of Liquid Hand Soap Do You Use Most Often?,” *Statista - The Statistics Portal, Statista*. [Online]. Available: https://www.statista.com/statistics/276375/us-households-brands-of-liquid-hand-soap-used/. [Accessed: 22-Jul-2017].
[69] W. a Jury and H. Vaux, “The role of science in solving the world’s emerging water problems,” *Proc. Natl. Acad. Sci.*, vol. 102, no. 44, pp. 15715–15720, 2005.
[70] M. A. Shannon, P. W. Bohn, M. Elimelech, J. G. Georgiadis, B. J. Mariñas, and A. M. Mayes, “Science and technology for water purification in the coming decades,” *Nature*, vol. 452, no. 7185, pp. 301–310, 2008.
[71] L. D. Nghiem and T. Fujioka, *Removal of Emerging Contaminants for Water Reuse by Membrane Technology*. Elsevier B.V., 2016.

[72] R. W. Holloway, L. Miller-Robbie, M. Patel, J. R. Stokes, J. Munakata-Marr, J. Dadakis, and T. Y. Cath, “Life-cycle assessment of two potable water reuse technologies: MF/RO/UV-AOP treatment and hybrid osmotic membrane bioreactors,” *J. Memb. Sci.*, vol. 507, pp. 165–178, 2016.
[73] A. S. Stillwell, D. C. Hoppock, and M. E. Webber, “Energy recovery from wastewater treatment plants in the United States: A case study of the energy-water nexus,” *Sustainability*, vol. 2, no. 4, pp. 945–962, 2010.
[74] A. Bernabeu, R. F. Vercher, L. Santos-Juanes, P. J. Simón, C. Lardín, M. A. Martínez, J. A. Vicente, R. González, C. Llosá, A. Arques, and A. M. Amat, “Solar photocatalysis as a tertiary treatment to remove emerging pollutants from wastewater treatment plant effluents,” *Catal. Today*, vol. 161, no. 1, pp. 235–240, 2011.
[75] J. M. Herrmann, “Heterogeneous photocatalysis: State of the art and present applications,” *Top. Catal.*, vol. 34, no. 1–4, pp. 49–65, 2005.
[76] C. McCullagh, N. Skillen, M. Adams, and P. K. J. Robertson, “Photocatalytic reactors for environmental remediation: A review,” *J. Chem. Technol. Biotechnol.*, vol. 86, no. 8, pp. 1002–1017, 2011.
[77] A. Mills and S. Le Hunte, “An overview of semiconductor photocatalysis,” *J. Photochem. Photobiol. A Chem.*, vol. 108, no. 1, pp. 1–35, 1997.
[78] W. H. Glaze, J.-W. Kang, and D. H. Chapin, “The Chemistry of Water Treatment Processes Involving Ozone, Hydrogen Peroxide and Ultraviolet Radiation,” *Ozone Sci. Eng.*, vol. 9, no. 4, pp. 335–352, 1987.
[79] M. A. Oturan and J.-J. Aaron, “Advanced Oxidation Processes in Water/Wastewater Treatment: Principles and Applications. A Review,” *Crit. Rev. Environ. Sci. Technol.*, vol. 44, no. 23, pp. 2577–2641, 2014.
[80] A. Fujishima and K. Honda, “Electrochemical Photolysis of Water at a Semiconductor Electrode,” *Nature*, vol. 238, no. 5358, pp. 37–38, 1972.
[81] S. N. Frank and A. J. Bard, “Heterogeneous Photocatalytic Oxidation of Cyanide Ion in Aqueous Solutions at TiO2 Powder,” *J. Am. Chem. Soc.*, vol. 99, no. 1, pp. 303–304, 1977.
[82] C. Dette, M. A. Pérez-Osorio, C. S. Kley, P. Punke, C. E. Patrick, P. Jacobson, F. Giustino, S. J. Jung, and K. Kern, “TiO2 anatase with a bandgap in the visible region,” *Nano Lett.*, vol. 14, no. 11, pp. 6533–6538, 2014.
[83] O. Alfano, D. Bahnemann, A. Cassano, R. Dillert, and R. Goslich, “Photocatalysis in water environments using artificial and solar light,” *Catal. Today*, vol. 58, no. 2–3, pp. 199–230, 2000.
[84] D. H. Chen, X. Ye, and K. Li, “Oxidation of PCE with a UV LED photocatalytic reactor,” *Chem. Eng. Technol.*, vol. 28, no. 1, pp. 95–97, 2005.
[85] R. Tayade, T. Natarajan, and H. Bajaj, “Photocatalytic Degradation of Methylene Blue Dye Using Ultraviolet Light Emitting Diodes Photocatalytic Degradation of Methylene Blue Dye Using Ultraviolet Light,” *Ind. Eng. Chem. Res.*, no. 48, pp. 10262–10267, 2009.
[86] W. Y. Wang and Y. Ku, “Photocatalytic degradation of Reactive Red 22 in aqueous solution by UV-LED radiation,” *Water Res.*, vol. 40, no. 12, pp. 2249–2258, 2006.
[87] R. Asahi, “Visible-Light Photocatalysis in Nitrogen-Doped Titanium Oxides,”

Science (80-.)., vol. 293, no. 5528, pp. 269–271, 2001.
[88] H. Tong, S. Ouyang, Y. Bi, N. Umezawa, M. Oshikiri, and J. Ye, "Nano-photocatalytic materials: Possibilities and challenges," *Adv. Mater.*, vol. 24, no. 2, pp. 229–251, 2012.
[89] E. Chatzisymeon, S. Foteinis, D. Mantzavinos, and T. Tsoutsos, "Life cycle assessment of advanced oxidation processes for olive mill wastewater treatment," *J. Clean. Prod.*, vol. 54, pp. 229–234, 2013.
[90] K. Maeda and K. Domen, "Photocatalytic water splitting: Recent progress and future challenges," *J. Phys. Chem. Lett.*, vol. 1, no. 18, pp. 2655–2661, 2010.
[91] Y. Qu and X. Duan, "Progress, challenge and perspective of heterogeneous photocatalysts," *Chem. Soc. Rev.*, vol. 42, no. 7, pp. 2568–2580, 2013.
[92] F. Han, V. S. R. Kambala, M. Srinivasan, D. Rajarathnam, and R. Naidu, "Tailored titanium dioxide photocatalysts for the degradation of organic dyes in wastewater treatment: A review," *Appl. Catal. A Gen.*, vol. 359, no. 1–2, pp. 25–40, 2009.
[93] R. J. Braham and A. T. Harris, "Review of major design and scale-up considerations for solar photocatalytic reactors," *Ind. Eng. Chem. Res.*, vol. 48, no. 19, pp. 8890–8905, 2009.
[94] D. Spasiano, R. Marotta, S. Malato, P. Fernandez-Ibañez, and I. Di Somma, "Solar photocatalysis: Materials, reactors, some commercial, and pre-industrialized applications. A comprehensive approach," *Appl. Catal. B Environ.*, vol. 170–171, pp. 90–123, 2015.
[95] D. Bahnemann, "Photocatalytic water treatment: Solar energy applications," *Sol. Energy*, vol. 77, no. 5, pp. 445–459, 2004.
[96] W. W. Shaner and W. S. Duff, "Solar Thermal Electric Power Systems : Comparison of Line-Focus Collectors," *Sol. Energy*, vol. 22, pp. 49–61, 1979.
[97] M. Mehos and C. Turchi, "Field testing solar photocatalytic detoxification on TCE contaminated groundwater," *Environ. Prog.*, vol. 12, no. 3, pp. 194–199, 1993.
[98] H. Price, E. Lüpfert, D. Kearney, E. Zarza, G. Cohen, R. Gee, and R. Mahoney, "Advances in Parabolic Trough Solar Power Technology," *J. Sol. Energy Eng.*, vol. 124, no. 2, p. 109, 2002.
[99] A. Fernández-García, E. Zarza, L. Valenzuela, and M. Pérez, "Parabolic-trough solar collectors and their applications," *Renew. Sustain. Energy Rev.*, vol. 14, no. 7, pp. 1695–1721, 2010.
[100] D. Y. Saltiel, C, Martin, A., and Goswami, "Performance Analysis of Solar Water Detoxification Systems by Detailed Simulation," in *ASME International Solar Energy Conference, Maui, HI*, 1992, pp. 21–28.
[101] IARC, "IARC Monographs on the Evaluation of Carcinogenic Risks to Humans," *J. Chem. Inf. Model.*, vol. 53, no. 9, pp. 40–74, 2012.
[102] J. Blanco, S. Malato, P. Fernández, a Vidal, a Morales, P. Trincado, J. . Oliveira, C. Minero, M. Musci, C. Casalle, M. Brunotte, S. Tratzky, N. Dischinger, K.-H. Funken, C. Sattler, M. Vincent, M. Collares-Pereira, J. . Mendes, and C. . Rangel, "Compound parabolic concentrator technology development to commercial solar detoxification applications," *Sol. Energy*, vol. 67, no. 4–6, pp. 317–330, 1999.
[103] S. Malato, J. Blanco, D. C. Alarcón, M. I. Maldonado, P. Fernández-Ibáñez, and W. Gernjak, "Photocatalytic decontamination and disinfection of water with solar

collectors," *Catal. Today*, vol. 122, no. 1–2, pp. 137–149, 2007.
[104] D. Robert and S. Malato, "Solar photocatalysis: A clean process for water detoxification," *Sci. Total Environ.*, vol. 291, no. 1–3, pp. 85–97, 2002.
[105] S. Malato, J. Blanco, A. Vidal, D. Alarcon, M. I. Maldonado, J. Caceres, and W. Gernjak, "Applied studies in solar photocatalytic detoxification: An overview," *Sol. Energy*, vol. 75, no. 4, pp. 329–336, 2003.
[106] J. A. Byrne, B. R. Eggins, N. M. D. Brown, B. McKinney, and M. Rouse, "Immobilisation of TiO2 powder for the treatment of polluted water," *Appl. Catal. B Environ.*, vol. 17, no. 1–2, pp. 25–36, 1998.
[107] C. F. Liriano-Jorge, U. Sohmen, A. Özkan, H. Gulyas, and R. Otterpohl, "TiO2 photocatalyst nanoparticle separation: Flocculation in different matrices and use of powdered activated carbon as a precoat in low-cost fabric filtration," *Adv. Mater. Sci. Eng.*, vol. 2014, 2014.
[108] L. K. Limbach, R. Bereiter, E. Muller, R. Krebs, R. Galli, and W. J. Srtark, "Removal of Oxide Nanoparticles in aModel Wastewater Treatment Plant:Influence of Agglomeration andSurfactants on Clearing Efficiency," *Enviromental Sci. Technol.*, vol. 42, no. 15, pp. 5828–5833, 2008.
[109] T. Waller, C. Chen, and S. L. Walker, "Food and Industrial Grade Titanium Dioxide Impacts Gut Microbiota," *Environ. Eng. Sci.*, vol. 34, no. 8, pp. 537–550, 2017.
[110] W. Gernjak, T. Krutzler, A. Glaser, and S. Malato, "Photo-Fenton treatment of water containing natural phenolic compounds Photo-Fenton treatment of water containing natural phenolic pollutants," *Chemosphere*, vol. 50, pp. 71–78, 2003.
[111] H. B. Thu, M. Karkmaz, E. Puzenat, C. Guillard, and J. M. Herrmann, "From the fundamentals of photocatalysis to its applications in environment protection and in solar purification of water in arid countries," *Res. Chem. Intermed.*, vol. 31, no. 4–6, pp. 449–461, 2005.
[112] N. N. Rao, V. Chaturvedi, and G. Li Puma, "Novel pebble bed photocatalytic reactor for solar treatment of textile wastewater," *Chem. Eng. J.*, vol. 184, pp. 90–97, 2012.
[113] I. Arslan, I. A. Balcioglu, and D. W. Bahnemann, "Photochemical treatment of simulated dyehouse effluents by novel TiO2 photocatalysts: Experience with the thin film fixed bed (TFFB) and double skin sheet (DSS) reactor," *Water Sci. Technol.*, vol. 44, no. 5, pp. 171–178, 2001.
[114] W. Gernjak, M. L. Maldonado, S. Malato, J. Cáceres, T. Krutzler, A. Glaser, and R. Bauer, "Pilot-plant treatment of olive mill wastewater (OMW) by solar TiO 2 photocatalysis and solar photo-Fenton," *Sol. Energy*, vol. 77, no. 5, pp. 567–572, 2004.
[115] P. Wyness, J. F. Klausner, D. Y. Goswami, and K. S. Schanze, "Performance of nonconcentrating solar photocatalytic oxidation reactors, Part II: Shallow pond configuration," *J. Sol. Energy Eng.*, vol. 116, no. 1, pp. 8–13, 1994.
[116] R. F. P. Nogueira and W. F. Jardim, "TiO2-Fixed-Bed Reactor for Water Decontamination Using Solar Light," *Sol. Energy*, vol. 56, no. 5, pp. 471–477, 1996.
[117] M. March, A. Martin, and C. Saltiel, "Performance modeling of nonconcentrating solar detoxification systems," *Sol. Energy*, vol. 54, no. 3, pp. 143–151, 1995.

[118] M. V. Shankar, S. Anandan, N. Venkatachalam, B. Arabindoo, and V. Murugesan, "Novel thin-film reactor for photocatalytic degradation of pesticides in an aqueous solution," *J. Chem. Technol. Biotechnol.*, vol. 79, no. 11, pp. 1279–1285, 2004.
[119] P. K. J. Robertson, M. Adams, and I. Campbell, "Novel photocatalytic reactor development for removal of hydrocarbons from water," *Int. J. Photoenergy*, vol. 2008, 2008.
[120] L. Zou, Y. Li, and E. Hu, "Photocatalytic Decolorization of Lanasol Blue CE Dye Solution Using a Flat-Plate Reactor," *J. Environ. Eng.*, vol. 131, no. 1, pp. 102–107, 2005.
[121] I. Boiarkina, S. Norris, and D. A. Patterson, "The case for the photocatalytic spinning disc reactor as a process intensification technology: Comparison to an annular reactor for the degradation of methylene blue," *Chem. Eng. J.*, vol. 225, pp. 752–765, 2013.
[122] I. Boiarkina, S. Pedron, and D. A. Patterson, "An experimental and modelling investigation of the effect of the flow regime on the photocatalytic degradation of methylene blue on a thin film coated ultraviolet irradiated spinning disc reactor," *Appl. Catal. B Environ.*, vol. 110, pp. 14–24, 2011.
[123] G. Balasubramanian, D. D. Dionysiou, M. T. Suidan, V. Subramanian, I. Baudin, and J. M. Laîné, "Titania powder modified sol-gel process for photocatalytic applications," *J. Mater. Sci.*, vol. 38, no. 4, pp. 823–831, 2003.
[124] M. R. Hoffmann, S. T. Martin, W. Choi, and D. W. Bahnemann, "Environmental Applications of Semiconductor Photocatalysis," *Chem. Rev.*, vol. 95, no. 1, pp. 69–96, 1995.
[125] J. Theurich, M. Lindner, and D. W. Bahnemann, "Photocatalytic Degradation of 4-Chlorophenol in Aerated Aqueous Titanium Dioxide Suspensions: A Kinetic and Mechanistic Study," *Langmuir*, vol. 12, no. 26, pp. 6368–6376, 1996.
[126] U. I. Gaya, "Heterogeneous Photocatalysis Using Inorganic Semiconductor Solids," pp. 43–53, 2014.
[127] K. Vasanth Kumar, K. Porkodi, and A. Selvaganapathi, "Constrain in solving Langmuir-Hinshelwood kinetic expression for the photocatalytic degradation of Auramine O aqueous solutions by ZnO catalyst," *Dye. Pigment.*, vol. 75, no. 1, pp. 246–249, 2007.
[128] I. Boiarkina, S. Norris, and D. A. Patterson, "Investigation into the effect of flow structure on the photocatalytic degradation of methylene blue and dehydroabietic acid in a spinning disc reactor," *Chem. Eng. J.*, no. 222, pp. 159–171, 2013.
[129] I. Boiarkina, S. Pedron, and D. A. Patterson, "An experimental and modelling investigation of the effect of the flow regime on the photocatalytic degradation of methylene blue on a thin film coated ultraviolet irradiated spinning disc reactor," *Appl. Catal. B Environ.*, vol. 110, pp. 14–24, 2011.
[130] G. D. Fulford, "The Flow of Liquids in Thin Films," *Adv. Chem. Eng.*, vol. 5, no. C, pp. 151–236, 1964.
[131] Y. Q. Yu and X. Cheng, "Experimental study of water film flow on large vertical and inclined flat plate," *Prog. Nucl. Energy*, vol. 77, pp. 176–186, 2014.
[132] C. -Y Wang, "Liquid film flowing slowly down a wavy incline," *AIChE J.*, vol. 27, no. 2, pp. 207–212, 1981.
[133] B. E. Logan and S. W. Hermanowicz, "Application of the penetration theory to

oxygen transfer to biofilms," *Biotechnol. Bioeng.*, vol. 29, no. 6, pp. 762–766, 1987.
[134] L. K. Brumfield, R. N. Houze, and T. G. Theofanous, "Turbulent Mass Transfer At Free , Gas-Liquid Interfaces with Applications To Film Flows," *Int. J. Gynecol. Pathol.*, vol. 18, pp. 1077–1081, 1974.
[135] L. Lei, N. Wang, X. M. Zhang, Q. Tai, D. P. Tsai, and H. L. W. Chan, "Optofluidic planar reactors for photocatalytic water treatment using solar energy," *Biomicrofluidics*, vol. 4, no. 4, p. 43004, 2010.
[136] H. Lin and K. T. Valsaraj, "An optical fiber monolith reactor for photocatalytic wastewater treatment," *AIChE J.*, vol. 52, no. 6, pp. 2271–2280, 2006.
[137] a Houas, "Photocatalytic degradation pathway of methylene blue in water," *Appl. Catal. B Environ.*, vol. 31, no. 2, pp. 145–157, 2001.
[138] A. Visan, D. Rafieian, W. Ogieglo, and R. G. H. Lammertink, "Modeling intrinsic kinetics in immobilized photocatalytic microreactors," *Appl. Catal. B Environ.*, vol. 150–151, pp. 93–100, 2014.
[139] R. Gorges, S. Meyer, and G. Kreisel, "Photocatalysis in microreactors," *J. Photochem. Photobiol. A Chem.*, vol. 167, no. 2–3, pp. 95–99, 2004.
[140] J. Kulas, I. Roušar, J. Krýsa, and J. Jirkovský, "Photocatalytic degradation rate of oxalic acid on the semiconductive layer of n-TiO2 particles in the batch mode plate reactor Part I: Mass transfer limits," *J. Appl. Electrochem.*, vol. 28, no. 8, pp. 843–853, 1998.
[141] N. Miranda-García, S. Suárez, M. I. Maldonado, S. Malato, and B. Sánchez, "Regeneration approaches for TiO2 immobilized photocatalyst used in the elimination of emerging contaminants in water," *Catal. Today*, vol. 230, pp. 27–34, 2014.
[142] U. S. E. P. Agency, "Building Statistics in the U.S.," 2009.
[143] U. N. E. P. (UNEP)., "Buildings and Climate Change," 2009.
[144] B. Fuller and P. Romer, "Urbanization As Opportunity," 2014.
[145] D. H. W. Li, L. Yang, and J. C. Lam, "Zero energy buildings and sustainable development implications - A review," *Energy*, vol. 54, pp. 1–10, 2013.
[146] M. Younger, H. R. Morrow-Almeida, S. M. Vindigni, and A. L. Dannenberg, "The Built Environment, Climate Change, and Health. Opportunities for Co-Benefits," *Am. J. Prev. Med.*, vol. 35, no. 5, pp. 517–526, 2008.
[147] K. Hua, "Intelligent controls for cyber physical energy buildings," in *2013 IEEE/CIC International Conference on Communications in China - Workshops, CIC/ICCC 2013*, 2013, pp. 120–124.
[148] G. A. Niklasson and C. G. Granqvist, "Electrochromics for smart windows: thin films of tungsten oxide and nickel oxide, and devices based on these," *J. Mater. Chem.*, vol. 17, no. 2, pp. 127–156, 2007.
[149] A. Fidar, F. A. Memon, and D. Butler, "Environmental implications of water efficient microcomponents in residential buildings," *Sci. Total Environ.*, vol. 408, no. 23, pp. 5828–5835, 2010.
[150] B. Howard, L. Parshall, J. Thompson, S. Hammer, J. Dickinson, and V. Modi, "Spatial distribution of urban building energy consumption by end use," *Energy Build.*, vol. 45, pp. 141–151, 2012.
[151] A. Siddiqi and O. L. de Weck, "Quantifying End-Use Energy Intensity of the

Urban Water Cycle," *J. Infrastruct. Syst.*, vol. 19, no. 4, pp. 474–485, 2013.
[152] B. Penate, F. Cirez, F. J. Dominguez, V. J. Subiela, and L. Vera, "Design and testing of an isolated commercial EDR plant driven by solar photovoltaic energy," *Desalin. Water Treat.*, vol. 51, no. 4–6, pp. 1254–1264, 2013.
[153] L. Mei, D. Infield, U. Eicker, and V. Fux, "Thermal modelling of a building with an integrated ventilated PV facade," *Energy Build.*, vol. 35, no. 6, pp. 605–617, 2003.
[154] S. Coonen, "Building Integrated Photovoltaics," in *ORNL Solar Summit*, 2016.
[155] M. Ritzen, Z. Vroon, and C. Geurts, "Building integrated photovoltaics," in *Photovoltaic Solar Energy: From Fundamentals to Applications*, John Wiley & Sons, Ltd., 2017, pp. 579–589.
[156] W. Lee, J. Song, J. H. Son, M. P. Gutierrez, T. Kang, D. Kim, and L. P. Lee, "Solar optics-based active panel for solar energy storage and disinfection of greywater," *Biomicrofluidics*, vol. 10, no. 5, 2016.
[157] K. Kim, "Beyond Green : Growing Algae Facade," in *Proceedings of the 2013 ARCC Architectural Research Conference: The Visibility of Research*, 2013, pp. 500–505.
[158] T. Granata, M. Krehel, S. Wittkopf, and M. Egli, "A Hybrid Facade That Combines an Algal Bioreactor With Photovoltaics," in *CISBAT*, 2015, pp. 567–572.
[159] G. M. Elrayies, "Microalgae: Prospects for greener future buildings," *Renew. Sustain. Energy Rev.*, vol. 81, no. August 2016, pp. 1175–1191, 2018.
[160] J. Al Dakheel and K. Tabet Aoul, "Building Applications, Opportunities and Challenges of Active Shading Systems: A State-of-the-Art Review," *Energies*, vol. 10, no. 10, p. 1672, 2017.
[161] M. Bernardi, N. Ferralis, J. H. Wan, R. Villalon, and J. C. Grossman, "Solar energy generation in three dimensions," *Energy Environ. Sci.*, vol. 5, no. 5, p. 6880, 2012.
[162] A. H. C. Chan, C. K. Chan, J. P. Barford, and J. F. Porter, "Solar photocatalytic thin film cascade reactor for treatment of benzoic acid containing wastewater," *Water Res.*, vol. 37, no. 5, pp. 1125–1135, 2003.
[163] T. Mateus and A. C. Oliveira, "Energy and economic analysis of an integrated solar absorption cooling and heating system in different building types and climates," *Appl. Energy*, vol. 86, no. 6, pp. 949–957, 2009.
[164] B. M. Ross, V. Rao, Y. Park, H. Kagey, S. Hermanovitz, P. Guitterez, and L. P. Lee, "Optical Design of a Vertically-Integrated Multi-Step (VIMS) Solar Photocatalytic Reactor," pp. 1–12.
[165] J.-M. Chern and S.-P. Yang, "Measuring and Modeling of Oxygen Transfer Rate in a Drop Structure," *Ind. Eng. Chem. Res.*, vol. 43, no. 23, pp. 7657–7663, 2004.
[166] J. R. Bolton, K. G. Bircher, W. Tumas, and C. A. Tolman, "Figures-of-merit for the technical development and application of advanced oxidation technologies for both electric- and solar-driven systems (IUPAC Technical Report)," *Pure Appl. Chem.*, vol. 73, no. 4, pp. 627–637, 2001.
[167] R. Dillert, S. Vollmer, M. Schober, J. Theurich, D. Bahnemann, H.-J. Arntz, K. Pahlmann, J. Wienefeld, T. Schmedding, and G. Sager, "Photocatalytic Treatment of an Industrial Wastewater in the Double-Skin Sheet Reactor," *Chem. Eng.*

Technol., vol. 22, no. 11, p. 931, 1999.
[168] P. H. Gleick, “Basic water requirements for human activities: Meeting basic needs,” *Water Int.*, vol. 21, no. 2, pp. 83–92, 1996.
[169] World Health Organization, “Overview of greywater management Health considerations,” 2006.
[170] R. van Grieken, J. Marugán, C. Sordo, and C. Pablos, “Comparison of the photocatalytic disinfection of E. coli suspensions in slurry, wall and fixed-bed reactors,” *Catal. Today*, vol. 144, no. 1–2, pp. 48–54, 2009.
[171] P. G. Loutzenhiser, H. Manz, C. Felsmann, P. A. Strachan, T. Frank, and G. M. Maxwell, “Empirical validation of models to compute solar irradiance on inclined surfaces for building energy simulation,” *Sol. Energy*, vol. 81, no. 2, pp. 254–267, Feb. 2007.
[172] S. Freitas, C. Catita, P. Redweik, and M. C. Brito, “Modelling solar potential in the urban environment: State-of-the-art review,” *Renew. Sustain. Energy Rev.*, vol. 41, pp. 915–931, Jan. 2015.
[173] A. M. Omer, “Energy, environment and sustainable development,” *Renew. Sustain. Energy Rev.*, vol. 12, no. 9, pp. 2265–2300, 2008.
[174] A. Ghaffarianhoseini, N. D. Dahlan, U. Berardi, A. Ghaffarianhoseini, N. Makaremi, and M. Ghaffarianhoseini, “Sustainable energy performances of green buildings: A review of current theories, implementations and challenges,” *Renew. Sustain. Energy Rev.*, vol. 25, pp. 1–17, 2013.
[175] R. Krippner, T. Herzog, and W. Lang, *Facade Construction Manual*. Birkhäuser, 2012.
[176] A. E. Del Grosso and P. Basso, “Adaptive building skin structures,” *Smart Mater. Struct.*, vol. 19, no. 12, 2010.
[177] A. GhaffarianHoseini, A. GhaffarianHoseini, U. Berardi, J. Tookey, D. H. W. Li, and S. Kariminia, “Exploring the advantages and challenges of double-skin façades (DSFs),” *Renew. Sustain. Energy Rev.*, vol. 60, pp. 1052–1065, 2016.
[178] M. Coulis, “Maintaining Façade & Envelope Integrity,” *Buildings: Smarter Facility MAnagement*, 2009. [Online]. Available: https://www.buildings.com/article-details/articleid/9024/title/maintaining-facade-envelope-integrity. [Accessed: 09-Dec-2017].
[179] C. Balas-Ramirez, J. J. Sendra, R. Suárez, E. D. Fernandez-Nieto, and G. Narbona-Reina, “The mur neutralisant as an active thermal system : Saint Gobain tests (1931) versus CFD simulation (2015),” in *Le Corbusier, 50 Years Later International Congress*, 2015, no. 1931, pp. 708–722.
[180] W. Ding, Y. Hasemi, and T. Yamada, “Natural ventilation performance of a double-skin facade with a solar chimney,” *Energy Build.*, vol. 37, no. 4, pp. 411–418, 2005.
[181] S. A. Memon, “Phase change materials integrated in building walls: A state of the art review,” *Renew. Sustain. Energy Rev.*, vol. 31, pp. 870–906, 2014.
[182] K. Kim and D. Ph, “Beyond Green : Growing Algae Facade,” in *ARCC 2013 | The Visibility of Research Sustainability: Visualization Sustainability and Performance*, 2013, pp. 500–505.
[183] J. Shen, X. Zhang, T. Yang, L. Tang, A. Cheshmehzangi, Y. Wu, G. Huang, D. Zhong, P. Xu, and S. Liu, “Characteristic study of a novel compact Solar Thermal

Facade (STF) with internally extruded pin-fin flow channel for building integration," *Appl. Energy*, vol. 168, pp. 48–64, 2016.
[184] T. Matuska and B. Sourek, "Facade solar collectors," *Sol. Energy*, vol. 80, no. 11, pp. 1443–1452, 2006.
[185] C. Peng, Y. Huang, and Z. Wu, "Building-integrated photovoltaics (BIPV) in architectural design in China," *Energy Build.*, vol. 43, no. 12, pp. 3592–3598, 2011.
[186] R. Compagnon, "Solar and daylight availability in the urban fabric," *Energy Build.*, vol. 36, no. 4, pp. 321–328, 2004.
[187] B. P. Jelle, C. Breivik, and H. Drolsum Røkenes, "Building integrated photovoltaic products: A state-of-the-art review and future research opportunities," *Sol. Energy Mater. Sol. Cells*, vol. 100, no. 7465, pp. 69–96, 2012.
[188] E. Skoplaki and J. A. Palyvos, "On the temperature dependence of photovoltaic module electrical performance: A review of efficiency/power correlations," *Sol. Energy*, vol. 83, no. 5, pp. 614–624, 2009.
[189] P. Eiffert and A. Thompson, "U.S. Guidelines for the Economic Analysis of Building-Integrated Photovoltaic Power Systems," 2000.
[190] S. Krauter, "Increased electrical yield via water flow over the front of photovoltaic panels," *Sol. Energy Mater. Sol. Cells*, vol. 82, no. 1–2, pp. 131–137, 2004.
[191] T. T. Chow, "A review on photovoltaic / thermal hybrid solar technology," *Appl. Energy*, vol. 87, no. 2, pp. 365–379, 2010.
[192] M. Wolf, "Performance analyses of combined heating and photovoltaic power systems for residences," *Energy Convers.*, vol. 16, no. 1–2, pp. 79–90, 1976.
[193] J. . Kern, E. C. and M. C. Russell, "Combined photovoltaic and thermal hybrid collector systems," in *Photovoltaic Specialists Conference, 13th, Washington, D.C., June 5-8*, 1978.
[194] T. Yang and A. K. Athienitis, "A review of research and developments of building-integrated photovoltaic/thermal (BIPV/T) systems," *Renew. Sustain. Energy Rev.*, vol. 66, pp. 886–912, 2016.
[195] A. K. Athienitis, J. Bambara, B. O'Neill, and J. Faille, "A prototype photovoltaic/thermal system integrated with transpired collector," *Sol. Energy*, vol. 85, pp. 139–143, 2011.
[196] M. N. Chong, B. Jin, C. W. K. Chow, and C. Saint, "Recent developments in photocatalytic water treatment technology: A review," *Water Res.*, vol. 44, no. 10, pp. 2997–3027, 2010.
[197] R. Charron and A. K. Athienitis, "Optimization of the performance of double-façades with integrated photovoltaic panels and motorized blinds," *Sol. Energy*, vol. 80, no. 5, pp. 482–491, 2006.
[198] H. Davidsson, B. Perers, and B. Karlsson, "System analysis of a multifunctional PV/T hybrid solar window," *Sol. Energy*, vol. 84, no. 3, pp. 365–372, 2010.
[199] T. T. Chow, J. W. Hand, and P. A. Strachan, "Building-integrated photovoltaic and thermal applications in a subtropical hotel building," *Appl. Therm. Eng.*, vol. 23, no. 16, pp. 2035–2049, 2003.
[200] P. Dupeyrat, C. Menezo, M. Rommel, and H. M. Henning, "Efficient single glazed flat plate photovoltaic-thermal hybrid collector for domestic hot water system," *Sol. Energy*, vol. 85, no. 7, pp. 1457–1468, 2011.

[201] S. M. Hosseini Hashemi, J.-W. Choi, and D. Psaltis, “Solar thermal harvesting for enhanced photocatalytic reactions.,” *Phys. Chem. Chem. Phys.*, vol. 16, no. 11, pp. 5137–41, 2014.
[202] N. Wang, F. Tan, L. Wan, M. Wu, and X. Zhang, “Microfluidic reactors for visible-light photocatalytic water purification assisted with thermolysis,” *Biomicrofluidics*, vol. 8, no. 5, 2014.
[203] M. Gutierrez and L. P. Lee, “Multiscale Design and Integration of Sustainable Building Functions,” *Science (80-.).*, vol. 341, no. July, pp. 247–249, 2013.
[204] H. Liu, X. Wang, and D. Wu, “Fabrication of Graphene/TiO_2/Paraffin Composite Phase Change Materials for Enhancement of Solar Energy Efficiency in Photocatalysis and Latent Heat Storage,” *ACS Sustain. Chem. Eng.*, vol. 5, no. 6, pp. 4906–4915, 2017.
[205] “ASHRAE 93-2010 (RA 2014) - Methods of Testing to Determine the Thermal Performance of Solar Collectors,” Atlanta, GA, 2010.
[206] S. Fischer, W. Heidemann, H. Müller-Steinhagen, B. Perers, P. Bergquist, and B. Hellström, “Collector test method under quasi-dynamic conditions according to the European Standard EN 12975-2,” *Sol. Energy*, vol. 76, no. 1–3, pp. 117–123, 2004.
[207] J. S. Coventry and K. Lovegrove, “Development of an approach to compare the ‘value’ of electrical and thermal output from a domestic PV/thermal system,” *Sol. Energy*, vol. 75, no. 1, pp. 63–72, 2003.
[208] T. Takashima, T. Tanaka, T. Doi, J. Kamoshida, T. Tani, and T. Horigome, “New proposal for photovoltaic-thermal solar energy utilization method,” *Sol. energy*, vol. 52, no. 3, pp. 241–245, 1994.
[209] B. J. Huang, T. H. Lin, W. C. Hung, and F. S. Sun, “Performance evaluation of solar photovoltaic/thermal systems,” *Sol. Energy*, vol. 70, no. 5, pp. 443–448, 2001.
[210] A. Bertrand, A. Mastrucci, N. Schüler, R. Aggoune, and F. Maréchal, “Characterisation of domestic hot water end-uses for integrated urban thermal energy assessment and optimisation,” *Appl. Energy*, vol. 186, pp. 152–166, 2017.
[211] A. Bertrand, R. Aggoune, and F. Maréchal, “In-building waste water heat recovery: An urban-scale method for the characterisation of water streams and the assessment of energy savings and costs,” *Appl. Energy*, vol. 203, p. 983, 2017.
[212] W. S. Duff and D. A. Hodgson, “A simple high efficiency solar water purification system,” *Sol. Energy*, vol. 79, no. 1, pp. 25–32, 2005.
[213] N. J. Peill and M. R. Hoffmann, “Development and Optimization of a TiO2-Coated Fiber-Optic Cable Reactor: Photocatalytic Degradation of 4-Chlorophenol,” *Environ. Sci. Technol.*, vol. 29, no. 12, pp. 2974–2981, 1995.
[214] M. Pelaez, N. T. Nolan, S. C. Pillai, M. K. Seery, P. Falaras, A. G. Kontos, P. S. M. Dunlop, J. W. J. Hamilton, J. A. Byrne, K. O’Shea, M. H. Entezari, and D. D. Dionysiou, “A review on the visible light active titanium dioxide photocatalysts for environmental applications,” *Appl. Catal. B Environ.*, vol. 125, pp. 331–349, 2012.